Characterization and Adhesion Evaluation of Hydrothermally Deposited BNT Films on Titanium Substrates

Fangchao XU

A dissertation submitted to
Kochi University of Technology
in partial fulfillment of the requirements
for the degree of

Doctor of Engineering

Graduate School of Engineering
Kochi University of Technology
Kochi, Japan

August 2009

Characterization and Adhesion Evaluation of Hydrothermally Deposited BNT Films on Titanium Substrates **Fangchao XU**

Characterization and Adhesion Evaluation of Hydrothermally Deposited BNT Films on Titanium Substrates

Fangchao XU

A dissertation submitted to
Kochi University of Technology
in partial fulfillment of the requirements
for the degree of

Doctor of Engineering

Department of Engineering
Graduate School of Engineering
Kochi University of Technology
Kochi, Japan

August 2009

ABSTRACT

Piezoelectric materials have been extensively used in smart devices such as sensors and actuators. Nowadays, lead zirconate titanate $Pb(Zr_x,Ti_{1-x})O_3$ (abbreviated as PZT) and PZT-based ceramics are the most commonly used piezoelectric materials due to their excellent piezoelectric properties. However, lead oxide (PbO) in PZT has a strong toxicity to the human body. Hence, there is a great need to develop lead-free piezoelectric ceramics for replacing PZT. In recent years, $(Bi_{1/2}Na_{1/2})TiO_3$ (abbreviated as BNT) has been extensively studied as one of promising lead-free piezoelectric ceramics. On the other hand, piezoelectric films have attracted more and more attentions with the great development of Micro-electromechanical Systems (abbreviated as MEMS), especially in the development of micro-sensors and micro-actuators. In this dissertation, an attempt to deposit BNT film on titanium substrate was made using a hydrothermal method.

In the hydrothermal synthesis of BNT films on titanium substrates, hydrated bismuth nitrate ($Bi(NO_3)_3 \cdot 5H_2O$), titanium oxide(TiO_2) and sodium hydroxide(NaOH) were used as starting materials. We employed a 2-step process: nucleation and crystal growth. A series of samples were prepared with varying the concentrations of $Bi(NO_3)_3$ and TiO_2 starting materials. The properties of deposited BNT films were characterized using SEM, EDX, XRD, LCR and other instruments, and then investigated with respect to the concentrations of $Bi(NO_3)_3$ and TiO_2 starting materials. First of all, XRD diffraction patterns confirmed the generation of BNT crystal with a rhombohedral crystal structure in the deposited films. However, Bi_2O_3 impurity was also found, and its amount increased with increasing the $Bi(NO_3)_3$ concentration. With assumption of deposited films as a system of $(1-x)(Bi_{1/2}Na_{1/2})TiO_3$-$xBi_2O_3$, the BNT content was calculated from the Bi/Ti ratio of the EDX results. With the evaluation target of the calculated BNT content, the optimized synthesis condition was determined as follows: $Bi(NO_3)_3$ of 1.2 mol/l and TiO_2 of 0.5 mol/l. In addition, the unimorph cantilever type actuators were fabricated by BNT deposited samples, and their piezoelectric responses were measured under a DC and AC field. This actuation test confirmed the piezoelectric activity of deposited BNT films, and

it was noted that the piezoelectricity strength of the deposited BNT film was greatly dependent on the crystallization level of BNT. The piezoelectric response of the tested unimorph actuator was stronger in the case of higher BNT diffraction peaks.

The performance and reliability of film/substrate structures are determined to a large extent by the interfacial strength. A quantitative evaluation of the adhesion strength is demanded in the design and fabrication of the film base component. As yet, there is no accepted convention for defining the adhesion strength between the film and substrate. In an effort to quantitatively assess the adhesion strength between the deposited BNT film and titanium substrate, a tensile test, indentation test and scratch test were carried out in this dissertation. The critical force or substrate strain inducing film exfoliation or delamination was determined with the aid of FEM analysis in their respective load condition. In practical evaluation of film adhesion, which test method to use depends on the comparability of the results to the actual operational environment of the film/substrate system. In addition, film adhesion measurements showed that the appropriate pretreatment of titanium substrate such as chemical polish and mechanical polish can improve the adhesion strength of BNT films on titanium substrates.

TABLE OF CONTENTS

LIST OF FIGURES

LIST OF TABLES

Chapter 1

Introduction

This chapter briefly introduces the background for the conducted research. It then motivates the necessity of the research and outlines the objectives and structure of this disseration.

1.1. Motivation and Objectives

Piezoelectricity is exhibited in some materials which are called piezoelectric materials. If a mechanical stress is applied to such piezoelectric materials, an electrical charge will be generated on their opposite faces. This phenomenon is called the direct piezoelectric effect. The converse piezoelectric effect occurs when an applied electrical field causes a mechanical stress in the piezoelectric materials.

The direct piezoelectric effect was discovered by the brothers Pierre Curie and Jacques Curie in 1880 [(1)]. They found that if certain crystals were subjected to mechanical strain, they became electrically polarized and the degree of polarization was proportional to the applied strain. In 1881, Lippmann mathematically proved that applying a voltage to a piezoelectric material induces strain in the material [(2)]. The Curie brothers immediately obtained quantitative proof of this effect.

Piezoelectric materials are capable of acting as either a sensor or an actuator, or both, owing to the direct and converse piezoelectric effects. Nowadays, piezoelectric materials have been extensively used in microelectronic and micromechanical systems (MEMS) [(3)-(10)]. Among piezoelectric materials, lead zirconate titanate $Pb(Zr_x, Ti_{1-x})O_3$ (abbreviated as PZT) and PZT-based ceramics are the most commonly used piezoelectric materials due

to their excellent piezoelectric properties [11]-[16]. However, the toxicity of lead oxide in PZT does harm to human and environment, and then causes a serious problem of environment pollution [17]. The European Union (EU) introduced legislation for use of lead free materials in 2003 [18]. The dangers of lead (Pb) are well recognized, and laws are being introduced internationally to curb its use. Therefore, to reduce and eliminate lead pollution, more and more attentions have been paid to lead-free piezoelectric ceramics [19] - [25].

Bismuth sodium titanate $(Bi_{1/2}Na_{1/2})TiO_3$ (abbreviated as BNT) is considered to be one of promising lead-free piezoelectric ceramics [26]-[28]. In this work, BNT films were deposited on pure titanium substrates by the hydrothermal method. On the other hand, with the trend of miniaturization of smart devices such as micro-sensors and micro-actuators, thin films of piezoelectric materials have been intensely studied [29]-[33]. Kanda et al. reported that PZT films were successfully deposited on pure titanium substrates by the hydrothermal method [34]-[35]. The hydrothermal synthesis of BNT powder was reported by Pookmanee et al [36]. However, there have been few reports about the development of BNT films. The desire for lead free piezoelectric materials and the strong driving force for the miniaturization of intelligent systems motivate the present research.

Based on the background as described above, the objective of this thesis is first to develop BNT films on titanium substrates by a hydrothermal method, with investigating the effects of the concentrations of starting materials on the characteristics of BNT films; and second to quantitatively evaluate the adhesion of BNT films to titanium substrates in different load conditions by a tensile test, indentation test and scratch test with the aid of FEM analysis.

1.2. Thesis Outline

This dissertation is organized as follows:

Chapter 1 motivates the necessity of the research and outlines the objectives and structure of this dissertation.

In Chapter 2, the related background and previous research on piezoelectric materials are reviewed, including the relation between the crystal symmetry and the piezoelectricity, the piezoelectric constitutive relation, and piezoelectric materials with the perovskite structure. The synthesis methods of piezoelectric films are also reviewed, especially introducing the hydrothermal method.

Chapter 3 firstly presents the hydrothermal synthesis of BNT films on titanium substrates; secondly, we characterize the properties of deposited BNT films, such as microstructure, crystal structure, element compositions, relative permittivity and piezoelectric performance; thirdly, we make optimization of synthesis condition on the evaluation target of the BNT content; finally, we investigate the characteristics of deposited BNT films with respect to the concentrations of the starting materials.

In chapter 4, a tensile test is performed to evaluate the adhesion of deposited BNT films to titanium substrates. We investigate the behavior of film exfoliation using the replica method, and determine the critical substrate strain inducing film exfoliation with the aid of finite element analysis (FEM).

In chapter 5, an indentation test is performed to evaluate the adhesion of deposited BNT films to titanium substrates. We investigate the behavior of film delamination by observing the morphology of the indentations using the laser microscope system, and then determine the critical substrate strain inducing film delamination with the aid of finite element analysis.

In chapter 6, a scratch test is performed to evaluate the adhesion of deposited BNT films to titanium substrates. Some of Ti substrates are pretreated by chemical polish and mechanical polish respectively prior to BNT film deposition with a view of investigating the effects of substrate surface pretreatments on the adhesion of BNT films. We determine the critical force from the variations of the tangential force and the acoustic

emission (AE) signals with the normal force.

In chapter 7, we make a summary on the basis of experimental results and investigations.

References

(1) J. F. Tressler, S. Alkoy and R. E. Newnham, Piezoelectric Sensors and Sensor Materials, *Journal of Electroceramics*, Vol.2, No.4(1998), pp.257-272.

(2) K. Uchino, J. H. Zheng, A. Joshi, Y. H. Chen, S. Yoshikawa, S. Hirose, S. Takahashi and J. W. C. De Vries, High Power Characterization of Piezoelectric Materials, *Journal of Electroceramics*, Vol.2, No.1(1998), pp.33-40.

(3) L. V. Antoshkin, N. N. Botygina, O. N. Emaleev, P. A. Konyaev, V. P. Lukin and A. P. Yankov, A Piezoelectric Drive for Two-Coordinate Angular Mirror Control, *Instruments and Experimental Techniques*, Vol.45, No.1(2002), pp.132-134.

(4) A. O. Vatul'yan and A. A. Rynkova, Flexural Vibrations of a Piezoelectric Bimorph with a Cut Internal Electrode, *Journal of Applied Mechanics and Technical Physics*, Vol.42, No.1(2001), pp.164-168.

(5) M. Ozawa, T. Hatanaka and H. Hasegawa, Internal Friction of 2 and 8 mol % Y_2O_3-ZrO_2 Polycrystals Measured by a Resonance-Piezoelectric Method at Around 100 kHz, *Journal of Materials Science Letters*, Vol.10, No.13(1991), pp.774-775.

(6) F. Calame and P. Muralt, Novel 3D PZT Thin Film Structure for Micromechanics, *Journal of Electroceramics*, Vol.19, No.4(2007), pp.399-402.

(7) Y. Miyahara, M. Deschler, T. Fujii, S. Watanabe and H. Bleuler, Non-contact Atomic Force Microscope with a PZT Cantilever Used for Deflection Sensing, Direct Oscillation and Feedback Actuation, *Applied Surface Science*, Vol.188, No.3-4(2002), pp.450-455.

(8) R. N. Torah, S. P. Beeby, M. J. Tudor and N. M. White, Thick-Film Piezoceramics and Devices, *Journal of Electroceramics*, Vol.19, No.1(2007), pp.95-110.

(9) K. Uchino, S. Cagatay, B. Koc, S. Dong, P. Bouchilloux and M. Strauss, Micro Piezoelectric Ultrasonic Motors, *Journal of Electroceramics*, Vol.13, No.1-3 (2004), pp.393-401.

(10) P. Marin-Franch, D. L. Tunnicliffe and D. K. Das-Gupta, Dielectric Properties and Spatial Distribution of Polarization of Ceramic + Polymer Composite Sensors, *Materials Research Innovations*, Vol.4, No.5-6(2001), pp.334-339.

(11) K. Morimoto, A. Uematsu, S. Sawai, K. Hisano and T. Yamamoto, Simultaneous Measurement of Thermophysical Properties and Dielectric Properties of PZT-Based Ferroelectric Ceramics by Thermal Radiation Calorimetry, *International Journal of Thermophysics*, Vol.24, No.3(2003), pp.821-835.

(12) A. Navarro, S. A. Rocks and R. A. Dorey, Micromoulding of Lead Zirconate Titanate (PZT) Structures for MEMS, *Journal of Electroceramics*, Vol.19, No.4(2007), pp.321-326.

(13) Klaus Prume, Paul Muralt, Florian Calame, Thorsten Schmitz-Kempen and Stephan Tiedke,

Extensive Electromechanical Characterization of PZT Thin Films for MEMS Applications by Electrical and Mechanical Excitation Signals, *Journal of Electroceramics*, Vol.19, No.4(2007), pp.407-411.

(14) S. Narendra Babu, A. Siddeshwar, K. Srinivas, S. V. Suryanarayana and T. Bhimasankaram, Magnetoelectric Properties of Ni/PZT/Ni Layered Composite for Low Field Applications, *Journal of Materials Science*, Vol.44, No.15(2009), pp.3948-3951.

(15) C. Pramila, T. C. Goel and P. K. C. Pillai, Piezoelectric, Pyroelectric and Dielectric Properties of La- and Sm-Doped PZT Ceramics, *Journal of Materials Science Letters*, Vol.12, No.21(1993), pp.1657-1658.

(16) S. N. Kallaev, G. G. Gadzhiev, I. K. Kamilov, Z. M. Omarov, S. A. Sadykov and L. A. Reznichenko, Thermal Properties of PZT-based Ferroelectric Ceramics, *Physics of the Solid State*, Vol.48, No.6 (2006), pp.1169-1170.

(17) D. Q. Xiao , D. M. Lin and J. G. Zhu, Investigation on the Design and Synthesis of New Systems of BNT-Based Lead-Free Piezoelectric Ceramics, *Journal of Electroceramics*, Vol.16, No.4(2006), pp.271–275.

(18) M. Demartin Maeder, D. Damjanovic, and N. Setter, Lead Free Piezoelectric Materials, *Journal of Electroceramics,* Vol.13, No.1-3(2004), pp.385-392.

(19) K. Prasad, Lily, K. Kumari and K. P. Chandra, Electrical Properties of a Lead-Free Perovskite Ceramic: $(Na_{0.5}Sb_{0.5})TiO_3$, *Applied Physics A: Materials Science & Processing*,Vol.88, No.2(2007), pp.377-383.

(20) Y. Wu, H. Zhang, Y. Zhang, J. Y. Ma and D. H. Xie, Lead-Free Piezoelectric Ceramics with Composition of $(0.97-x)Na_{1/2}Bi_{1/2}TiO_3$-$0.03NaNbO_3$-$xBaTiO_3$, J*ournal of Materials Science*, Vol.38, No.5(2003), pp.987-994.

(21) S. H. Choy, X. X. Wang and H. L. W Chan, Electromechanical and Ferroelectric Properties of $(Bi_{1/2}Na_{1/2})TiO_3$-$(Bi_{1/2}K_{1/2})TiO_3$-$(Bi_{1/2}Li_{1/2})TiO_3$-$BaTiO_3$ Lead-Free Piezoelectric Ceramics for Accelerometer Application, *Applied Physics A: Materials Science & Processing*,Vol.89, No.3(2007), pp.775-781.

(22) X. X. Wang, H. L. W. Chan and C. L. Choy, $(Bi_{0.5}Na_{0.5})_{0.94}Ba_{0.06}TiO_3$ Lead-Free Ceramics with Simultaneous Addition of CeO_2 and La_2O_3, *Applied Physics A: Materials Science & Processing*, Vol.80, No.2(2005), pp.333-336.

(23) S. J. Zhang, R. Xia and Thomas R. Shrout, Lead-free Piezoelectric Ceramics vs. PZT?, *Journal of Electroceramics*, Vol.19, No.4 (2007), pp.251-257.

(24) T. Takenaka, H. Nagata, Y. Hiruma, Y. Yoshii and K. Matumoto, Lead-free Piezoelectric Ceramics Based on Perovskite Structures, *Journal of Electroceramics*, Vol.19, No.4 (2007), pp.259-265.

(25) S. H. Choy, X. X. Wang, H. L.W. Chan and C. L. Choy, Study of Compressive Type Accelerometer Based on Lead-free BNKBT Piezoceramics, *Applied Physics A: Materials*

Science & Processing, Vol.82, No.4 (2006), pp.715-718.

(26) A. Thanaboonsombut and N. Vaneesorn, Effect of Attrition Milling on the Piezoelectric Properties of $Bi_{0.5}Na_{0.5}TiO_3$-Based Ceramics, *Journal of Electroceramics*, Vol.21, No.1-4 (2008), pp.414-417.

(27) O. Khamman, A. Watcharapasorn, K. Pengpat and T. Tunkasiri, Fine Grained Bismuth Sodium Titanate Ceramics Prepared via Vibro-Milling Method, *Journal of Materials Science*, Vol.41, No.16 (2006), pp.5391-5394.

(28) C. R. Zhou and X. Y. Liu, Dielectric and Piezoelectric Properties of $Bi_{0.5}Na_{0.5}TiO_3$–$BaNb_2O_6$ Lead-free Piezoelectric Ceramics, *Journal of Materials Science: Materials in Electronics*, Vol.19, No.1 (2008), pp.29-32.

(29) H.Y. Guo, J.B. Xu, Ian H. Wilson, Z. Xie and E.Z. Luo, Study of Microscopic Piezoelectricity of $(Pb_{0.76}Ca_{0.24})TiO_3$ Thin Films, *Physics Letters A*, Vol.294, No.3-4(2002), pp.217-221.

(30) H. X. Cao and Z. Y. Li, Piezoelectric Properties of Epitaxial $Ba_{0.6}Sr_{0.4}TiO_3$ Thin Films, *Physics Letters A*, Vol.334, No.5-6(2005), pp.429-435.

(31) P. F. Liu, J. H. Qiu and Q. Jiang, Dielectric Behavior of Ferroelectric Thin Films Grown on Orthorhombic Substrates, *Physics Letters A*, Vol.357, No.6(2006), pp.485-490.

(32) B. M. Gol'tsman, V. V. Lemanov, A. I. Dedyk, S. F. Karmanenko and L. T. Ter-Martirosyan, Dielectric Properties of Planar Structures Based on Ferroelectric $Ba_{0.5}Sr_{0.5}TiO_3$ Films, *Technical Physics Letters*, Vol.23, No.8(1997), pp.594-596.

(33) N. A. Pertsev, A. G. Zembil'gotov and R. Wazer, Effective Dielectric and Piezoelectric Constants of Thin Polycrystalline Ferroelectric Films, *Physics of the Solid State*, Vol.40, No.12(1998), pp.2002-2008.

(34) T. Kanda, T. Morita, M. K. Kurosawa and T. Higuchi, Sensitivity of a Miniaturized Touch Probe Sensor Using PZT Thin Film, *Ultrasonics,* Vol.40, No.1-8(2002), pp.61-65.

(35) P. Pookmanee, P. Uriwilost and S. Phanickpat, Hydrothermal Synthesis of Fine Bismuth Powders, *Ceramics International*, Vol.30, No.7(2004), pp.1913-1915.

(36) E. B. Arau´Jo and J. A. Eiras, Effect of Substrate Characteristics on Dielectric Properties of PZT Thin Films Obtained from Oxide Precursors, *Journal of Materials Science Letters*, Vol.18, No.20(1999), pp.1679-1681.

Chapter 2

Literature Review

This chapter reviews the related background and previous research in the field of piezoelectric materials, which are essential to understand the present dissertation. It mainly includes fundamentals of piezoelectricity and ferroelectricity, crystal symmetry and piezoelectric materials with the perovskite structure. The synthesis methods of piezoelectric films are also reviewed, especially introducing the hydrothermal method.

2.1. Piezoelectricity and Ferroelectricity

Piezoelectricity is the ability of some of dielectric materials to develop electrical polarization in respond to mechanical strain (stress). Ferroelectricity is exhibited in some of dielectric materials which possess a spontaneous polarization even when they are unstrained [(1)]. Ferroelectric materials are a subset of piezoelectric materials. The relationships between dielectric, piezoelectric and ferroelectric materials are illustrated in Figure 2.1. All the ferroelectric materials are piezoelectric materials, while not all the piezoelectric materials possess ferroelectric properties. In this section, the fundamentals of piezoelectricity and ferroelectricity are presented from the viewpoint of microstructure.

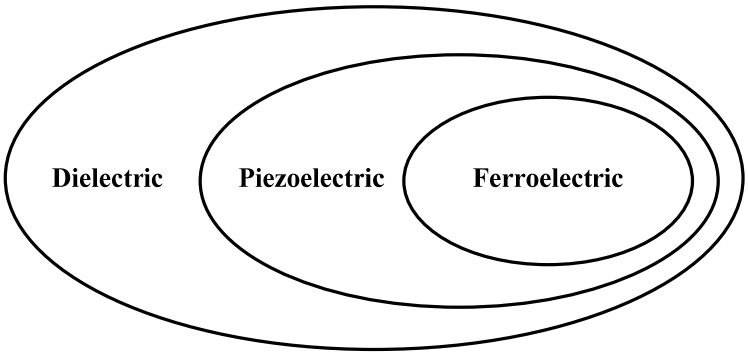

Figure 2.1 Relationship between dielectric, piezoelectric and ferroelectric materials

2.1.1. Crystal Structure

Piezoelectricity is attributed to the lack of a center of symmetry of the crystallographic unit cell [(2)]. Deformation of such a unit cell leads to polarization. Figure 2.2 provides an explanation of why the piezoelectric effect exists. In the unstressed unit cell, the center of positive charges coincides with the center of negative charges. As shown in Figure 2.2a, the unit cell with a center of symmetry deforms when subjected to a compressive stress, but the centers of positive and negative charges are not separated, thus no piezoelectricity is observed in the bulk material. In Figure 2.2b, the unit cell with a noncentrosymmetric structure deforms when subjected to a compressive stress, and the centers of positive and negative charges are separated. This results in the net polarization of the unit cell, thus piezoelectricity is observed in the bulk material.

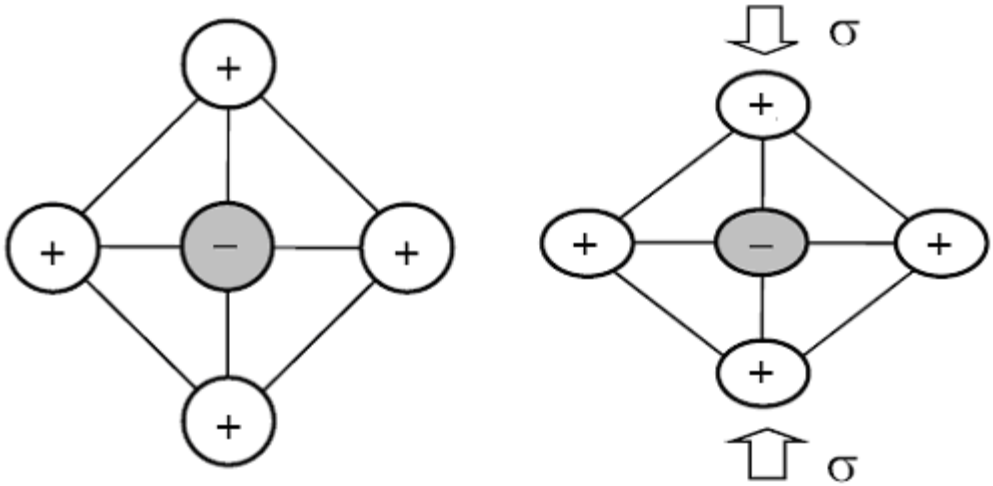

(a)

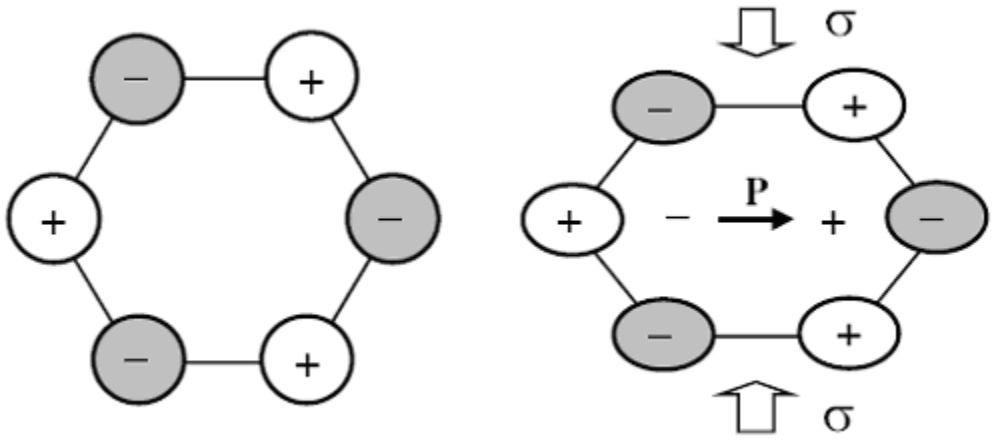

(b)

Figure 2.2 Origin of piezoelectricity: (a) centrosymmetric crystal structure; (b) noncentrosymmetric crystal structure

Piezoelectricity is exhibited in some materials (crystal or non-crystalline) that do not have a center of symmetry. As BNT film, the focus of this dissertation, is one of polycrystals, the relationship between crystal structure and piezoelectricity is solely discussed in this section. Crystals are classified into seven crystal systems according to their atomic lattices. The seven crystal systems are further divided into 32 point groups or

crystal structures, each of which exhibits unique symmetric elements such as reflection, rotation and translation [3]. In the 32 point groups, 11 point groups with a center of symmetry can not support piezoelectricity; the other 21 point groups lack a center of symmetry, thus support piezoelectricity with one exception (point group 432) [4]. In other words, crystals belonging to one of these 20 point groups exhibit piezoelectricity. Microscopic dipoles are formed in piezoelectric materials by the displacement between the positive and negative charges in the unit cell. 10 of the 20 piezoelectric point groups have no net polarization, as the microscopic dipoles sum to zero except when the crystal is strained. The remaining 10 piezoelectric point groups exhibit a spontaneous polarization even when the crystal is unstrained. These crystals are referred to as pyroelectric materials. The spontaneous polarization is a result of a displacement between the centers of positive and negative charges in the crystal unit cell and changes when the material is heated uniformly causing a charge to develop on the surface [5]. Ferroelectric materials are a subset of pyroelectric materials, and defined as pyroelectric materials with a switchable spontaneous polarization [6]. Ferroelectric materials include the structures of tungsten bronze, perovskite, pyrochlore and bismuth layer [7]. BNT crystal has a perovskite structure [8]. As described above, the crystal structures of piezoelectric, pyroelectric and ferroelectric materials are depicted schematically in Figure 2.3 [9]-[10]. It can be concluded that the necessary condition for piezoelectricity to exist is a noncentrosymmetric crystal structure, and the necessary conditions for ferroelectricity to exist are a noncentrosymmetric crystal structure and a switchable spontaneous polarization.

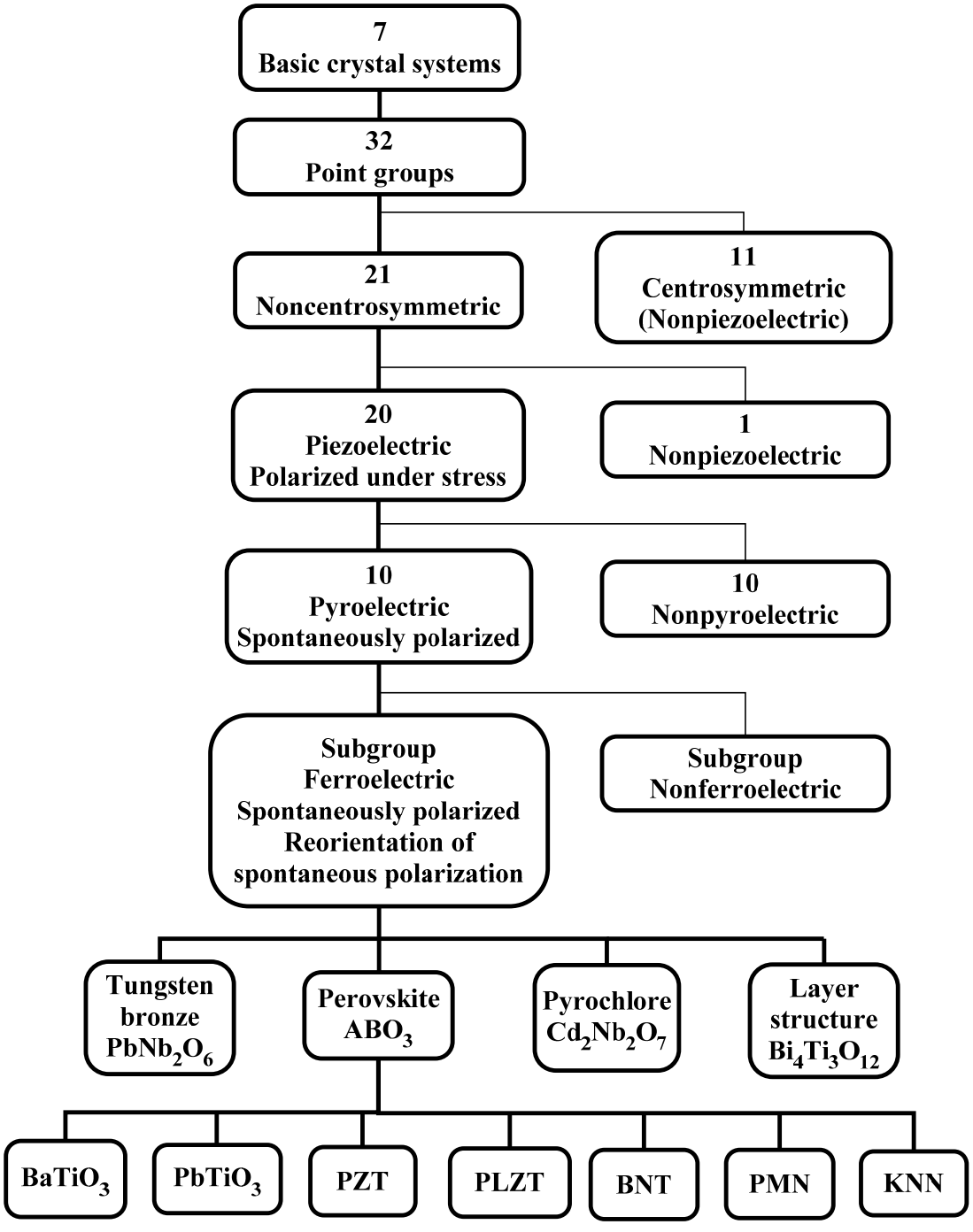

Figure 2.3 Crystal structures of piezoelectric, pyroelectric and ferroelectric materials

2.1.2. Piezoelectricity

It has been more than one hundred years since piezoelectricity was discovered in 1880 by the Curie brothers [11]. "Piezo" is derived from the Greek word *piezein* meaning "to press" [12]. Piezoelectricity is the ability of some materials to convert mechanical energy to electric energy (direct piezoelectric effect) or electric energy to mechanical energy (converse piezoelectric effect). The direct and converse piezoelectric effects are illustrated in Figure 2.4.

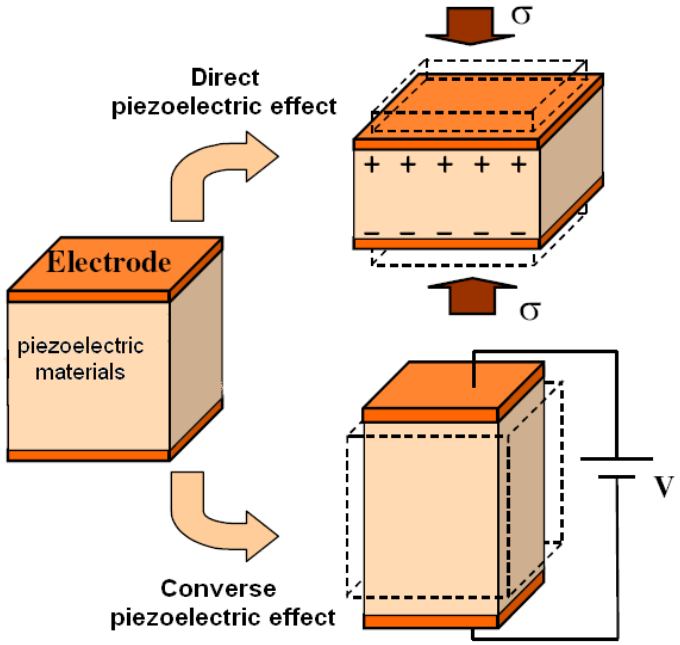

Figure 2.4 The direct and converse piezoelectric effects

The constitutive relation describing the electromechanical effect is given by the following two equations [13].

$$D = dT \tag{2.1}$$

$$S = dE \tag{2.2}$$

Where, D: charge density, C/m^2;

d: piezoelectric constant, C/N;

T: stress, N/m^2;

S: strain;

E: electric field, V/m.

Equation (2.1) describes the charge density change if a stress is applied to the crystal, and this effect is called the direct piezoelectric effect. In other words, the direct piezoelectric effect describes the material's ability to produce a voltage when mechanically strained and can be utilized in sensor applications. Similarly, the converse piezoelectric effect in Equation (2.2) states that the crystal will become strained if an electric field E is applied to the crystal. Therefore, the converse piezoelectric effect can be utilized in actuator applications. If considering the linear elastic and dielectric relations, the piezoelectric constitutive equations can be expressed in the tensor form [14]:

$$D_m = d_{mi} T_i + \varepsilon_{mk}^T E_k \tag{2.3}$$

$$S_i = s_{ij}^E T_j + d_{mi} E_m \tag{2.4}$$

Where s is the elastic compliance, ε is the permittivity, and the subscripts i, j, m and k indicate the direction of stress, strain or electric field. The superscript E indicates that the elastic compliance is measured under the constant electric field (short-circuit condition), and the superscript T indicates that the permittivity is measured under zero stress.

The piezoelectric constant d is an important parameter in the quantitative description of piezoelectricity. The general matrix of the piezoelectric constant is given by the following expression [15].

$$d_{mi} = \begin{bmatrix} d_{11} & d_{12} & d_{13} & d_{14} & d_{15} & d_{16} \\ d_{21} & d_{22} & d_{23} & d_{24} & d_{25} & d_{26} \\ d_{31} & d_{32} & d_{33} & d_{34} & d_{35} & d_{36} \end{bmatrix} \tag{2.5}$$

The first subscript refers to the direction of polarization generated in the bulk material or the direction of the applied electric field. The second subscript refers to the direction of the applied stress or the direction of induced strain. The direction of polarization is

usually chosen to coincide with the Z-axis of a rectangular system. If the directions of X, Y and Z are represented by 1, 2 and 3 respectively, and the shears about these axes are represented by 4, 5 and 6 respectively, as shown in Figure 2.5, the tensor of piezoelectric constant is expressed into the matrix(Equation 2.5).

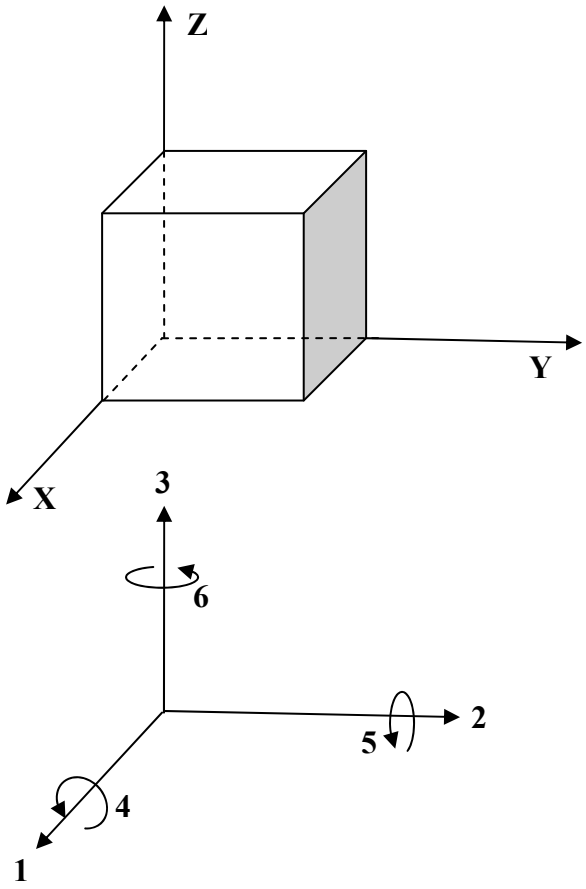

Figure 2.5 Designation of the axes and directions of deformation

The piezoelectric constants d_{31}, d_{33} and d_{15} are illustrated in Figure 2.6 as examples.

d_{31}: the polarization in the 3 direction induced by unit applied stress in the 1 direction, or the strain induced in the 1 direction by unit electric field in the 3 direction.

d_{33}: the polarization in the 3 direction induced by unit applied stress in the 3 direction, or the strain induced in the 3 direction by unit electric field in the 3 direction.

d_{15}: the polarization in the 1 direction induced by unit applied shear stress in the 5 direction, or the shear strain induced in the 5 direction by unit electric field in the 1 direction.

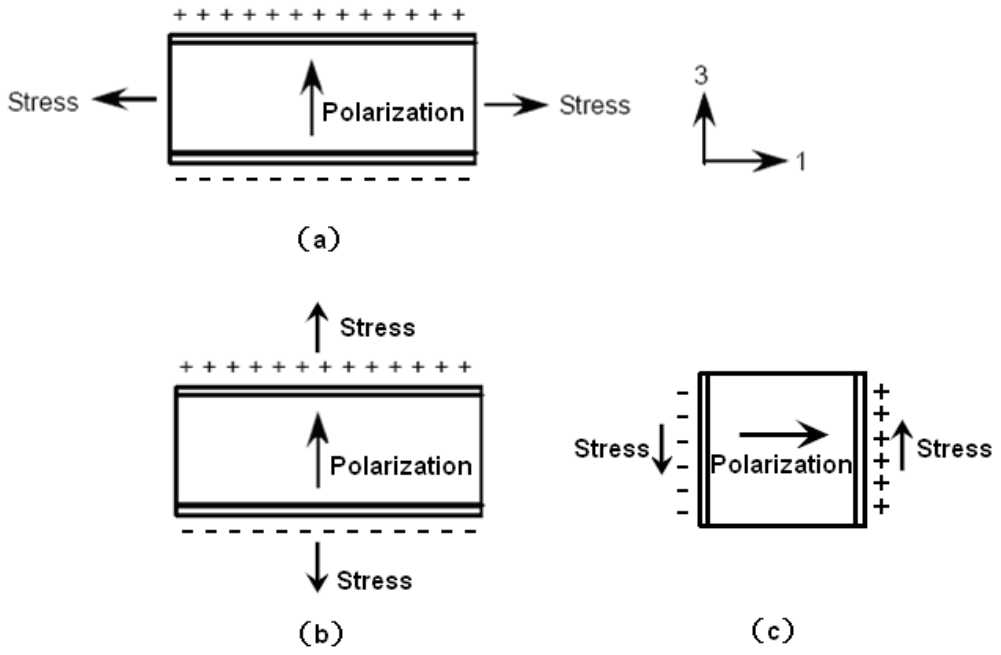

Figure 2.6 Schematic illustrations of piezoelectric coefficients: (a) d_{31}; (b) d_{33}; (c) d_{15}

2.1.3. Ferroelectricity

Ferroelectricity was first discovered in Rochelle salt (sodium potassium tartrate tetrahydrate, $NaKC_4$-H_4O_6•$4H_2O$) in 1921 by J. Valasek [16]. The name ferroelectricity stems from the hysteretic nature of dielectric displacement with applied field, analogous to the hysteresis in magnetization with magnetic field present in ferromagnets. The word ferroelectricity was thus chosen out of convenience and in no way implies that iron is a necessary component to all crystals displaying the ferroelectric phenomenon.

Ferroelectric materials are a subset of pyroelectric materials, which are in turn, a subset of piezoelectric materials. As such, ferroelectrics possess a spontaneous electric dipole moment, develop charges on their surfaces when subjected to a stress and deform when subjected to an electric field. Although each unit cell of ferroelectric materials has a spontaneous polarization, these polarizations are randomly orientated. Therefore unpoled ferroelectric materials have no net remnant polarization, and they must be polarized to exhibit a bulk piezoelectric effect. In addition, ferroelectric materials generally exhibit a ferroelectric behavior below a certain temperature and a paraelectric behavior above this temperature. This structural phase transition from a high-temperature nonferroelectric paraelectric phase to a low-temperature ferroelectric phase occurs at what is called the Curie point (T_c) [17]. Typically, a ferroelectric material in the paraelectric phase is centrosymmetric, which means it exhibits no piezoelectricity, and in the case of BNT, the crystal structure is cubic and hence neither pyroelectric nor piezoelectric [18].

The distinction between pyroelectric and ferroelectric materials is that the direction of the spontaneous polarization in ferroelectrics can be switched by an applied electric field. The polarization reversal can be observed by measuring the ferroelectric hysteresis. A typical *D*-*E* hysteresis loop of a ferroelectric material is shown in Figure 2.7. Here, *D* and *E* mean electrical displacement and electrical field strength, respectively.

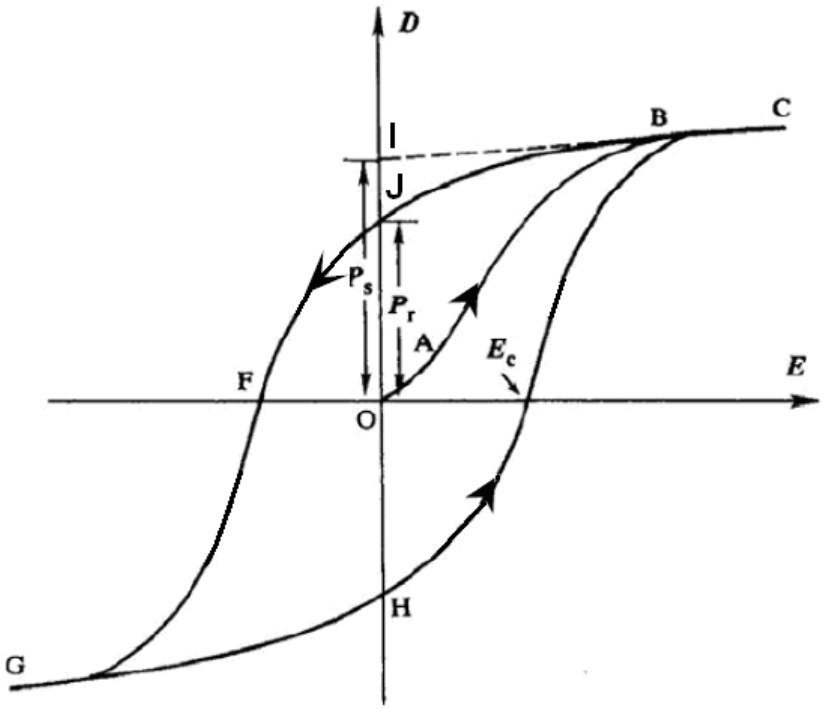

Figure 2.7 A typical *D*-*E* hysteresis loop of ferroelectric materials [19]

As shown in Figure 2.7, initially the unpoled ferroelectric material has zero polarization (origin point O). If only a small electric field is applied across the sample, only a linear relationship between *D* and *E* is observed, because the electric field strength is not large enough to switch domains and the ferroelectric material behaves as a normal dielectric material (OA). A domain is a region with a uniform polarization, surrounded by regions with other polarization directions. As the electric field strength increases, a number of negative domains will switch over to the positive direction and the polarization will increase rapidly (AB) until all the domains are aligned in the positive direction (BC). This is a state of saturation in which the ferroelectric material is composed of just a single domain. As the electric field strength decreases, the polarization will generally decrease but does not return to zero with the removal of the applied electric field. This is because some of the domains remain aligned in the positive direction and the ferroelectric material will exhibit a remnant polarization (OJ, P_r). The

linear extrapolation of the segment BC back to the polarization axis (CBI) represents a linear dielectric and piezoelectric response. The polarization value at point I is the spontaneous polarization (P_s). The electric field required to reduce the polarization P to zero is called the coercive field strength (OF, E_c). Further increase of the electric field strength in the reverse direction will cause a complete alignment of the dipoles in this direction and the cycle can be completed by reversing the field direction once again. The relation between D and E is represented by a hysteresis loop (CJFGHC) as shown in the figure. Hysteresis loop is an important characteristic of ferroelectric materials.

2.2. Piezoelectric Materials

After the piezoelectric effect was discovered in quartz crystal, many materials with piezoelectric property were discovered and synthesized. Nowadays, quartz is still a widely used piezoelectric material for overall stability with respect to time and temperature and is noted for its capability of frequency control [20]. Quartz is naturally piezoelectric (non-ferroelectric) with an essentially linear response, even when very high electric or stress fields are imposed. However, the piezoelectric effect exhibited in natural materials such as quartz, tourmaline, Rochelle salt, etc. is very low [21]-[22]. Thus, polycrystalline ferroelectric ceramic materials such as $BaTiO_3$ and PZT have been developed with improved properties. Ferroelectric ceramics have become an important group of piezoelectric materials.

Ferroelectric ceramics require poling to exhibit the piezoelectric behavior [23]. Poling or polarization is normally achieved at an elevated temperature by applying a high electric field across the material. The orientations of domains in ferroelectric ceramics determine whether or not the ferroelectric ceramics exhibit piezoelectricity. The domains are randomly oriented in the ferroelectric ceramics before poling. Owing to the random distribution of domains throughout the ferroelectric ceramics, no overall polarization or piezoelectricity is exhibited. The domains switch to the applied electric field and align in the same orientation during the poling process. After poling, the domains stay roughly in the same orientation though the electric field is removed. When a stress or an electric field is applied to such poled ferroelectric ceramics, the domains experience the response proportional to the applied stress or electric field, and this results in the display of piezoelectricity. As a consequence, these ferroelectric ceramics become to possess piezoelectricity after poling.

2.2.1. Perovskite Structure

Perovskite is the mineral name of calcium titanate ($CaTiO_3$) [24]. Ferroelectric ceramics with the perovskite crystal structure are probably the most important class of ferroelectric materials for technological applications. For example, barium titanate ($BaTiO_3$), lead titanate ($PbTiO_3$), PZT, lead lanthanum zirconate titanate (PLZT) and BNT have the perovskite structure [25]. The general chemical formula of the perovskite structure is ABO_3 where O is oxygen. A denotes a monovalent, divalent or trivalent metal cation with a large radius, and B denotes a pentavalent, tetravelent or trivalent metal cation with a small radius. As shown in Figure 2.8, the perovskite structure (unit cell) can be described as a cubic structure with A ions at the corners, O ions at the face centers and smaller B ion filling the cubic center.

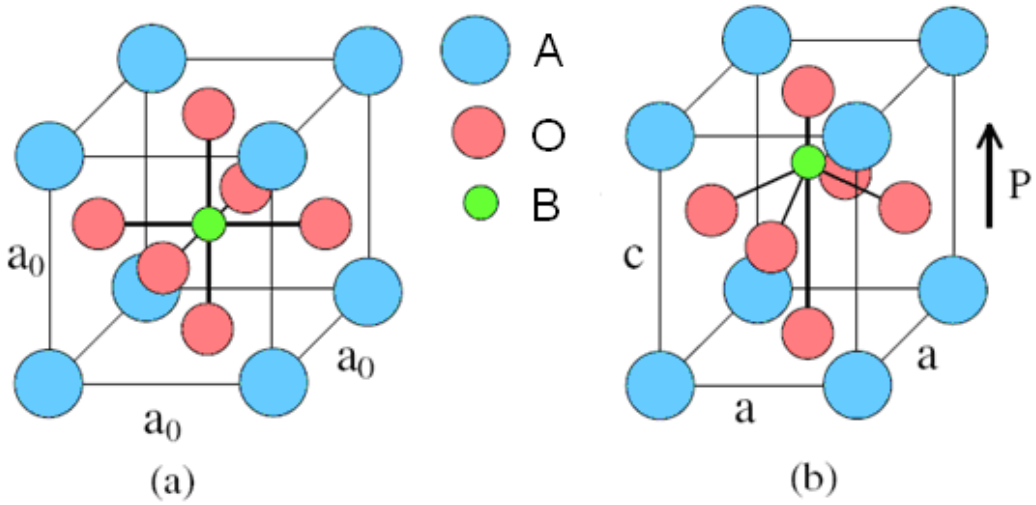

Figure 2.8 Perovskite structure (ABO_3): (a) paraelectric cubic phase above the Curie temperature; (b) ferroelectric tetragonal phase below the Curie temperature

Figure 2.8 compares the unit cells of the paraelectric cubic phase and the ferroelectric tetragonal phase. Above the Curie temperature, the ferroelectric ceramics exhibit the simple cubic symmetry (Figure 2.8(a)). This structure is centrosymmetric with positive and negative charge centers coinciding, so there are no dipoles present in the material. Below the Curie temperature, however the ceramics take on the ferroelectric phase in which the positive and negative charge centers no longer coincide. As an example of ferroelectric structure below T_c, tetragonal symmetry is presented in Figure 2.8(b). As a consequence, each unit cell then has a built-in electric dipole which may be reversed, and also switched to a certain allowed direction by the application of an electric field or stress. It is shown in Figure 2.9 that the tetragonal phase may undergo 90° or 180° polarization switching among the six equivalent polarization directions. The polarization switching induced by an electric field is called ferroelectric switching (90° or 180°), and that induced by a stress is called ferroelastic switching (90°). A stress does not induce 180° switching because 180° switching doesn't accompany a change of spontaneous strain.

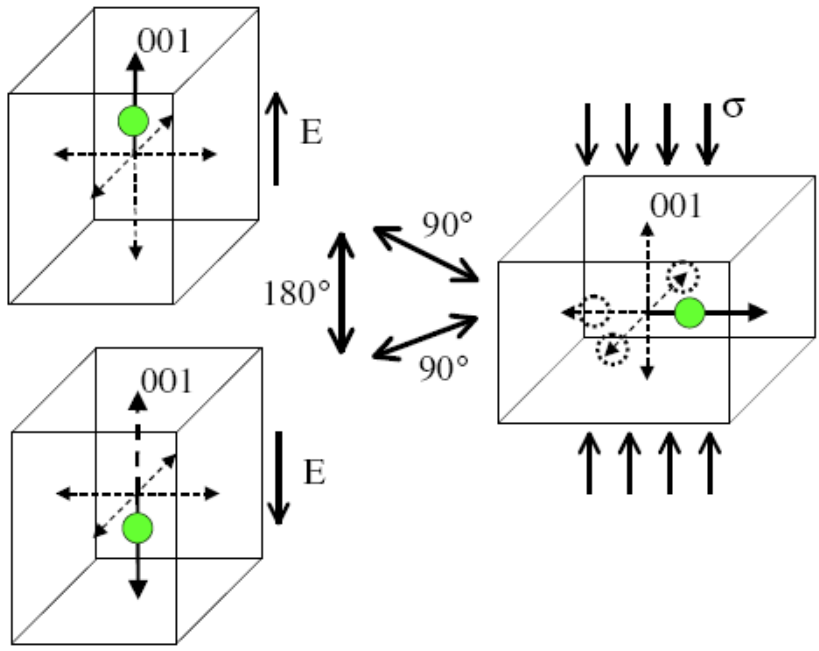

Figure 2.9 Polarization switching of the tetragonal phase. A stress induces 90° ferroelastic switching; an electric field induces 90° or 180° ferroelectric switching [26]

An electric dipole is one of necessary conditions for ferroelectric ceramics to exhibit piezoelectricity. As described above, the ferroelectric ceramics with electric dipoles will exhibit piezoelectricity after poling. As shown in Figure 2.10, the domains are randomly oriented before poling, and then aligned roughly in the direction of the applied electric field after 90° and 180° switching. As a result, the ferroelectric materials with a perovskite structure become to exhibit piezoelectricity after poling.

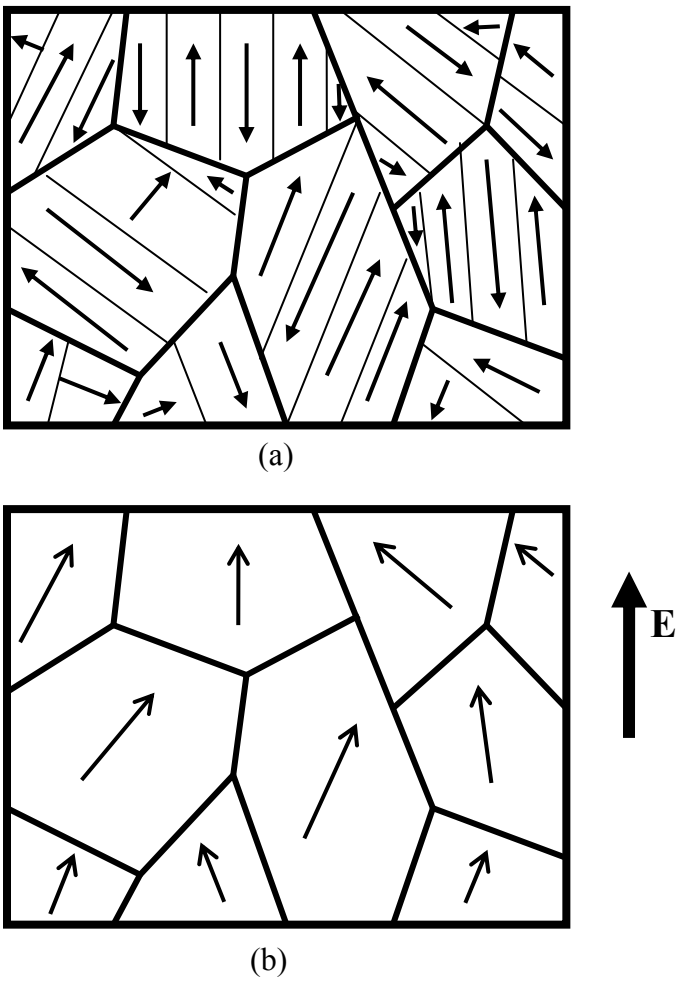

(a)

(b)

Figure 2.10 Schematic diagram of domains in ferroelectric ceramics with a perovskite structure: (a) before poling; (b) after poling

2.2.2. PZT

PZT, one of the perovskite family, has been widely used because of their superior piezoelectric and dielectric properties. In the perovskite structure of PZT, Pb cations occupy the corners of a cube, with O anions at the face centers and a Zr or Ti cation at the center of the unit cell. In fact, PZT is a solid solution of lead zirconate($PbZrO_3$), and lead titanate($PbTiO_3$). Both $PbTiO_3$ and $PbZrO_3$ have the perovskite structure. Below their respective Curie temperatures, $PbTiO_3$ has a tetragonal ferroelectric phase; whereas $PbZrO_3$ has an orthorhombic antiferroelectric phase [27]. The Ti^{4+} cations in $PbTiO_3$ can be partially substituted by Zr^{4+} with a molar ratio X to form a binary system (solid solution) with the following chemical formula $Pb(Zr_x,Ti_{1-x})O_3$. The percentage of $PbZrO_3$ or $PbTiO_3$ in the solid solution determines not only the phase of the solution at a particular temperature but also certain properties like the piezoelectric constant.

Figure 2.11 shows the phase diagram of PZT solid solution system. The Curie temperature is the boundary between the cubic paraelectric phase and the various possible ferroelectric/antiferroelectric phases. T_c varies from 230°C to 490°C depending upon the Zr/Ti ratio. Above T_c, paraelectric cubic phase exists in PZT and the Zr/Ti ions are located at the exact center of the unit cell, regardless of the composition. Below T_c, a morphotropic phase boundary (MPB) divides the ferroelectric region in two parts, which are the rhombohedral (Zr-rich side) and the tetragonal (Ti-rich side). The MPB is located near X~50%, and is almost a vertical straight line. Hence, the transition is practically temperature independent. PZT solid solutions with compositions close to or at the MPB are quite interesting, because they have high dielectric and piezoelectric properties. In the tetragonal phase, there are six equivalent (100) polarization directions; whereas in the rhombohedral phase, there are eight equivalent (111) variants. Within the MPB region, the 6 domain states of the tetragonal coexist with the 8 domain states of the rhombohedral. This results in 14 possible directions for the spontaneous polarization. Consequently, the compositions near the morphotropic boundary show maximum dielectric, ferroelectric and piezoelectric properties.

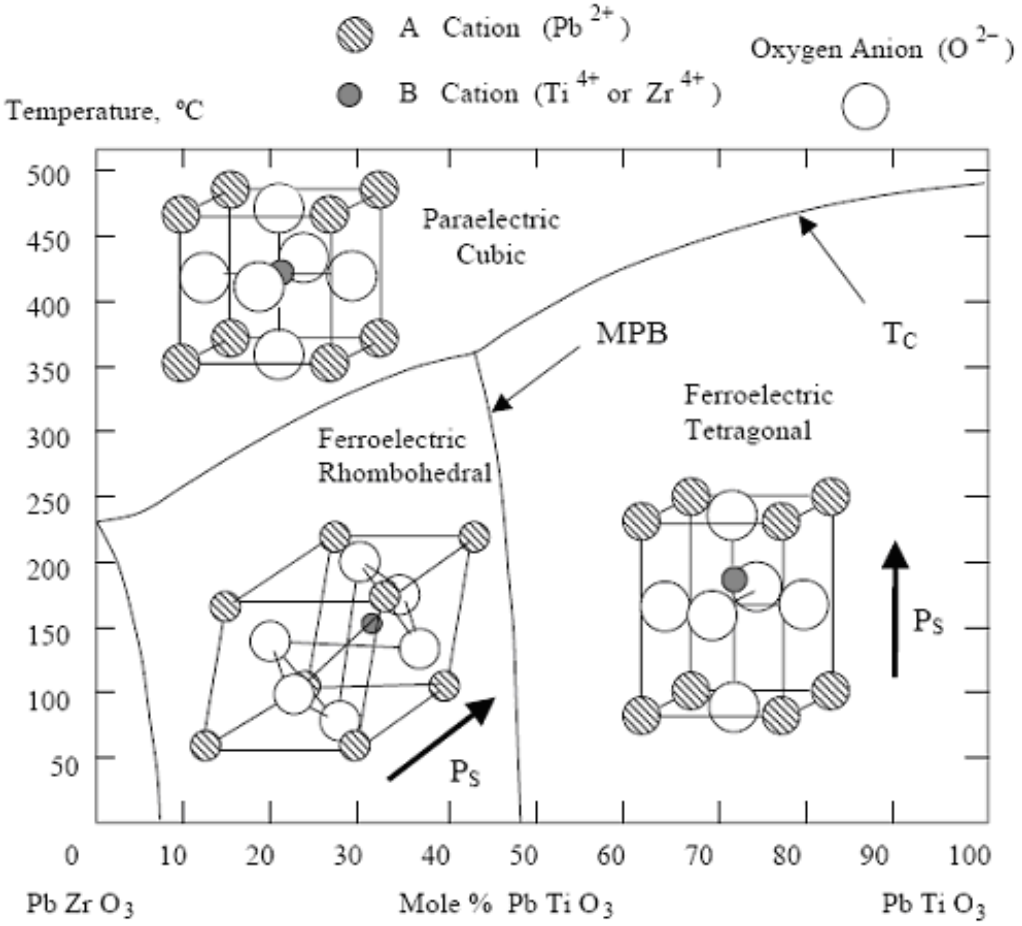

Figure 2.11 Phase diagram of PZT solid solution system [28]

2.2.3. Lead-free Piezoelectric Materials

To date, PZT and PZT-based ceramics are the most widely used piezoelectric materials for piezoelectric actuators, sensors and transducers due to their excellent piezoelectric properties. However, the hazardous lead content present within these materials raises serious environmental concerns. For example, in the typical composition of PZT, $Pb(Zr_{0.52}Ti_{0.48})O_3$, lead takes up to more than 60 wt.% of the material [29]. The toxicity of lead presents serious threat to human health. Once absorbed by a human body, lead occupies the bonding sites where calcium is supposed to be. Because calcium is a crucial messenger to nerve pulse transmission, heart activity and blood clotting, the replacement by lead disrupts the functioning of brain neurotransmitter and the central nervous system is seriously jeopardized [30]. Moreover, lead can accumulate in human organisms and is difficult to remove. There are two major ways that lead gets into the environment: the disposal of discarded lead-contained devices and the evaporation of lead oxide during the processing of lead-based materials. Most wastes are disposed of by the landfill method. After lead-contained devices are buried in the ground, toxic lead can dissolve into the underground water during the acid rain falls contaminating the water source that people need for everyday life. During the processing of lead-based materials, the evaporation of lead oxide is inevitable due to its low melting point (888°C) and high vapor pressure [31].

In addition, in the biosensing applications where the biosensor needs to be utilized inside human body, it's required that the sensing materials, for instance, the piezoelectric materials need to be biocompatible with the interior environment of human body. Lead-based piezoelectric materials are obviously not suitable for these applications.

With the above concerns, regulations and policies against lead-based materials have been increasingly enacted throughout the world. In 2003, European Union (EU) issued the decree of Waste Electrical and Electronic Equipment Directive (WEEE), in which the hazardous substance directive (RoHS) strictly prohibited the use of the six materials listed in Table 2.1 in the manufacturing of electronic equipment. These hazardous materials had to be eliminated from all new electrical products on market since July 1, 2006. Lead was in the first place in these six hazardous substances. In Asia, Japan, China,

and South Korea have also enacted similar policies and legislation to control the usage of lead-contained materials [32]. However, lead-based piezoelectric materials are exempted from the list of the banned materials in these directives or regulations due to the fact that the piezoelectric properties of current lead-free candidates were still inferior to the lead-based materials. Therefore, there has been a growing interest in developing alternative lead-free piezoelectric materials that can eventually replace the current lead-based ones.

Table 2.1 Restriction of Hazardous Substances (RoHS) [33]

Number	Hazardous substance	Chemical formula or symbol
1	Lead	Pb
2	Mercury	Hg
3	Cadmium	Cd
4	Hexavalent chromium	Cr^{6+}
5	Polybrominated biphenyls	PBB
6	Polybrominated diphenyl ether	PBDE

In recent years, an intensive research effort has been spent on the search for alternative environment friendly lead-free materials all around the world. Among all the lead-free piezoelectric materials, two classes have drawn a lot of attention: bismuth layer structure type (BLSF) and perovskite structure type. Table 2.2 shows the current major lead-free piezoelectric materials and their primary properties in comparison to those of PZT.

Table 2.2 Primary properties of current major lead-free piezoelectric materials and PZT

	BLSF	Perovskite structure type			
	$Bi_4Ti_3O_{12}$	$BaTiO_3$	BNT	$(Na_{0.5}K_{0.5})NbO_3$	PZT
T_c (°C)	683	120	320	420	300~400
d_{33} (pC/N)	<10	190	120~200	100~416	200~500
d_{31} (pC/N)	----	-78	-7.5	-30~-152	-130
ε_r (at 1kHz)	100~200	1500~6000	~1700	200~500	1000~4000
References	(34)	(35)	(36)	(37)	(38)

In the current lead-free piezoelectric materials which are studied intensively, bismuth sodium titanate (BNT), discovered by Smolenskii et al. in 1960 [39], is considered to be one of promising lead-free piezoelectric ceramics. BNT belongs to the perovskite family (ABO_3) with bismuth cations(Bi^{3+}) and sodium cations (Na^{+}) at the A-sites, and titanium cation (Ti^{4+}) at the B-site. BNT has a relatively large remnant polarization (P_r=38μC/cm^2) and coercive field (E_c=73 kV/cm) at room temperature. It also has a relatively high Curie temperature (T_c=320°C) [40]. In addition, BNT has a rhombohedral symmetry at room temperature. Therefore, BNT piezoelectric ceramics show a great prospect not only for environment protection but also for various applications.

2.3. Synthesis Methods of Piezoelectric Films

Recently, with the rapid development of Micro-electromechanical Systems (MEMS) engineering, there is an increasing trend for the miniaturization of smart devices such as micro-sensors and micro-actuators. With the driving force towards miniature devices, piezoelectric films have been intensely investigated on their fabrication and characterization. Among film fabrication techniques, chemical vapor deposition (CVD), pulse laser deposition (PLD), sol-gel, RF magnetron sputtering and hydrothermal synthesis have been investigated to fabricate films on various substrates [(41)-(46)]. Figure 2.12 shows the diagram of film fabrication methods, most of which could be categorized into the following categories.

(1) Vapor phase deposition;

(2) Liquid phase deposition

A general definition for vapor phase deposition is the transportation of evaporated molecules from a source material onto a substrate. The initial step of vapor deposition is to obtain the gaseous form of the source molecules. The vaporized source material is then condensed onto a substrate to form a film. There are two general types of vapor deposition techniques: Physical vapor deposition (PVD) and chemical vapor deposition (CVD). In PVD methods, the solid or liquid source material is vaporized by evaporation, laser ablation, or sputtering at high vacuum conditions. In CVD methods, chemical reactions occur during thin film deposition. These reactions can happen between source gases prior to deposition, or between source molecules and substrate during condensation. CVD can be performed under high vacuum or atmospheric pressures, depending on the desired chemical reaction.

In the liquid phase deposition, chemical solution deposition involves fabricating thin films from a chemical solution, drying to remove the liquid in the gel network and performing appropriate heat treatment to convert the as-deposited film into the desired crystalline phase.

Hydrothermal synthesis, one of chemical solution deposition methods, is a method for synthesizing crystals in an aqueous solution under high temperature and high pressure. Compared with other methods such as sol-gel method, CVD, PLD, or the RF

magnetron sputtering method, the hydrothermal method has four outstanding advantages as follows [47]-[51]:

(1) Films can grow on the curved substrate, allowing new kinds of micro-sensors and micro-actuators. Other methods are useful only for a flat-figure substrate. The hydrothermal method, however, utilizes a chemical reaction between the substrate and ions dissolved in the solution, so a film can be deposited over the entire substrate surface.

(2) Deposited films require no poling treatment. During the deposition, the polarization direction is aligned. The direction of the chemical reaction is vertical to the surface of the substrate. It has been assumed that this is why polarization direction is aligned. However, a detailed explanation of this phenomenon is not yet available.

(3) Deposited films require no annealing treatment. Other methods require that the deposited films be annealed to be crystallized. Therefore, it is easy to cause a crack in the deposited film because of the difference in the thermal expansion coefficient between the film and the substrate. The hydrothermal method utilizes a recrystallization reaction, so annealing is not necessary.

(4) The cost of the method is rather low.

In this dissertation, the hydrothermal method was developed to deposit BNT films on pure titanium substrates.

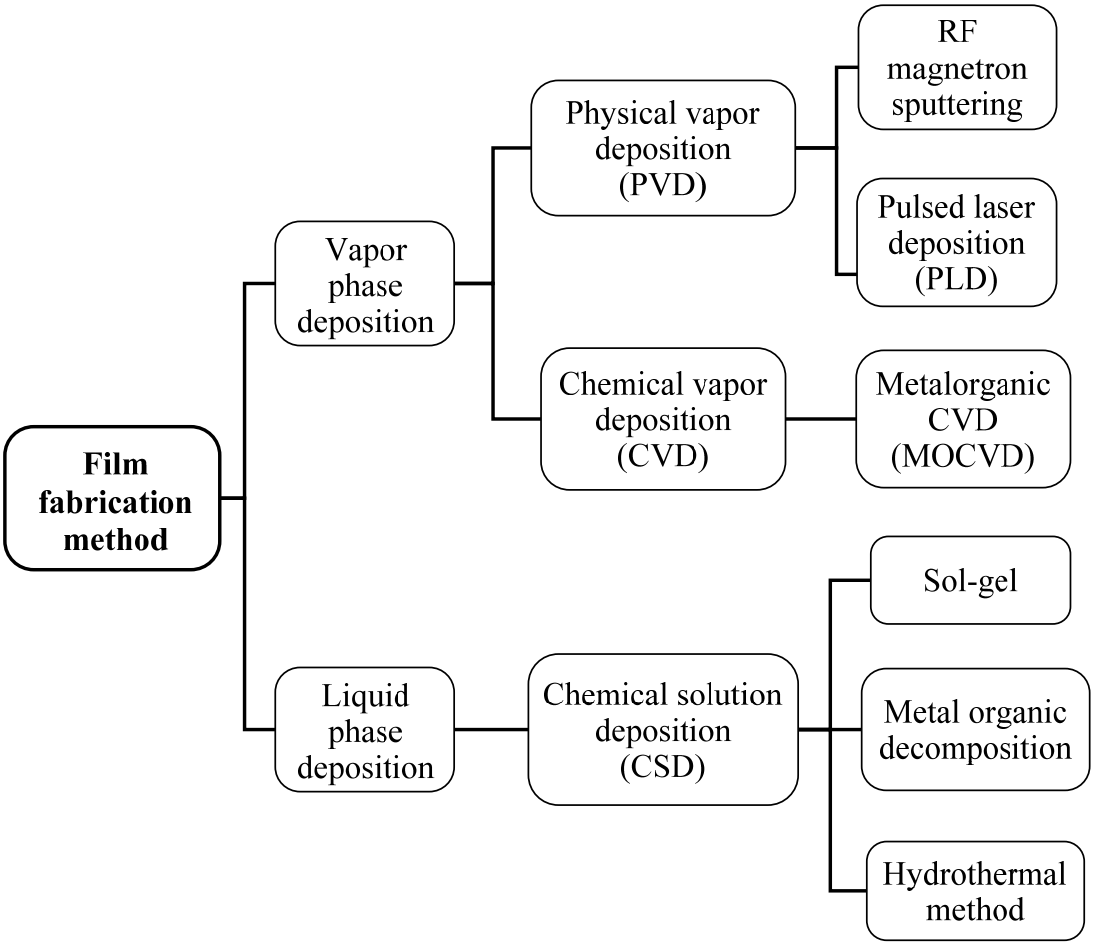

Figure 2.12 Diagram of film fabrication methods

References

(1) D. R. Uhlmann, J. T. Dawley, W. H. Poisl and B. J. J. Zelinski, Ferroelectric Films, *Journal of Sol-Gel Science and Technology*, Vol.19, No.1-3 (2000), pp.53-64.

(2) Yasutomo Uetsuji, Mitsuteru Horio and Kazuyoshi Tsuchiya, Optimization of Crystal Microstructure in Piezoelectric Ceramics by Multiscale Finite Element Analysis, *Acta Materialia*, Vol.56, No.9 (2008), pp. 1991-2002.

(3) Shigehiro Fujino, Combinatorial Discovery of a Morphotropic Phase Boundary in a Lead-free Piezoelectric Material [dissertation]. University of Maryland, 2008.

(4) Tanawadee Dechakupt, Microstructure-Processing-Property Relations in Chemical Solution Deposited Barium Titanate Films [dissertation]. The Pennsylvania State University, 2007.

(5) H. Chen, T. Q. Lü, C. W. Chen and W. W. Cao, Theoretical Studies on the Pyroelectric Properties of Two Component Composite Ferroelectric Thin Film, *Physics Letters* A, Vol.360, No.2(2006), pp.357-361.

(6) Irzaman, Y. Darvina, A. Fuad, P. Arifin, M. Budiman and M. Barmawi, Physical and Pyroelectric Properties of Tantalum-Oxide-Doped Lead Zirconium Titanate [$Pb_{0.9950}(Zr_{0.525}Ti_{0.465}Ta_{0.010})O_3$] Thin Films and Their Application for IR Sensors, *Physica Status Solidi (a*), Vol.199, No.3(2003), pp.416-424.

(7) Lang Chen, Effects of Electric Field on Piezoelectric Responses of Ferroelectric Thin Films [dissertation]. University of Maryland, 2005.

(8) D. Q. Xiao , D. M. Lin and J. G. Zhu, Investigation on the Design and Synthesis of New Systems of BNT-Based Lead-Free Piezoelectric Ceramics, *Journal of Electroceramics*, Vol.16, No.4(2006), pp.271–275.

(9) B. H. Chen, Fabrication, Characterization and Application of Lead Zirconate Titanate Thin films and Bulk Ceramics [dissertation]. National Cheng Kung University, 2004.

(10) Sudarsan Srinivasan, Piezoelectric, Dielectric and Ferroelectric Thin Films on Metal Substrates for Microelectronic Applications [dissertation]. North Carolina State University, 2005.

(11) Kwangtae Ha, A Combined Piezoelectric Composite Actuator and Its Application to Wing/Blade Tips [dissertation]. Georgia Institute of Technology, 2005.

(12) Sontipee Aimmanee, Deformation and Force Characteristics of Laminated Piezoelectric Actuators [dissertation]. The Virginia Polytechnic Institute and State University, 2004.

(13) I. Kanno, Y. Tazawa, T. Suzuki and H. Kotera, Piezoelectric Unimorph Miroactuators with X-shaped Structure Composed of PZT Thin Films, *Microsystem Technologies*, Vol.13, No.8-10 (2007), pp.825-829.

(14) Ling-Sheng Jang and Yung-Chiang Yu, Peristaltic Micropump System With Piezoelectric

Actuators, *Microsystem Technologies*, Vol.14, No.2 (2008), pp.241-248.

(15) Y. T. Hu, H. P. Hu and J. S. Yang, A Low Frequency Piezoelectric Power Harvester Using a Spiral-shaped Bimorph, *Science in China Series G: Physics Mechanics and Astronomy*, Vol.49, No.6 (2006), pp.649-659.

(16) S. Shah and M.S. Ramachandra Rao, Preparation and Dielectric Study of High-Quality PLZT X/65/35 (X = 6,7,8) Ferroelectric Ceramics, *Applied Physics A: Materials Science & Processing*, Vol.71, No.1 (2000), pp.65-69.

(17) D.-S. Paik, S.-E. Park, T. R. Shrout and W. Hackenberger, Dielectric and Piezoelectric Properties of Perovskite Materials at Cryogenic Temperatures, *Journal of Materials Science*, Vol.34, No.3 (1999), pp.469-473.

(18) Pusit Pookmanee, Gobwute Rujijanagul, Supon Ananta, Robert B. Heimann, Sukon Phanichphant, Effect of Sintering Temperature on Microstructure of Hydrothermally Prepared Bismuth Sodium Titanate Ceramics, *Journal of the European Ceramic Society*, Vol.24, No.2 (2004), pp.517-520.

(19) Adam Goff, Modeling and Synthesis of a Piezoelectric Ceramic-Reinforced Metal Matrix Composite [dissertation]. The Virginia Polytechnic Institute and State University, 2003.

(20) D. B. BalitskiЇ, O. Yu. Sil'vestrova, V. S. BalitskiЇ, Yu. V. PisarevskiЇ, D. Yu. PushcharovskiЇ and E. Philippot, Elastic, Piezoelectric, and Dielectric Properties of a-GeO_2 Single Crystals, *Crystallography Reports*, Vol.45, No.1(2000), pp.145-147.

(21) A. I. Burkhanov, A. V. Shil'nikov, A. V. Sopit, and A. G. Luchaninov, Dielectric and Electromechanical Properties of (1 –x) PMN–x PZT Ferroelectric Ceramics, *Physics of the Solid State*, Vol.42, No.5 (2000), pp.936-943.

(22) Adel Benhaj Jilani, Deformations of Piezoceramic-Composite Actuators [dissertation]. The Virginia Polytechnic Institute and State University, 2004.

(23) I. P. Pronin, E. Yu. Kaptelov, E. A. Tarakanov, T. A. Shaplygina, V. P. Afanas'ev and A. V. Pankrashkin, Self-Polarization and Migratory Polarization in Thin Lead Zirconate–Titanate Films, *Physics of the Solid State*, Vol. 44, No.4(2002), pp.769–773.

(24) L. B. Li, J. Zhang, Z. Yin and M. S. Zhang, Position-Thickness-Dependent Stresses and Stress-Induced Diffuse Dielectric Anomaly in Perovskite Ferroelectric Films, *Physics Letters A*, Vol.321, No.1 (2004), pp.67-73.

(25) Roxana M. Piticescu, Paula Vilarnho, Laura Madalina Popescu and Radu R. Piticescu, Perovskite Nanostructures Obtained by a Hydrothermal Electrochemical Process, *Journal of the European Ceramic Society*, Vol.26, No.14 (2006), pp.2945-2949.

(26) Huidong Li, Sodium Potassium Niobate-based Lead-free Piezoelectric Ceramics: Bulk and Freestanding Thick Films [dissertation]. Drexel University, 2008.

(27) D. A. Kiselev, A. L. Kholkin, A. A. Bogomolov, O. N. Sergeeva, E. Yu. Kaptelov, and I. P. Pronin, Piezo- and Pyroelectric Hysteresis in Thin Unipolar PZT Films, *Technical Physics Letters*, Vol.34,

No.8(2008), pp.646-649.

(28) Taeyun Kim, Lead Zirconate Titanate (PZT) Based Thin Film Capacitors for Embedded Passive Applications [dissertation]. North Carolina State University, 2003.

(29) Y. W. Liao, D. Q. Xiao and D. M. Lin, Piezoelectric and Ferroelectric Properties of $Bi_{0.5}(Na_{1-x-y}K_xAg_y)_{0.5}TiO_3$ Lead-free Piezoelectric Ceramics, *Applied Physics A: Materials Science & Processing*, Vol.90, No.1 (2008), pp.165-169.

(30) V. A. Dubok, Bioceramics-Yesterday, Today, Tomorrow, *Powder Metallurgy and Metal Ceramics*, Vol.39, No.7-8 (2000), pp.381-394.

(31) X. X. Wang, H. L. W. Chan and C. L. Choy, $(Bi_{0.5}Na_{0.5})_{0.94}Ba_{0.06}TiO_3$ Lead-free Ceramics with Simultaneous Addition of CeO_2 and La_2O_3, *Applied Physics A: Materials Science & Processing*, Vol.80, No.2 (2005), pp.333-336.

(32) Wataru Sakamoto, Yu-ki Mizutani, Naoya Iizawa, Toshinobu Yogo, Takashi Hayashi and Shin-ichi Hirano, Synthesis and Properties of Ferroelectric Si-doped $(Bi,Nd)_4Ti_3O_{12}$ Thin Films by Chemical Solution Deposition, *Journal of Electroceramics*, Vol.17, No.2-4 (2006), pp.293-297.

(33) Brian James Laughlin, Sputtered $(Ba_x, Sr_{1-x})TiO_3$, BST, Thin Films on Flexible Copper Foils for Use as a Non-linear Dielectric [dissertation]. North Carolina State University, 2006.

(34) Q. B. Yang, Y. X. Li, Q. R. Yin, P. L.Wang and Y. B. Cheng, $Bi_4Ti_3O_{12}$ Nanoparticles Prepared by Hydrothermal Synthesis, *Journal of the European Ceramic Society*, Vol.23, No.1 (2003), pp.161-166.

(35) Kyung Won Seo and Hyun Goo Kong, Hydrothermal Preparation of $BaTiO_3$ Thin Films, *Korean Journal of Chemical Engineering*, Vol.17, No.4 (2000), pp.428-432.

(36) Sossity A. Sheets, Dielectric and Electromechanical Properties of Barium and Zirconium Co-doped Sodium Bismuth Titanate [dissertation]. Massachusetts Institute of Technology, 2000.

(37) S. Gentil, D. Damjanovic and N. Setter, $Pb(Mg_{1/3}Nb_{2/3})O_3$ and $(1-x)Pb(Mg_{1/3}Nb_{2/3})O_3$-$xPbTiO_3$ Relaxor Ferroelectric Thick Films: Processing and Electrical Characterization, *Journal of Electroceramics*, Vol.12, No.3 (2004), pp.151-161.

(38) T. Tunkasiri, Ye Qin, W. Nhuapeng and W. Thamjaree, Structure and Electrical Properties of RF-Sputtering Deposited Thin Ferroelectric $Pb(Zr_{0.52}Ti_{0.48})O_3$ Films, *Journal of Materials Science Letters*, Vol.19, No.21(2000), pp.1913-1916.

(39) Timothy James Yosenick, Synthesis and Colloidal Properties of Anisotropic Hydrothermal Barium Titanate [dissertation]. The Pennsylvania State University, 2005.

(40) Nobuyoshi Fujiwara, Basic Study on Fabrication of Piezoelectrics-Titanium Composites by Hydrothermal Synthesis and Their Properties [dissertation]. Kochi University of Technology, 2006.

(41) K. H. Lai, C. Y. Chan, M. K. Fung, I. Bello, C. S. Lee and S. T. Lee, Mechanical Properties of

DLC Films Prepared in Acetylene and Methane Plasmas Using Electron Cyclotron Resonance Microwave Plasma Chemical Vapor Deposition, *Diamond and Related Materials*, Vol.10, No.9-10 (2001), pp.1862-1867.

(42) Raghuveer S. Makala, Pulsed Laser Deposition of Bi_2Te_3 Based Thermoelectric Thin Films [dissertation]. North Carolina State University, 2002.

(43) Y. D. Xia, G. H. Shi, D. Wu and Z. G. Liu, Dielectric Properties of Low Loss $Ba_{6-3x}Nd_{8+2x}Ti_{18}O_{54}$ Thin Films Prepared by Pulsed Laser Deposition for Microwave Applications, *Journal of Electronic Materials*, Vol.33, No.10 (2004), pp.1236-1239.

(44) J. M. Fernández-Pradas, M. V. García-Cuenca, L. Clèries, G. Sardin and J. L. Morenza, Influence of the Interface Layer on the Adhesion of Pulsed Laser Deposited Hydroxyapatite Coatings on Titanium Alloy, *Applied Surface Science*,Vol.195, No.1-4 (2002), pp.31-37.

(45) J. W. Zhai, X. Yao, B. Shen, L. Y. Zhang and Haydn Chen, Dielectric and Ferroelectric Properties of $Ba(Zr_{0.35}Ti_{0.65})O_3$ Thin Films Grown by a Sol-Gel Process, *Journal of Electroceramics*, Vol.11, No.3(2003), pp.157-161.

(46) Ian M. Reaney, David V. Taylor and Keith G. Brooks, Ferroelectric PZT Thin Films by Sol-Gel Deposition, *Journal of Sol-Gel Science and Technology*, Vol.13, No.1-3 (1998), pp.813-820.

(47) Kun-Ming Hung, Ching-Shieh Hsieh, Wein-Duo Yang and Yi-Jiun Sun, The Preparatory Optimal Conditions of Barium Titanate Thin Film from a Hydrothermal Method at Low Temperature, *Journal of Materials Science*, Vol.42, No.7 (2007), pp.2376-2382.

(48) P. A. Ndiaye, B. Loiseau, S. Minaud, P. Pernod and J. C. Tricot, $PbZr_x\ Ti_{1-x}\ O_3$ Hydrothermal Synthesis on Titanium Substrate for Actuators, *Microsystem Technologies*, Vol.6, No.1 (1999), pp.15-18.

(49) Y. H. Kitsunai, N. Kawashima, S. Takeuchi, M. Ishikawa, M. Kurosawa and E. Odaira, Development of Miniature Needle-Type Hydrophone with Lead Zirconate Titanate Polycrystalline Film Deposited by Hydrothermal Method, *Japanese Journal of Applied Physics*, Vol.45, No.5B (2006), pp.4688-4692.

(50) Z.-B. Wu, T. Tsukada and M. Yoshimura, Direct Synthesis of Potassium Tantalate Thin Films by Hydrothermal-Electrochemical Method, *Journal of Materials Science*, Vol.35, No.11 (2000), pp.2833-2839.

(51) S. Euphrasie, S. Daviero-Minaud and P. Pernod, PZT films Deposited by a Hydrothermal Method and Characterizations, *Materials Science and Engineering B*, Vol.104, No.3 (2003), pp.180-184.

Chapter 3

Synthesis and Characterization of BNT Films on Titanium Substrates

This chapter describes the technology for the synthesis of piezoelectric BNT films on pure titanium substrates by the hydrothermal method. BNT films are prepared with varying the concentrations of starting materials to obtain the optimum synthesis condition. The optimization of the synthesis condition with the evaluation target of the BNT content is presented. Characterizations of deposited BNT films are also presented. Correlations between their properties and synthesis conditions are discussed.

3.1. Introduction

Piezoelectric materials have been extensively used in smart devices such as sensors and actuators. Nowadays, PZT and PZT-based ceramics are the most commonly used piezoelectric materials due to their excellent piezoelectric properties [(1)]. However, because of the strong toxicity of lead oxide, the use of the lead-based ceramics has caused serious lead pollution and environmental problems [(2)]. Therefore, there is a great need to develop lead-free piezoelectric ceramics for replacing them. BNT, one of promising lead-free piezoelectric ceramics, belongs to the perovskite family (ABO_3-type) with a rhombohedral symmetry at ambient temperature [(3)]. BNT ceramics and some BNT-based ceramics have been studied extensively [(4)-(8)].

Recently, piezoelectric films have attracted more and more attentions in microelectronic and micromechanical systems, especially in the development of micro-sensors and micro-actuators [(9)]. Kanda et al. reported that PZT films were successfully deposited on pure titanium substrates by the hydrothermal method [(10)]. In this dissertation, we introduced the hydrothermal method to deposit BNT films on pure titanium substrates. Compared with other methods such as sol-gel method, chemical vapor deposition (CVD), or the puttering method, the hydrothermal method has two outstanding advantages: [(11)] (1) films can grow on the complex shaped or tiny substrates, allowing new kinds of micro-sensors and micro-actuators; (2) the deposited films require no post treatment (annealing or poling).

The hydrothermal synthesis of BNT powder was reported by Jing et al. [(12)] and Pookmanee et al. [(13)]. However, little investigation on the development of BNT films has been done by the hydrothermal method. Moreover, there has been no report on the optimization of hydrothermal synthesis conditions of BNT films. In this work, the characteristics of BNT films were investigated with varying the concentrations of starting materials.

3.2. Experimental

3.2.1. Materials and Apparatus

In this study, a pure titanium substrate (40×20×0.05mm) was used. The biocompatibility of titanium is a factor of primary consideration. In addition, the titanium metal exhibits some excellent properties such as high strength, low density and high corrosion-resistance. Moreover, titanium substrate helps to form BNT nuclei on its surface. The starting materials for hydrothermal synthesis of BNT films are as follows:

Bi precursor: hydrated bismuth nitrate, $Bi(NO_3)_3 \cdot 5H_2O$, hereinafter referred to as $Bi(NO_3)_3$.

Ti precursor: titanium oxide, TiO_2.

Na precursor: sodium hydroxide, NaOH.

Mineralizer: NaOH.

Table 3.1 shows the hydrothermal synthesis conditions of starting materials. In this study, the concentration of NaOH was kept constant. The experimental equipment for hydrothermal synthesis of BNT films is shown in Figure 3.1, and it is equipped with a rotation device. During the hydrothermal synthesis process, the reaction vessel was rotated at the speed of 12 rpm to stir the reaction solution. Figure 3.2 shows the reaction vessel with a Teflon cup of 40ml.

Table 3.1 Conditions of starting materials and symbols of samples

16 ml solution of NaOH(10mol/l)		4ml solution of $Bi(NO_3)_3$ (mol/l)			
		1.0	1.2	1.4	1.6
8 ml solution of TiO_2 (mol/l)	0.3	A	E	I	M
	0.4	B	F	J	N
	0.5	C	G	K	O
	0.6	D	H	L	P

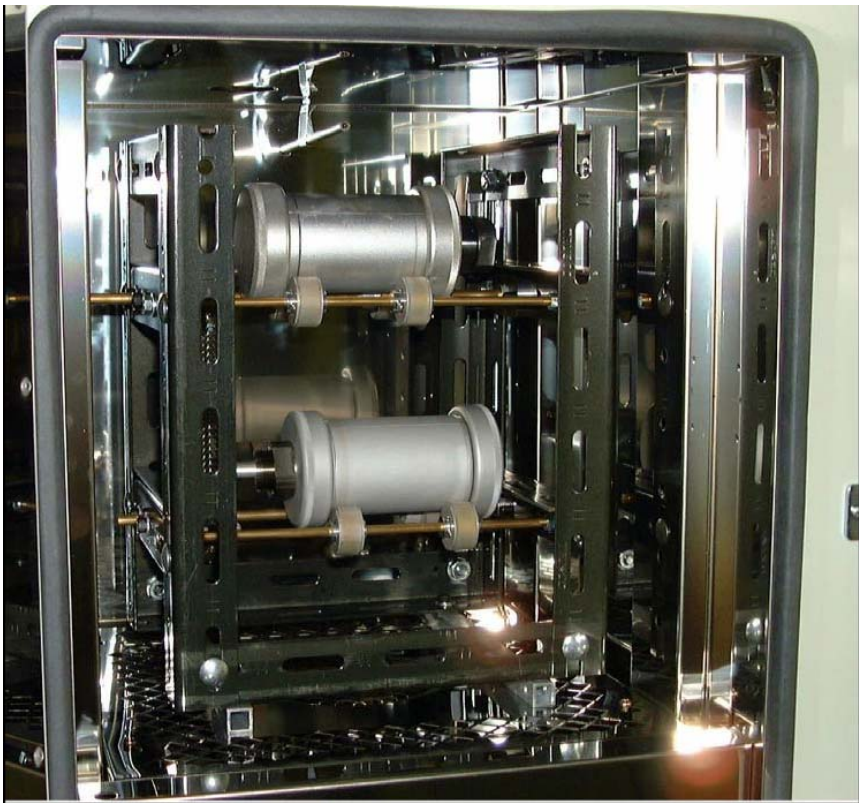

Figure 3.1 The experimental equipment for hydrothermal synthesis of BNT films

Figure 3.2 The reaction vessel for hydrothermal synthesis of BNT films

3.2.2. Hydrothermal Synthesis

The Hydrothermal method is the method of material synthesis or crystal growth in water under high temperature and pressure. Water exists as liquid under high pressure even if the temperature is above the boiling point of water at atmospheric condition. Reaction which is impossible under atmospheric pressure can occur under the above situation. It is said that various minerals are synthesized in the inside of the earth by the hydrothermal method.

Without considering the intermediate reaction steps, the total reaction, as showed in Equation (3.1), is desired to deposit BNT films on the surface of Ti substrates by the law of conservation of mass. The schematic illustration of the hydrothermal synthesis of BNT is shown in Figure 3.3.

$$2\mathrm{T}iO_2 + 4NaOH + Bi(NO_3)_3 \rightarrow 2Bi_{1/2}Na_{1/2}TiO_3 + 3NaNO_3 + 2H_2O \qquad (3.1)$$

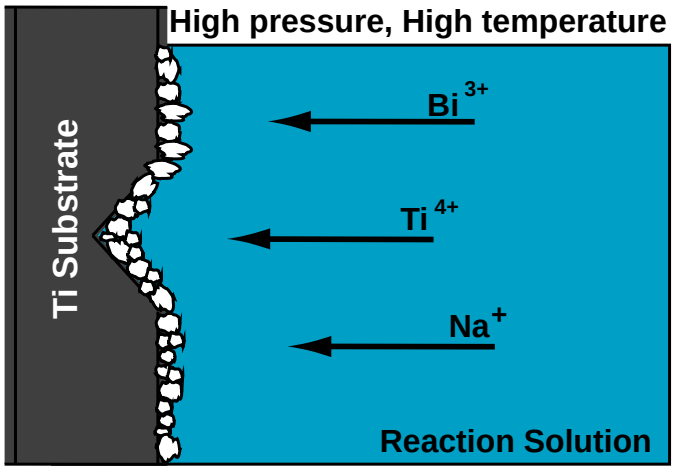

Figure 3.3 Schematic illustration of the hydrothermal synthesis of BNT

In this study, the hydrothermal method utilizes the chemical reaction at high temperature and pressure to grow BNT films on titanium substrates. Hence, the reaction vessel must be sealed to prevent the solution from evaporating. The reaction solution still exists as liquid in the process of hydrothermal synthesis. As shown in Figure 3.4, the

hydrothermal process of BNT films is a 2-step process: the first step is the nucleation process, and then the second step is the crystal growth process. After the nucleation process step, the reaction solution was renewed. BNT crystals were expected to grow in the second step. In this study, we repeated the second step once more to obtain a thicker film. After completion of each deposition, the sample was firstly cleaned in methanol using the ultrasonic cleaner, secondly rinsed by distilled water, and finally was dried using the blower.

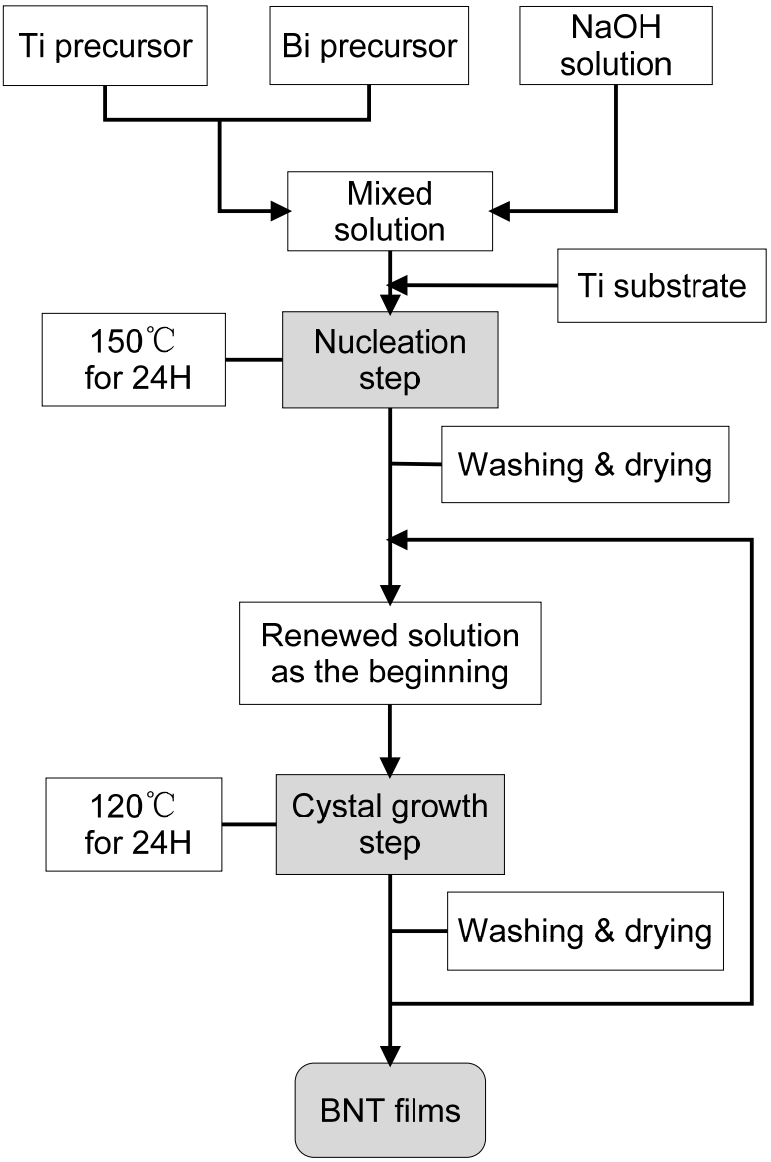

Figure 3.4 The process of the preparation of BNT films by the hydrothermal method

3.2.3. Characterization

3.2.3.1. SEM and EDX

A scanning electron microscopy (SEM) is an important tool to study the surface of thin films. The morphology and microstructures can be detected by using SEM. In this study, the grain shape and grain size of deposited BNT films were observed by SEM (Philips XL20) which is equipped with an energy dispersive X-ray spectrometer (EDX). The latter was used to make a quantitative analysis of element compositions of deposited BNT films. Before SEM observation, the sample with deposited BNT film was mounted on a special stage with a conductive tape, and then was sputtered with a thin layer of gold using a sputter coater (CRESSINGTON 108 AUTO).

3.2.3.2. XRD

X-ray diffraction (XRD) is one of the most popular and powerful technique to investigate the crystal structure of a material. In this study, crystal structures and crystallization levels of deposited BNT films were analyzed by XRD (JEOL JDX-3500) at the detection range (2θ) of 10-90º with a step of 0.05º. In an XRD pattern, amorphous materials don't have clearly defined peaks. BNT that has completed its structural change from the amorphous to the perovskite phase should only feature peaks associated with the established diffraction pattern for ideal BNT crystal. The Joint Committee for Powder Diffraction Studies (JCPDS) diffraction data defines the peaks associated with the rhombohedral structure of pure BNT, as well as their related relative intensities. BNT with the rhombohedral structure can be verified by JCPDS reference (file no. 36-0340).

3.2.3.3. Dielectric and Piezoelectric Properties

In order to evaluate the dielectric properties of deposited BNT films, punctiform conductive epoxies were laid on the film surface as electrodes. The areas of epoxy electrodes were measured using a laser microscope (VK-8510, Keyence). The dielectric loss and capacitance between the electrode and the titanium substrate (counter electrode) were measured at the frequency of 1 kHz using LCR Meter (Agilent 4284A). The piezoelectric constant d_{33} of the films was measured using a piezo-meter system (UK, Piezotest). The responses to applied DC and AC electric fields were measured on the unimorph cantilever type actuator.

3.3. Results and Discussion

3.3.1. Preparation of Starting Solution

It was noted that the order of mixing the precursors and the mineralizer for preparing the starting solution influenced greatly the quality of the prepared starting solution, thus affected the crystallization of deposited BNT films. The distinction between the different prepared starting solutions was visible to naked eye. The results are shown in Table 3.2. Mixing aqueous solutions of $Bi(NO_3)_3$ and TiO_2 and then adding NaOH aqueous solution led to no agglomerate, and then the starting solution close to a colloid was prepared. This is one of necessary conditions for hydrothermal synthesis of well crystallized BNT films. Figure 3.5 shows the XRD pattern of the specimen synthesized from the starting solution prepared in the order of (NaOH + $Bi(NO_3)_3$) + TiO_2 (TiO_2=0.5 mol/l, $Bi(NO_3)_3$=1.2 mol/l, NaOH=10 mol/l). Rather low BNT diffraction peaks observed indicate low crystallization of deposited BNT film.

Table 3.2 The order of mixing the precursors and the mineralizer for preparing the starting solution

Order of mixing	Prepared starting solution
(NaOH + $Bi(NO_3)_3$)+ TiO_2	Some agglomerates
(NaOH + TiO_2)+ $Bi(NO_3)_3$	Some agglomerates
($Bi(NO_3)_3$ + TiO_2)+ NaOH	No agglomerate

At the beginning of the hydrothermal synthesis, the titanium substrate reacted with the ions dissolved in the solution to form some nuclei on the substrate surface. This finally helps to increase the adhesion strength between deposited BNT film and the titanium substrate. The reaction of titanium substrate with the reaction solution was verified by the hydrothermal synthesis of BNT film without TiO_2 in the starting solution. Figure 3.6 shows the XRD pattern of the specimen synthesized under the condition without Ti precursor ($Bi(NO_3)_3$=1.2 mol/l, NaOH=10 mol/l). BNT diffraction peaks were found in this XRD pattern, and thus the generation of BNT crystal was confirmed. But the BNT diffraction peaks are very low. This indicates that the reaction of titanium substrate with the reaction solution occurred only in the nucleation stage, and the Ti precursor is necessary as a starting material for the crystal growth of BNT.

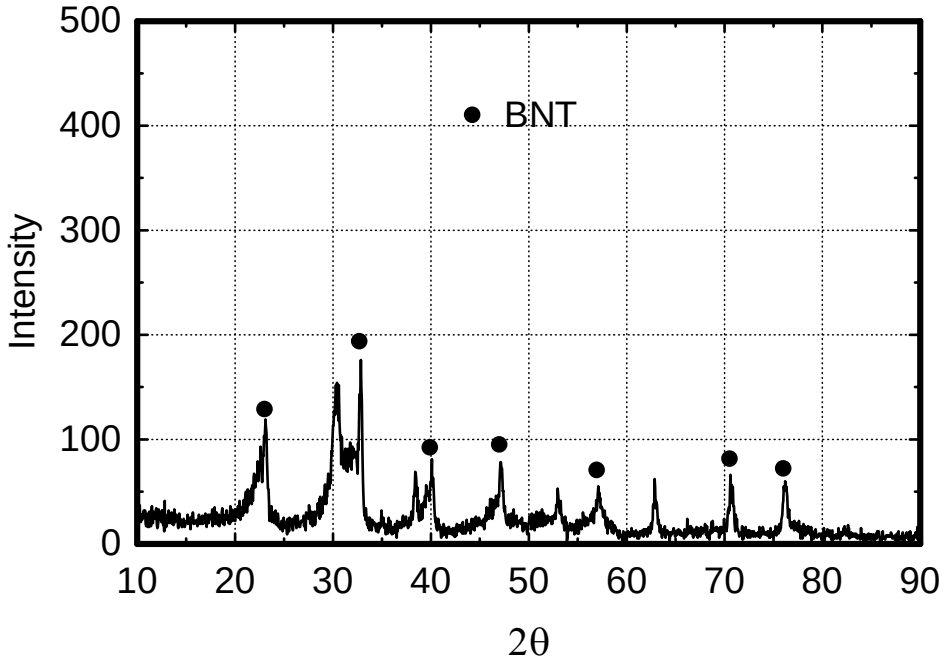

Figure 3.5 XRD pattern of the specimen synthesized from the prepared starting solution: (NaOH + $Bi(NO_3)_3$) + TiO_2(TiO_2=0.5 mol/l, $Bi(NO_3)_3$=1.2 mol/l, NaOH=10 mol/l)

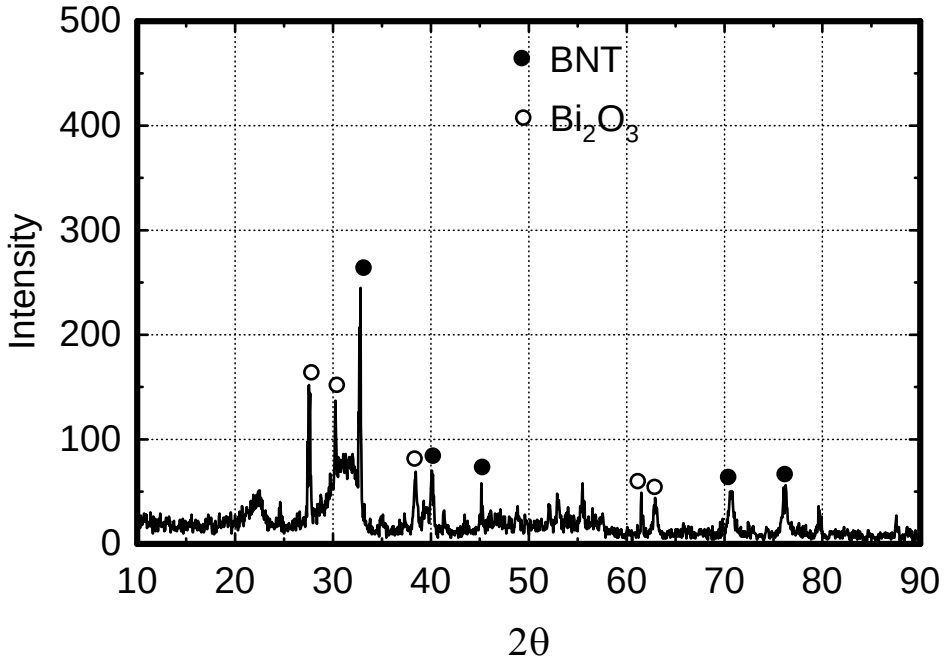

Figure 3.6 XRD pattern of the specimen synthesized under the condition without Ti precursor ($Bi(NO_3)_3$=1.2 mol/l, NaOH=10 mol/l)

3.3.2. Observation of Synthesis Process

To study the evolution of the hydrothermal deposition of BNT films on titanium substrates, the procedure of deposition was stopped at various appointed time after the beginning of the synthesis of BNT films, and then SEM observations were performed on the substrate surface. Figure 3.7 shows that some crystal nuclei were found on the substrate surface after 15 minutes of deposition, and BNT crystals were generated all over the substrate surface after one hour of deposition. However, the film thickness was less than 1 μm after one hour of deposition. The film thickness reached about 5 μm after 24 hours of deposition.

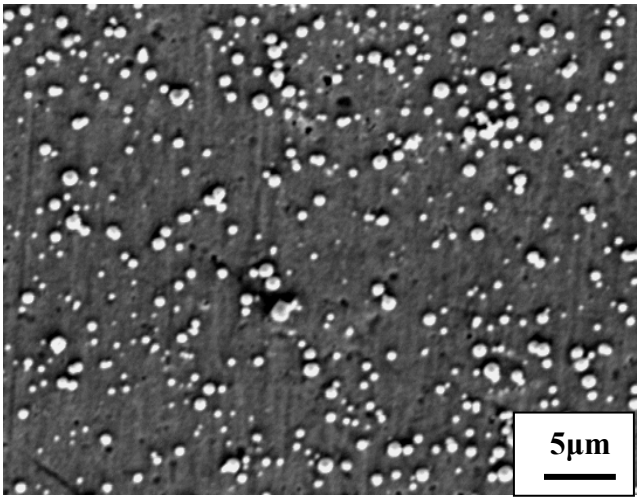

15 mins

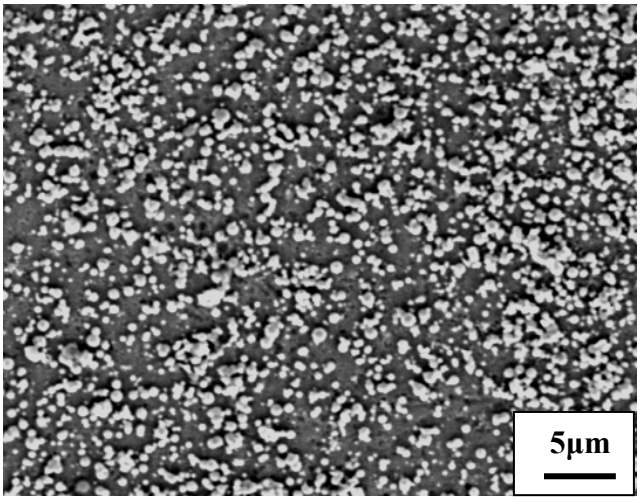

30 mins

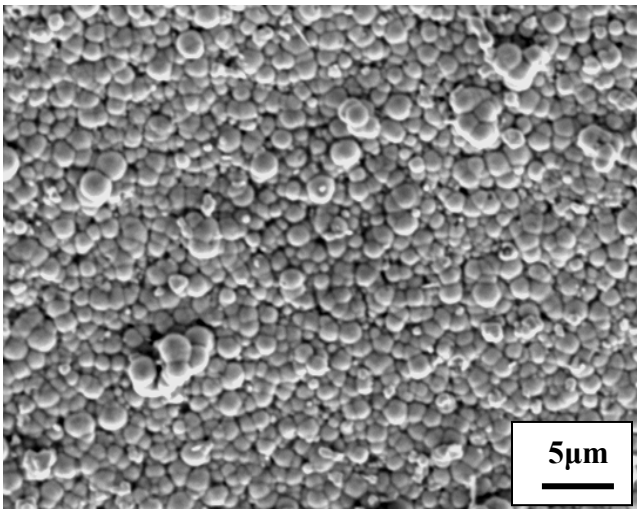

1 hr

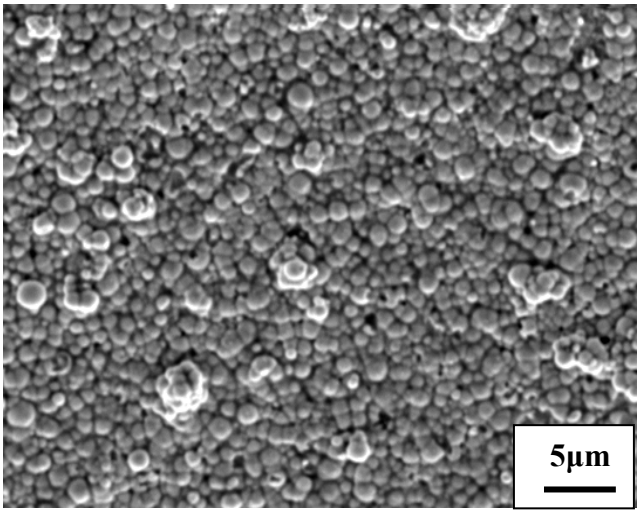

2 hr

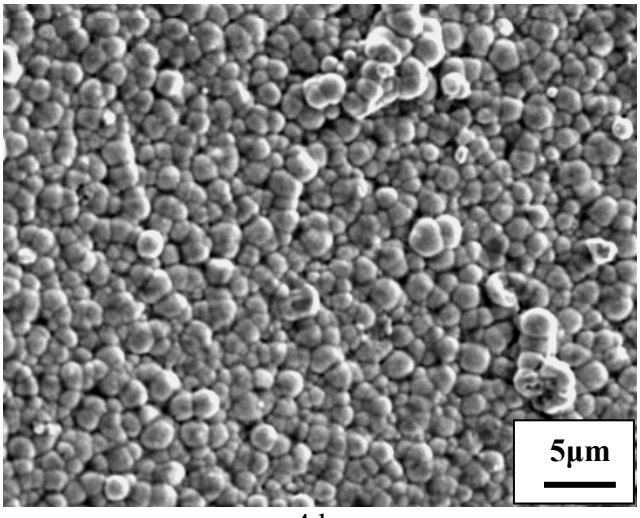

4 hr

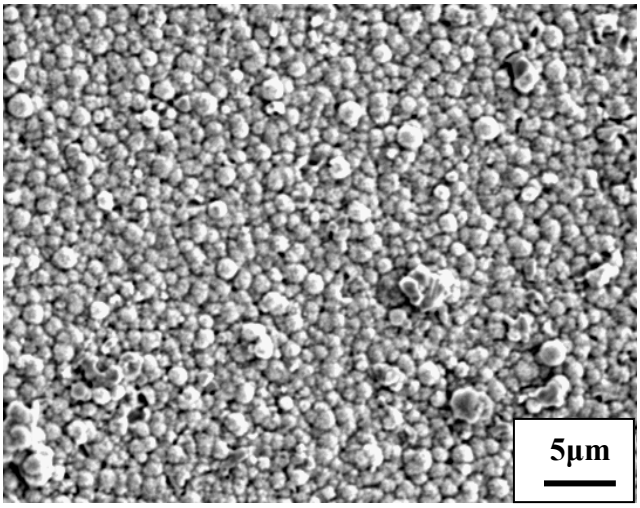

8 hr

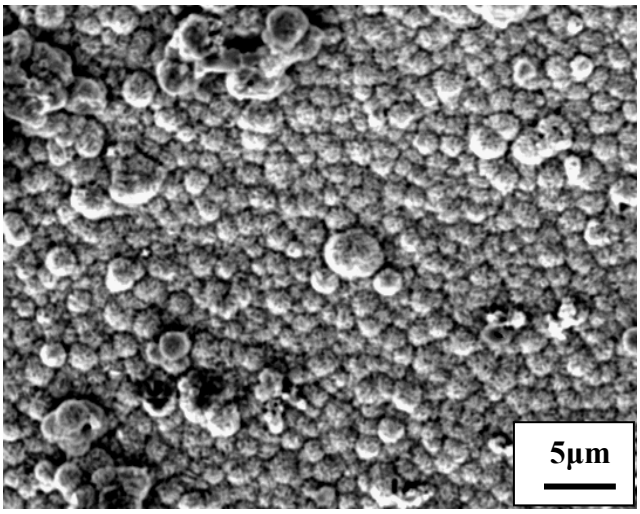

16 hr

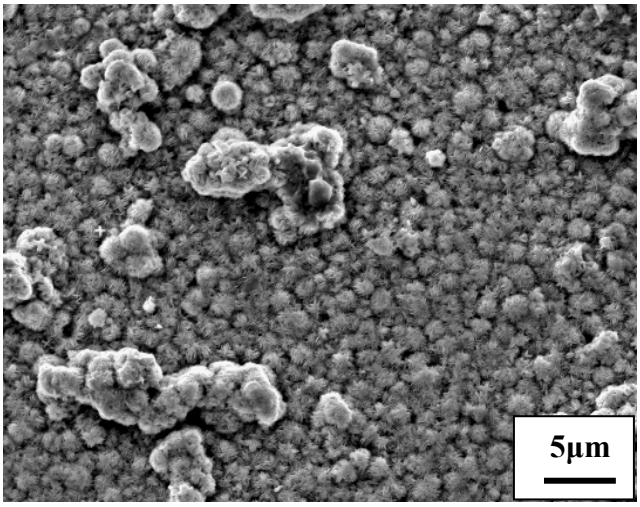

24 hr

Figure 3.7 SEM observations of substrate surface in the process of BNT crystallization

3.3.3. Film Thickness and Deposition Speed

The thicknesses of deposited films after the 1st, 2nd and 3rd deposition were measured respectively by a micrometer, and shown in Figures 3.8, 3.9 and 3.10, respectively. Not a big difference was found in the film thickness between all the samples after the 1st deposition. However, a great difference was found in Figures 3.9 and 3.10. It was found that the film tended to be thick in the case of high $Bi(NO_3)_3$ concentration after the 2nd or 3rd deposition. For the case of after the 3rd deposition, this tendency was clearly observed in Figure 3.11, which shows the variation of the film thickness with the $Bi(NO_3)_3$ concentration. In general, the film thickness increased with increasing the $Bi(NO_3)_3$ concentration, and then stayed almost the same as the $Bi(NO_3)_3$ concentration was more than 1.4mol/l.

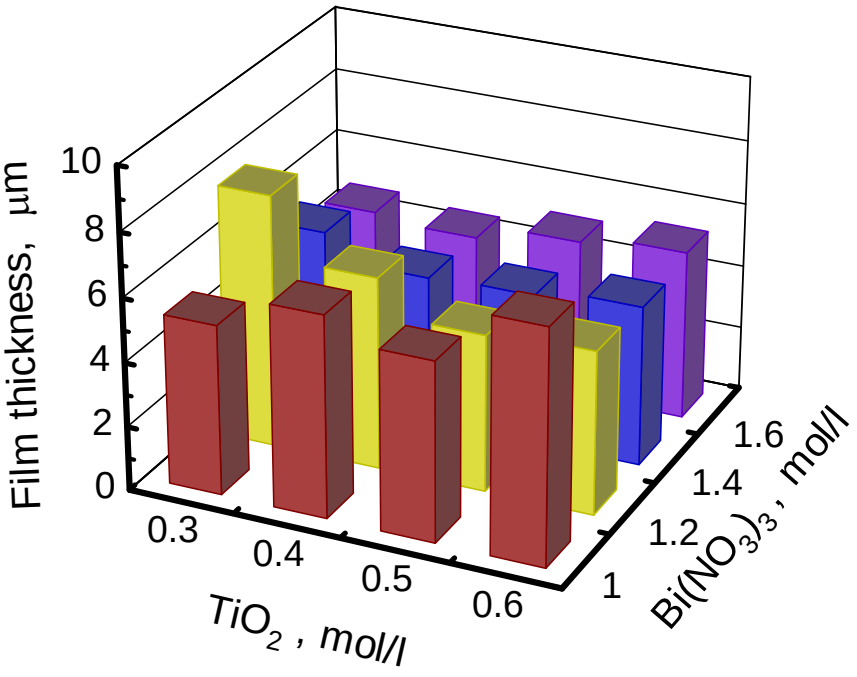

Figure 3.8 The film thickness after the 1st deposition

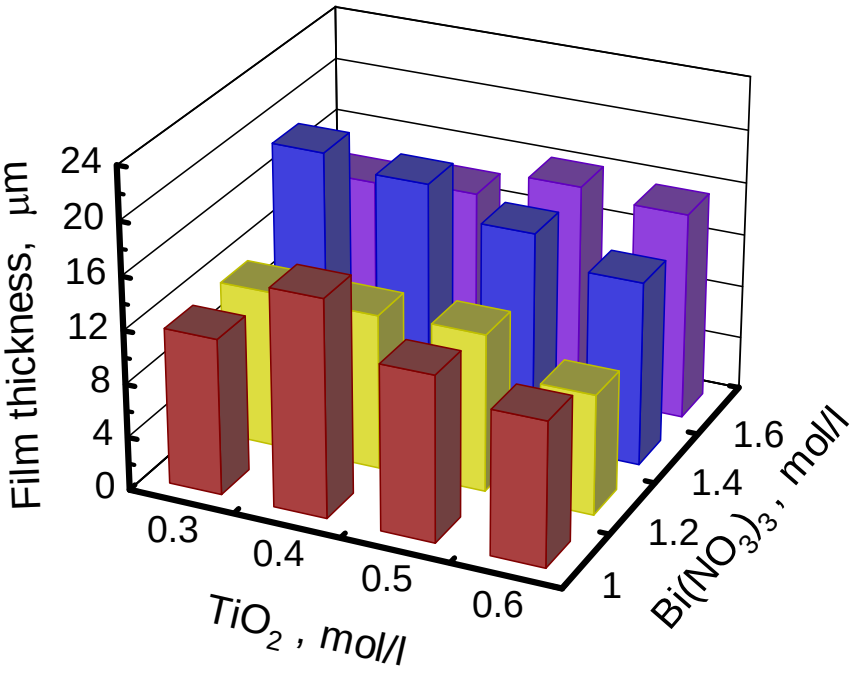

Figure 3.9 The film thickness after the 2nd deposition

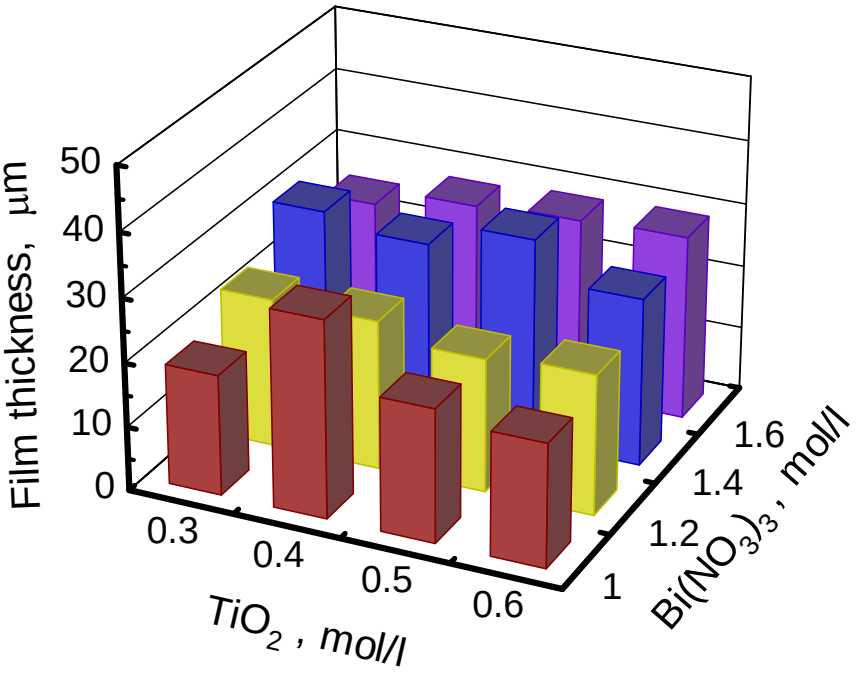

Figure 3.10 The film thickness after the 3rd deposition

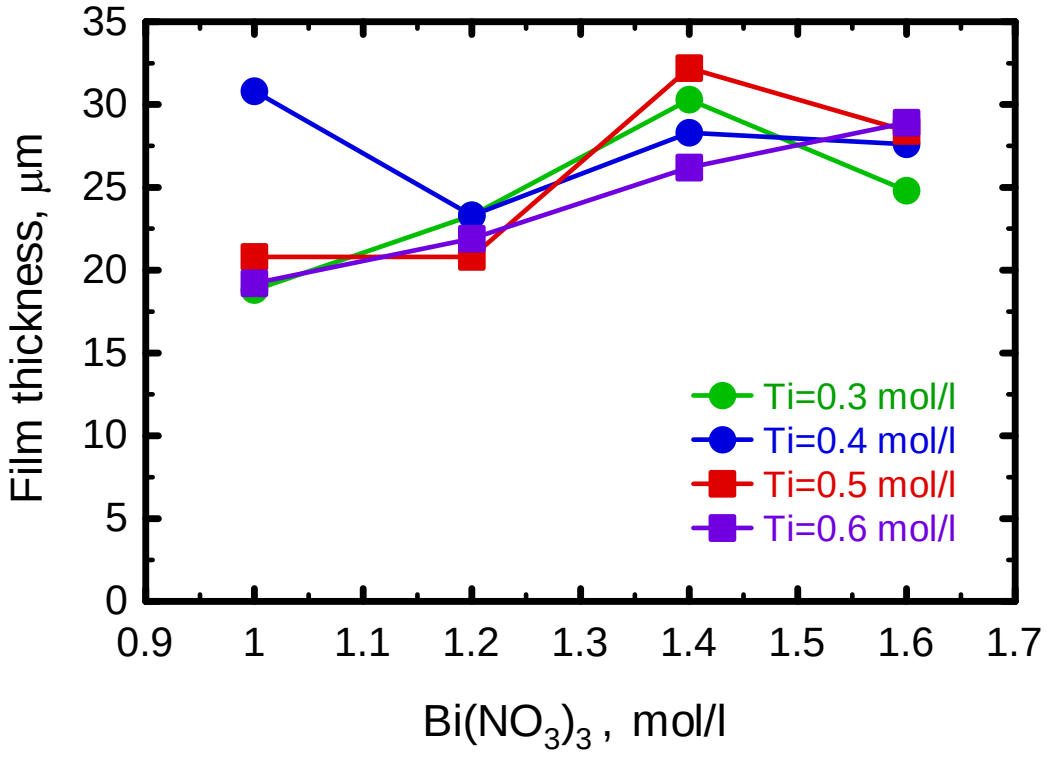

Figure 3.11 Variation of the film thickness with the $Bi(NO_3)_3$ concentration

Figure 3.12 shows the increase of the deposited film thickness for each deposition for all the samples. Only a small difference was found in the film thickness for the 1st deposition between these samples. However, the film thickness increases greatly in the 2nd and 3rd depositions. Figure 3.13 shows that the average deposition speeds for the 1st, 2nd and 3rd deposition were about 0.25, 0.35 and 0.45 μm/hr, respectively. For the 1st deposition, the deposition speed was relatively stable for all the synthesis conditions. However, for the 2nd and 3rd depositions, the deposition speed changed greatly with the synthesis condition. The maximum deposition speed reached 0.6 μm/hr for the 3rd deposition.

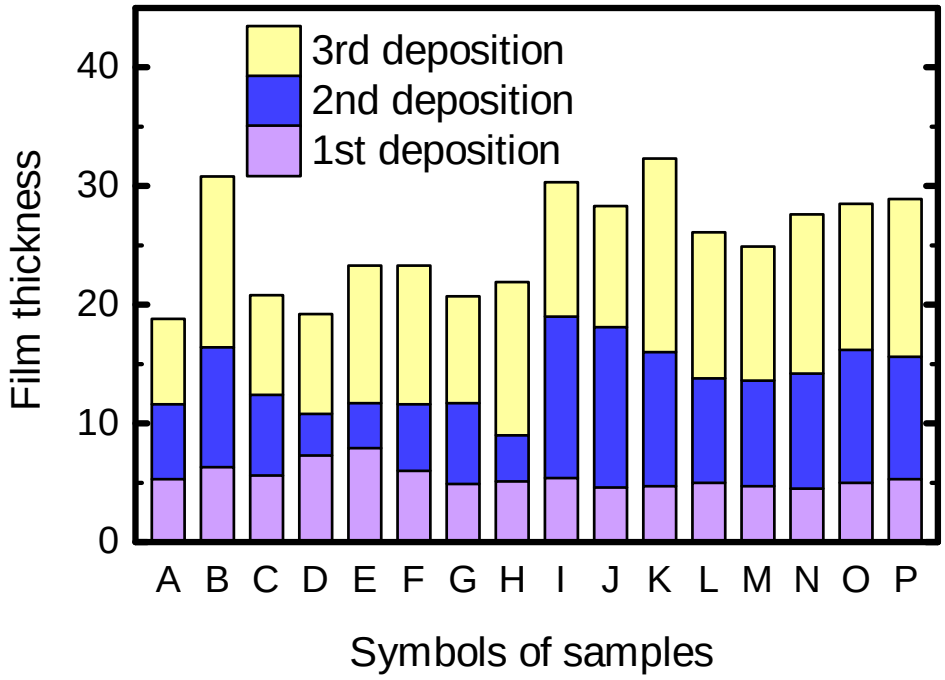

Figure 3.12 The increase of the deposited film thickness for each deposition

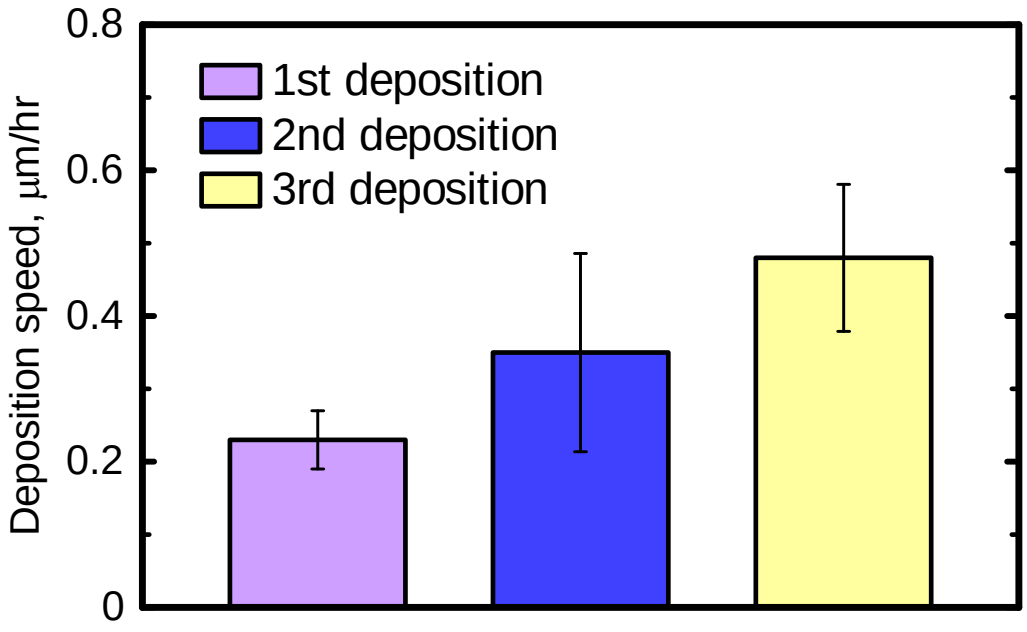

Figure 3.13 Deposition speed for each deposition

3.3.4. Morphology and Microstructure

SEM observations were performed on all the samples after the 1st, 2nd and 3rd deposition, respectively. As examples of observed samples, Figures 3.14, 3.15 and 3.16 show SEM images for sample G, K, O. Relatively homogenous granular BNT crystals (approximately 2 μm grain size) were observed after the 1st deposition. Some tetrahedral crystals were obviously found after the 2nd deposition, and the amount of this tetrahedral crystal increased greatly after the 3rd deposition, subsequently, the tetrahedral crystals were dispersed all over the film surface. This tetrahedral crystal was identified as Bi_2O_3 crystal by XRD analysis in Section 3.3.5. The great increase of the film thickness after the 2nd deposition may be primarily attributed to the generation of Bi_2O_3 crystal. The Bi_2O_3 impurity was more generated in the case of high $Bi(NO_3)_3$ concentrations. However it has no contribution to the piezoelectric property of deposited films, and thus the removal of Bi_2O_3 was desired. The Bi_2O_3 impurity can be removed by the immersion into concentrated nitric acid. The SEM images of sample G, K and O after the immersion are shown in Figures 3.14(d), 3.15(d) and 3.16(d), respectively. The thickness of etched BNT film was about 7 μm on each side regardless of the synthesis condition. The other properties of etched BNT films such as crystal structure, element composition, permittivity, piezoelectric constant etc. will be further investigated in our future research. In the present work, we focus on the characterization of as-deposited BNT films.

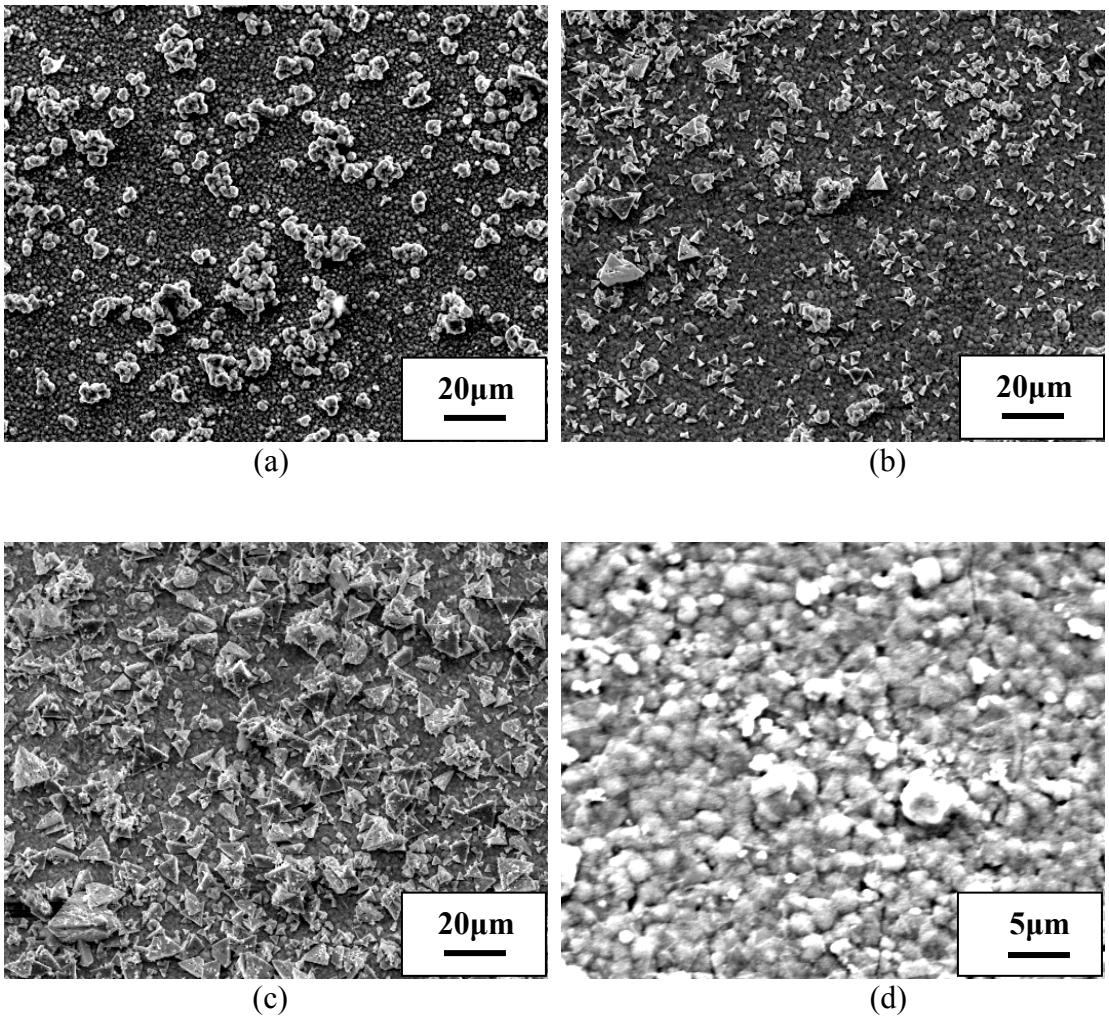

(a) (b)

(c) (d)

Figure 3.14 SEM images of BNT films (Sample G):
(a) after the 1st deposition; (b) after the 2nd deposition; (c) after the 3rd deposition;
(d) etched BNT film after the treatment of concentrated nitric acid

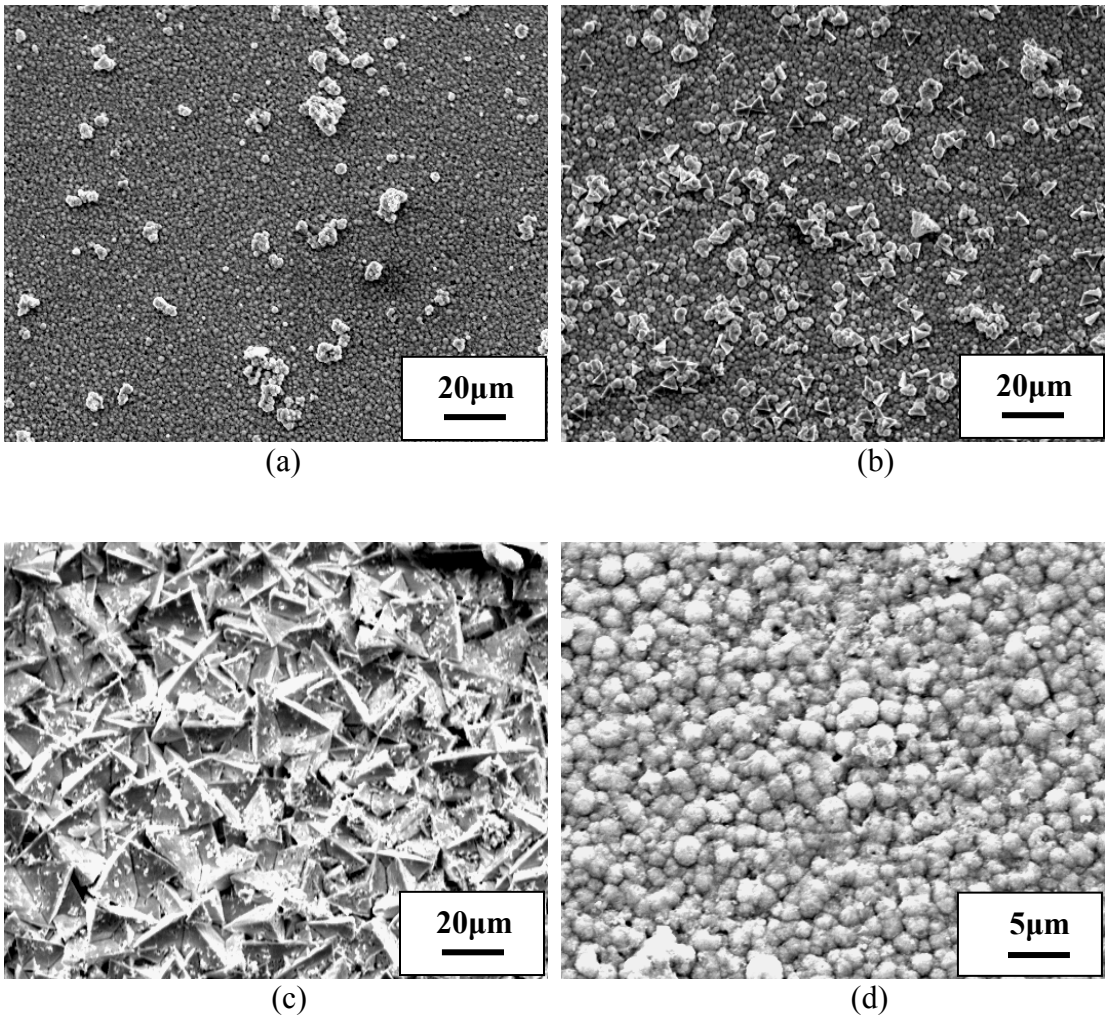

(a) (b)

(c) (d)

Figure 3.15 SEM images of BNT films (Sample K):
(a) after the 1st deposition; (b) after the 2nd deposition; (c) after the 3rd deposition;
(d) etched BNT film after the treatment of concentrated nitric acid

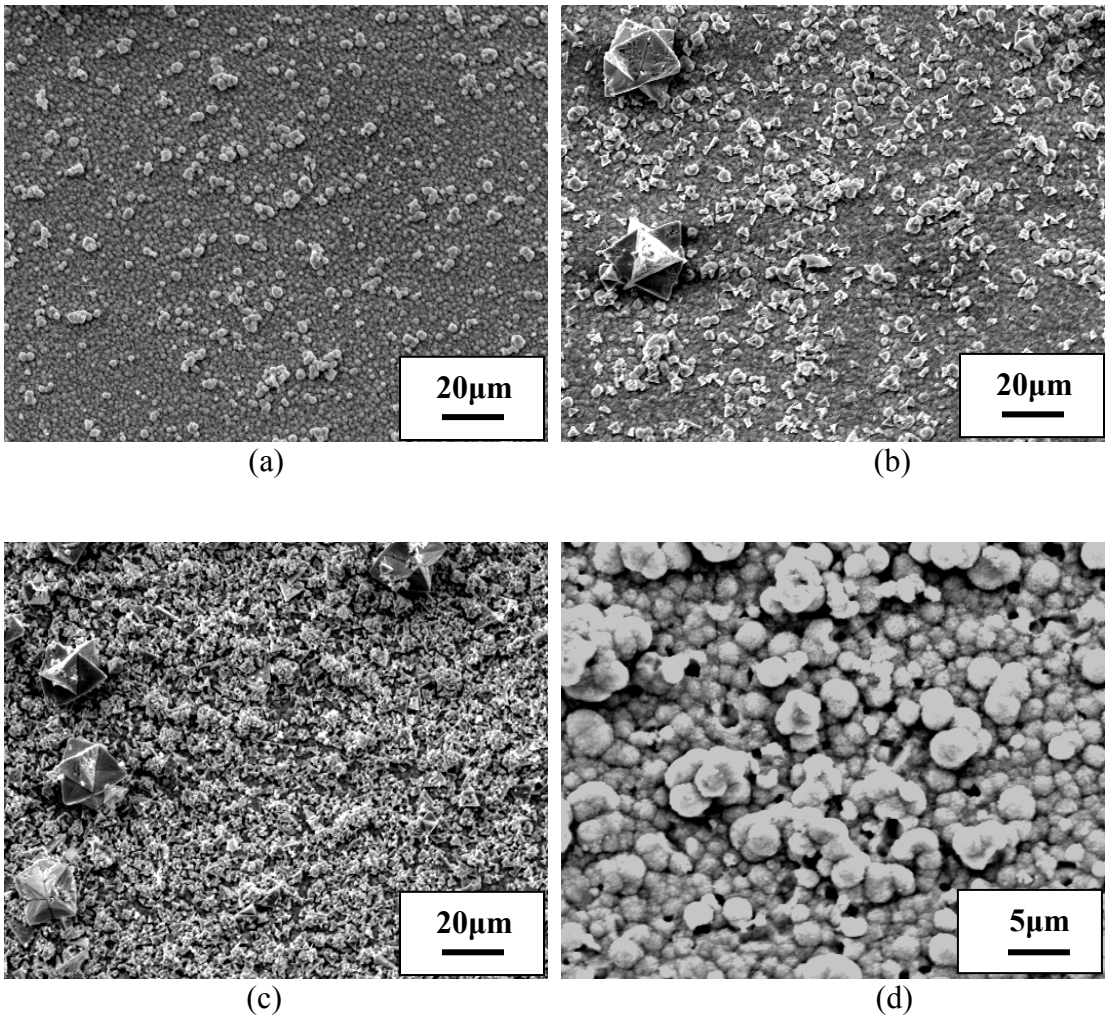

(a) (b)

(c) (d)

Figure 3.16 SEM images of BNT films (Sample O):

(a) after the 1st deposition; (b) after the 2nd deposition; (c) after the 3rd deposition;

(d) etched BNT film after the treatment of concentrated nitric acid

3.3.5. EDX and XRD Analysis

Deposited BNT films were quantitatively analyzed by EDX for all the samples, and their element compositions were shown in Figure 3.17. It can be seen that the element composition ratio (Bi/Na/Ti/O) of deposited BNT films is different from the stoichiometric ratio of BNT (10/10/20/60). This is thought to result from the generation of Bi_2O_3. The content of Bi_2O_3 will be calculated from the result of element compositions in Section 3.3.6. EDX analysis was also performed on sample G, K and O after the 1st, 2nd, 3rd deposition and etching treatment of concentrated nitric acid, respectively, and their results were shown in Figure 3.18. It can be found that the element composition ratio (Bi/Na/Ti/O) is relatively close to the stoichiometric ratio of BNT (10/10/20/60) for sample G, K and O after the 1st deposition.

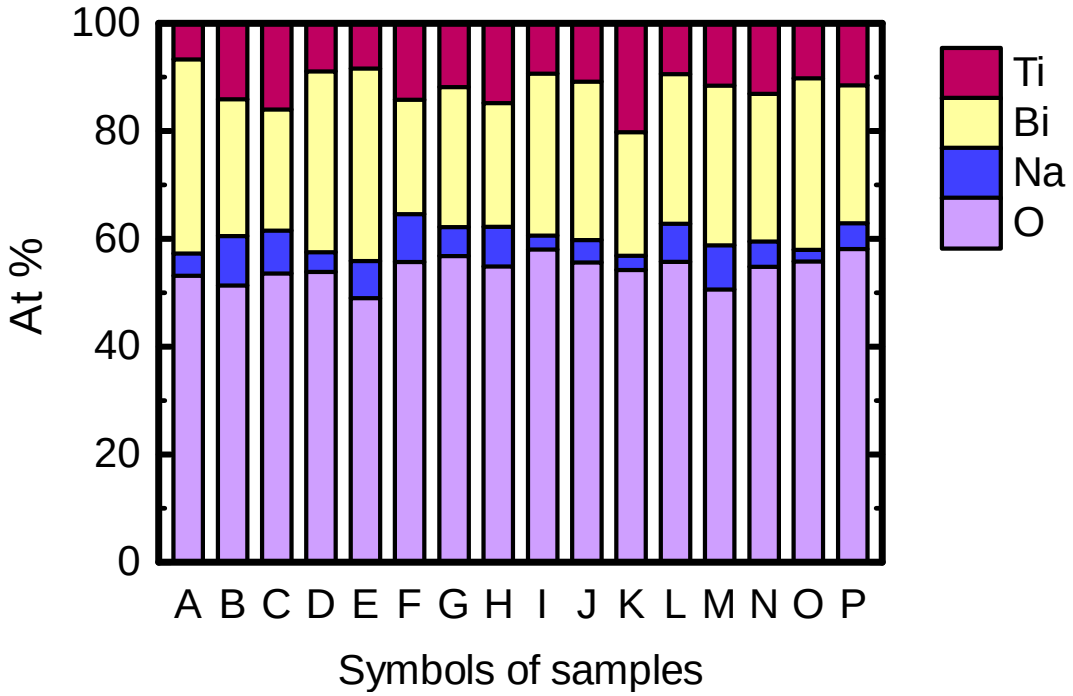

Figure 3.17 Quantitative analysis of element compositions of deposited films by EDX

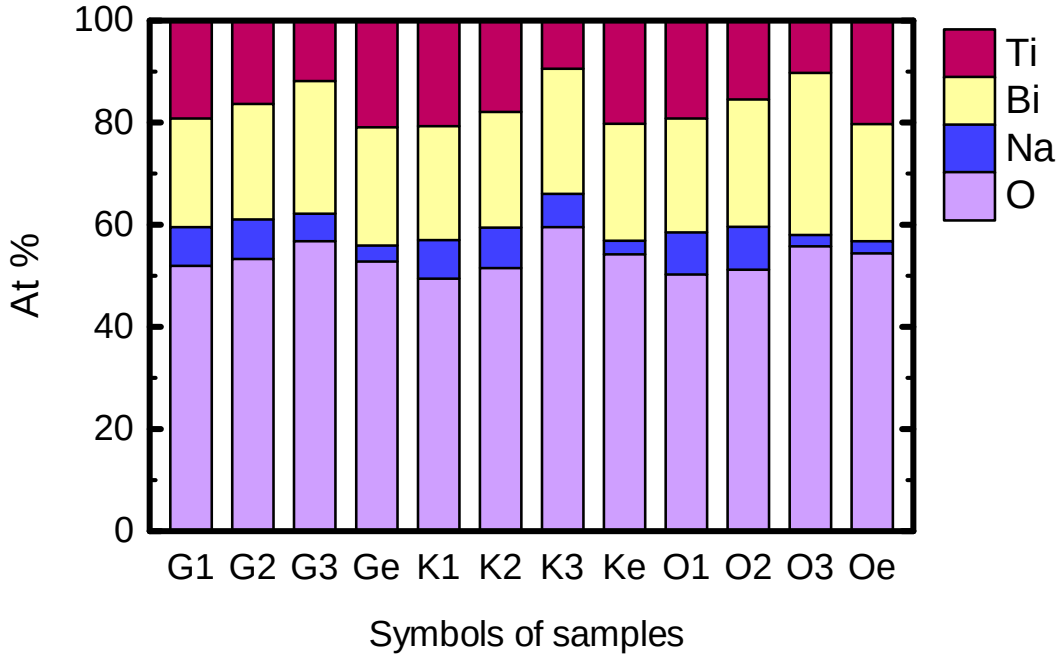

Note: (1) Gi, Ki and Oi indicate sample G, K and O after the 1st, 2nd or 3rd deposition, i=1, 2, 3;
(2) Ge, Ke and Oe indicate sample G, K and O after the etching treatment of concentrated nitric acid

Figure 3.18 Quantitative analysis of element compositions of sample G, K and O by EDX

All the samples were measured using XRD. The generations of BNT and Bi_2O_3 crystals were confirmed for each sample. As examples of measured XRD patterns, those of sample G, K and O ($Bi(NO_3)_3$ concentrations of the starting solution were 1.2, 1.4 and 1.6 mol/l respectively) are shown in Figure 3.19. The results show that sample G and K were nearly the same and more intense than sample O in the BNT diffraction peaks. Each diffraction peak of sample O was comparatively low, indicating that the crystallization level of sample O was not so high as that of sample G and K.

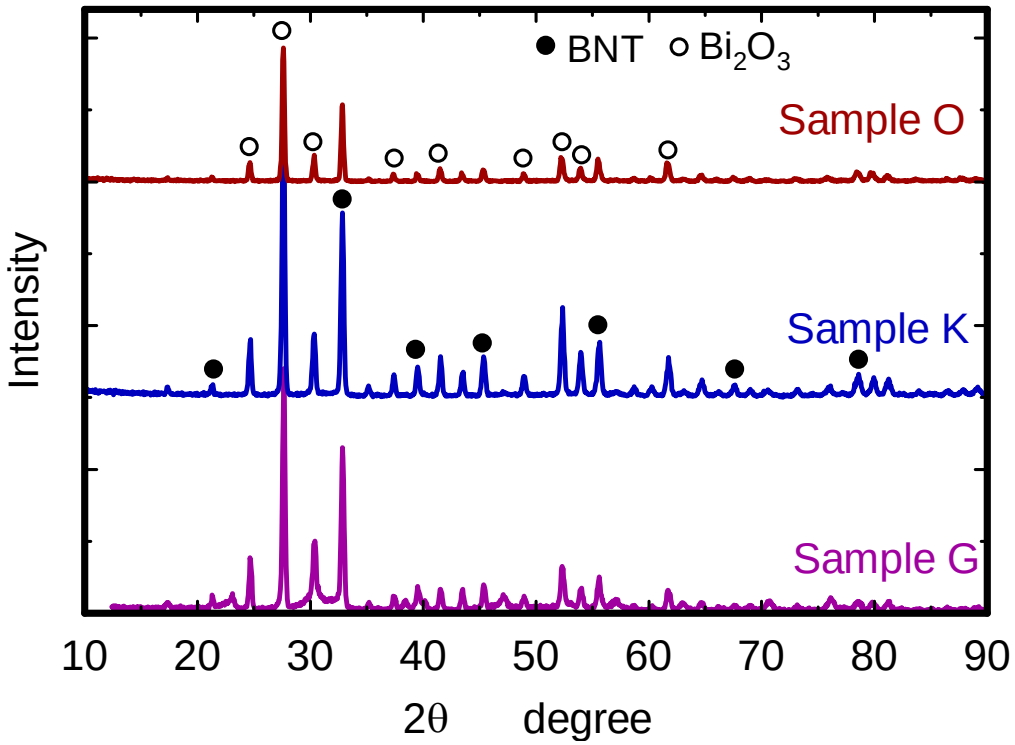

Figure 3.19 XRD patterns of sample G, K and O

3.3.6. Optimization of Synthesis Condition

It is evident that the homogeneity of deposited BNT films plays a vital role in determining their piezoelectric properties. However, the Bi_2O_3 impurity was found in deposited films from the results of XRD analysis and SEM observation. Without considering the other impurities of small quantity, we can assume deposited BNT films as a system of $(1-x)(Bi_{1/2}Na_{1/2})TiO_3$-$xBi_2O_3$. In other words, the element composition ratio (Bi/Na/Ti/O) of deposited BNT films is assumed to be (1+3x):(1-x):(2-2x):6. The value of x can be determined by the measured ratio of Bi/Na, Bi/Ti, Bi/O or etc. Since the change of the concentrations of Bi and Ti precursor is thought to directly affect the Bi/Ti ratio of deposited BNT films, the measured Bi/Ti ratio was used to calculate the values of x and 1-x, which indicate the contents of Bi_2O_3 and BNT. The composition ratios of BNT and Bi_2O_3 were shown in Figure 3.20 for all the samples. Figure 3.21 shows the composition ratio of BNT for sample G, K and O after the 1st, 2nd, 3rd deposition and etching treatment of concentrated nitric acid, respectively. The composition ratio of BNT decreased in the sequence of the 1st, 2nd and 3rd deposition. After etching treatment, it stayed almost the same, close to that of the sample after the 1st deposition.

The optimized synthesis condition was determined on the evaluation target of the calculated BNT content. Figures 3.22 and 3.23 show the correlation between the BNT content of deposited films and the $Bi(NO_3)_3$ and TiO_2 concentrations of starting solutions, respectively. In these two figures, fitting curves obtained by the least square method show that the BNT content reaches a maximum at the $Bi(NO_3)_3$ and TiO_2 concentrations of 1.2 and 0.5 mol/l, respectively. This indicates that the synthesis condition of G is optimum in our current research.

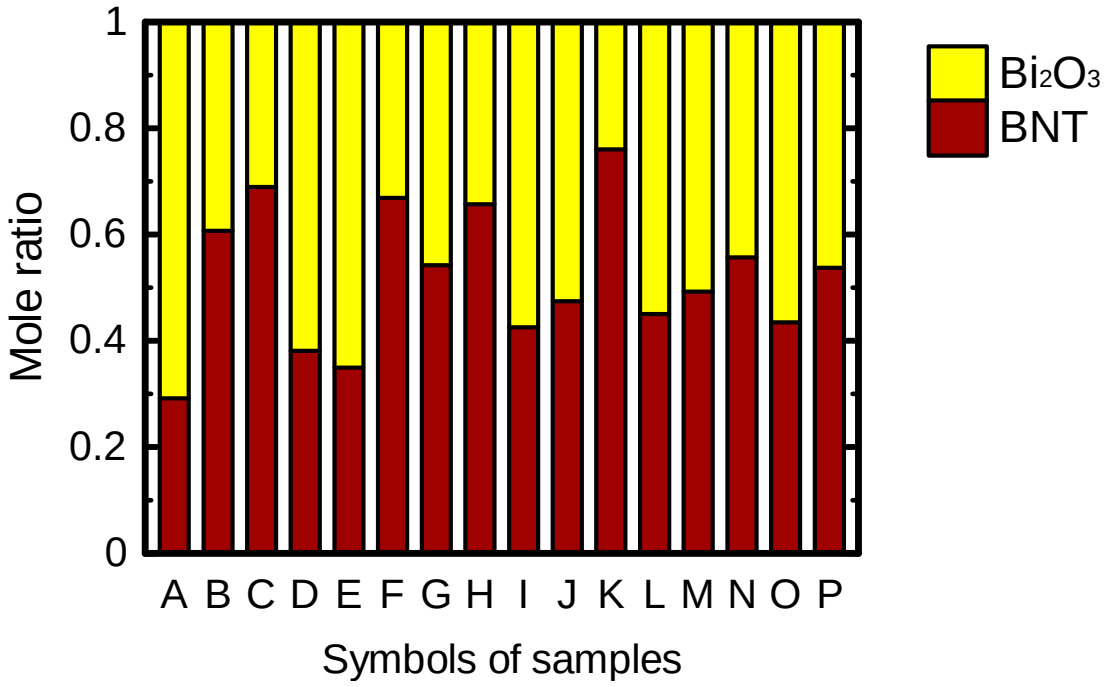

Figure 3.20 The composition ratio of calculated BNT and Bi_2O_3 content

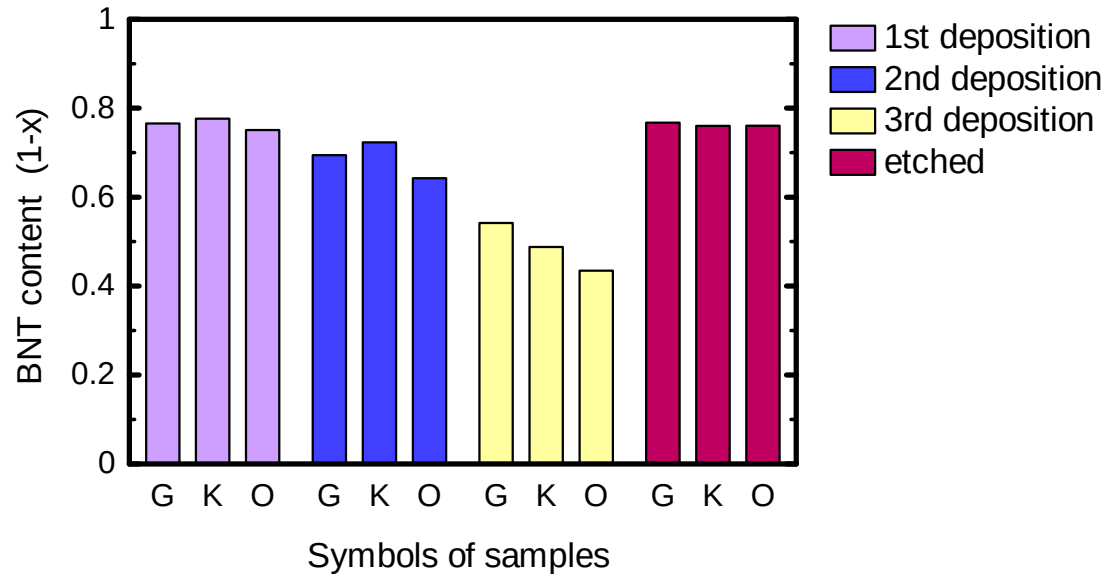

Figure 3.21 The composition ratio of calculated BNT content for sample G, K and O after the 1st, 2nd, 3rd deposition and etching treatment

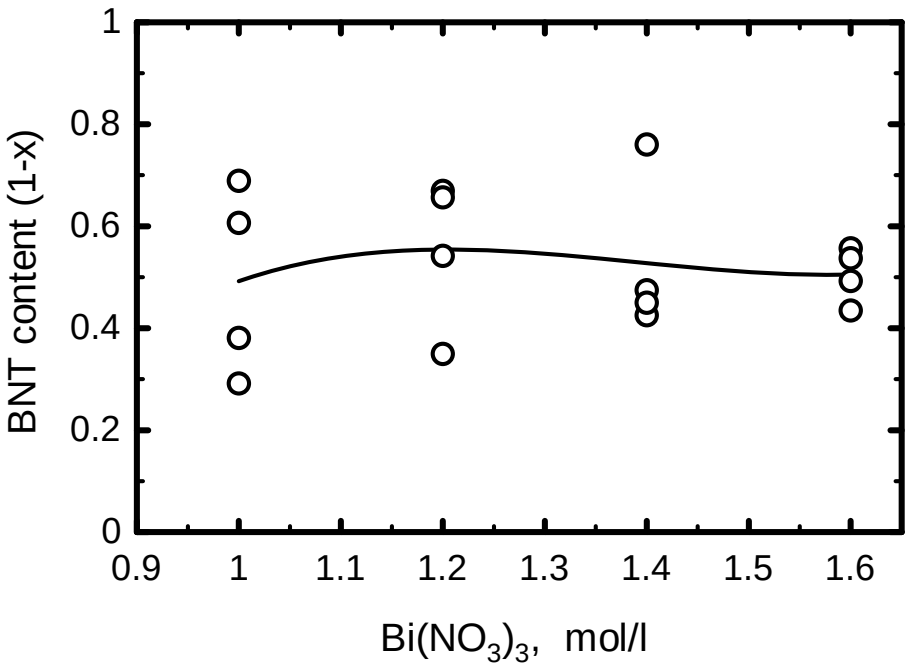

Figure 3.22 Correlation between the BNT content and the $Bi(NO_3)_3$ concentration

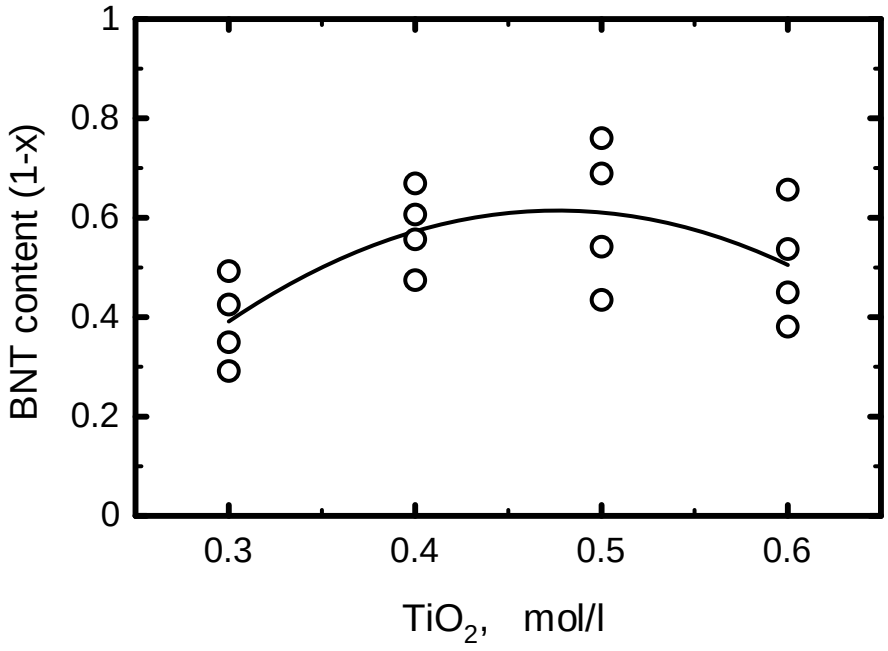

Figure 3.23 Correlation between the BNT content and the TiO_2 concentration

3.3.7. Permittivity and Dielectric Loss

The relative permittivity, ε_r, is a measurement describing the ability of a material to store charge. It was calculated from the following equation:

$$\varepsilon_r = \frac{C_p \cdot t}{A \cdot \varepsilon_0} \qquad (3.2)$$

where C_p is the capacitance(F), t is the film thickness(m), A is the top electrode area(m^2) , and ε_0 =8.85×10^{-12} F/m, which is the vacuum dielectric constant. Figure 3.24 shows the schematic illustration for measuring dielectric properties of deposited BNT films. Figure 3.25 shows the relative permittivity of deposited BNT films after the 3rd deposition. It shows that the relative permittivity was much larger in the case of the $Bi(NO_3)_3$ concentration of 1.6 mol/l, compared with the case of 1.4 mol/l. However, a small difference in the film thickness has been found between these two cases of 1.4 and 1.6 mol/l. The decrease in crystallization may be a factor to increase the relative permittivity of deposited films.

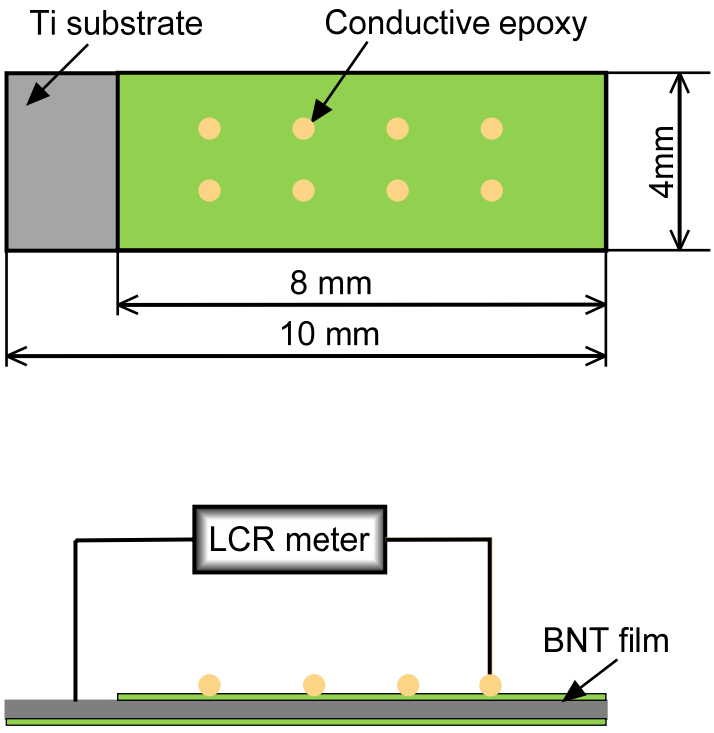

Figure 3.24 Schematic illustration for measuring dielectric properties of deposited BNT films

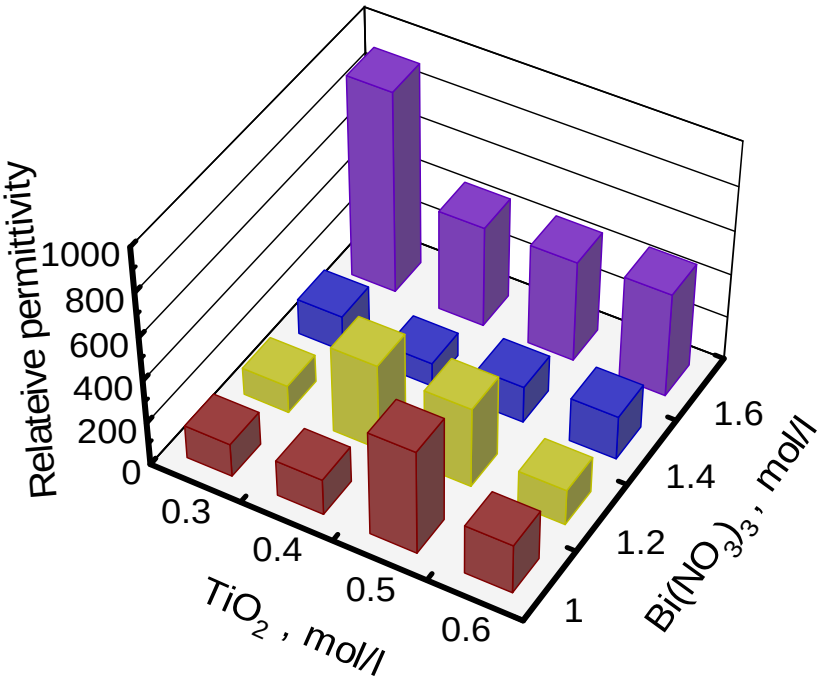

Figure 3.25 Relative permittivity of deposited BNT films after the 3rd deposition

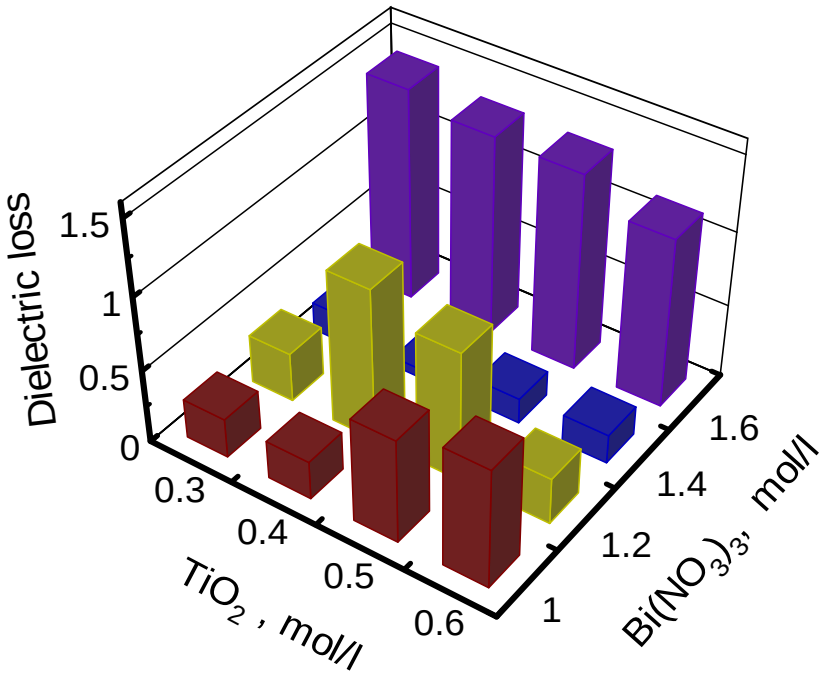

Figure 3.26 Dielectric loss of deposited BNT films after the 3rd deposition

As shown in Figure 3.26, the dielectric loss of deposited BNT films after the 3rd deposition varied with the synthesis conditions, and its change is similar to the result of relative permittivity (Figure 3.25). A correlation between the relative permittivity and dielectric loss was investigated and shown in Figure 3.27. The dielectric loss was positive correlated with the relative permittivity.

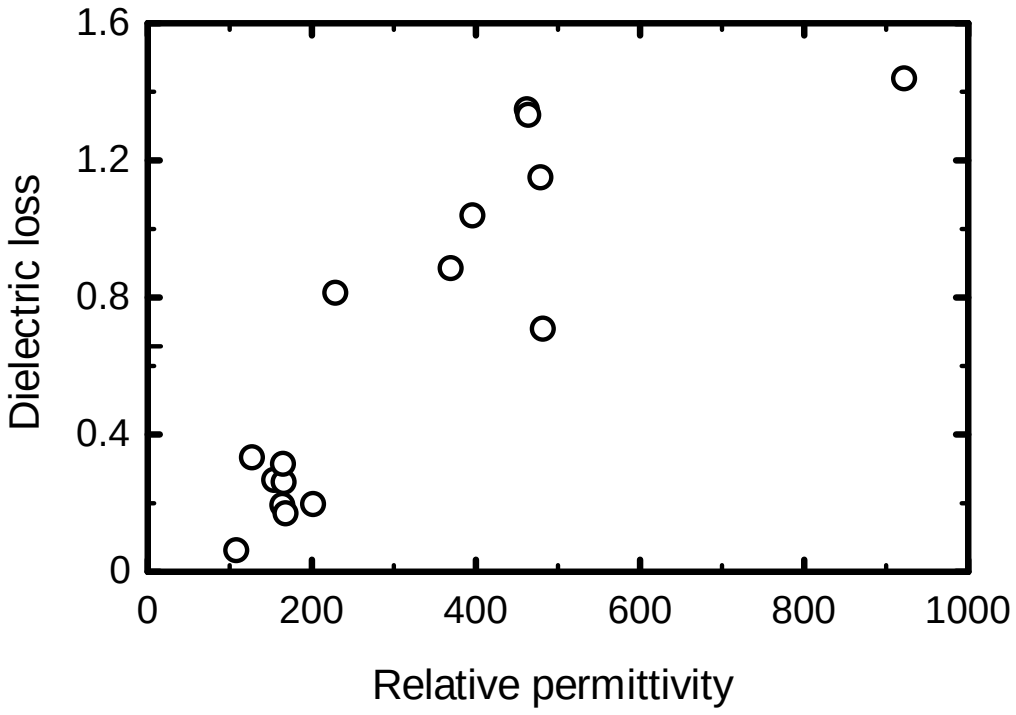

Figure 3.27 Correlation between the dielectric loss and relative permittivity

3.3.8. Piezoelectric Performance

3.3.8.1. The Piezoelectric Constant

The piezoelectric constant d_{33} was measured on the specimen, as shown in Figure 3.28. Gold was sputtered on one side of the specimen. The deposited BNT film on the other side was removed using an emery paper. Figure 3.29 shows the piezoelectric constant d_{33} of deposited BNT films after the 3rd deposition. It indicates that the piezoelectric constant may tend to be large in the case of low concentration of $Bi(NO_3)_3$. In contrast to the results of XRD patterns, the results of piezoelectric constant indicate that the BNT crystallization level can affect the piezoelectric constant of film, and high crystallization of BNT leads to large piezoelectric constant. For example, sample G and K were almost the same and larger than sample O in the piezoelectric constant. This is in agreement with their BNT crystallization levels. In addition, the correlation between the relative permittivity and piezoelectric constant of deposited films can not be found by comparing Figure 3.25 with Figure 3.29.

It is evident that the piezoelectric property of deposited BNT films is dependent on their BNT contents. Figure 3.30 shows the correlation between the piezoelectric constant and the BNT content. An obvious correlation was not found when the BNT content is less than 0.6, however the piezoelectric constant was positive correlated with the BNT content when the BNT content is more than 0.6.

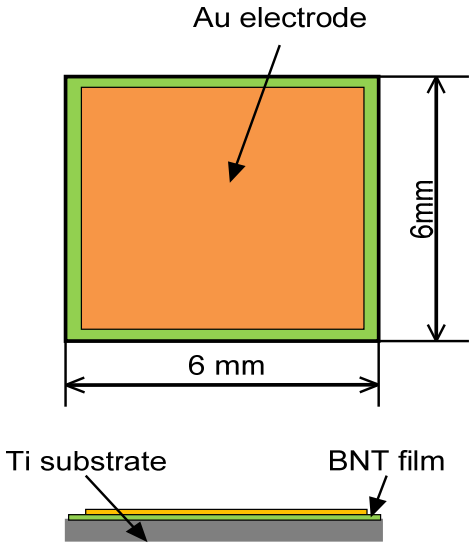

Figure 3.28 The specimen for measuring the piezoelectric constant d_{33} of deposited BNT film

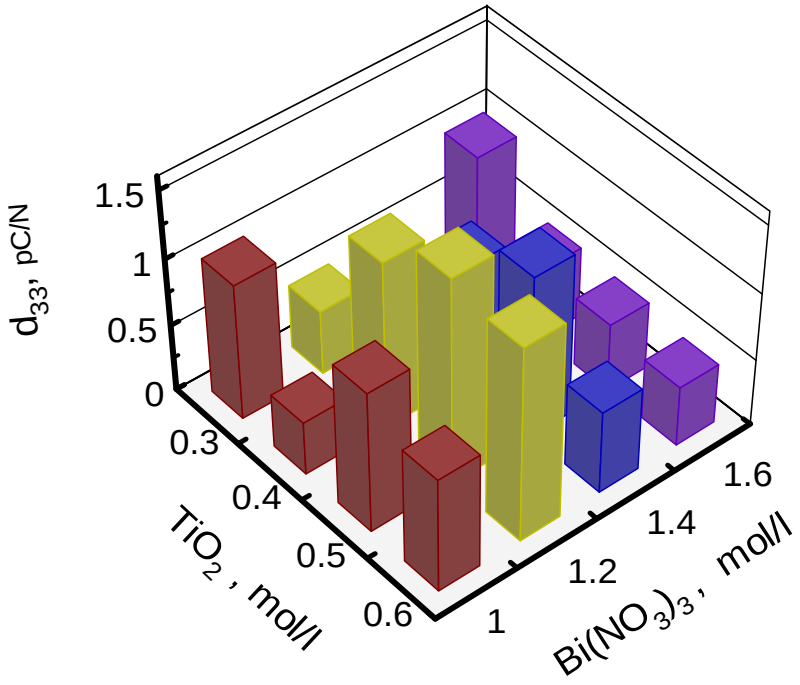

Figure 3.29 Piezoelectric constant of deposited BNT films after the 3rd deposition

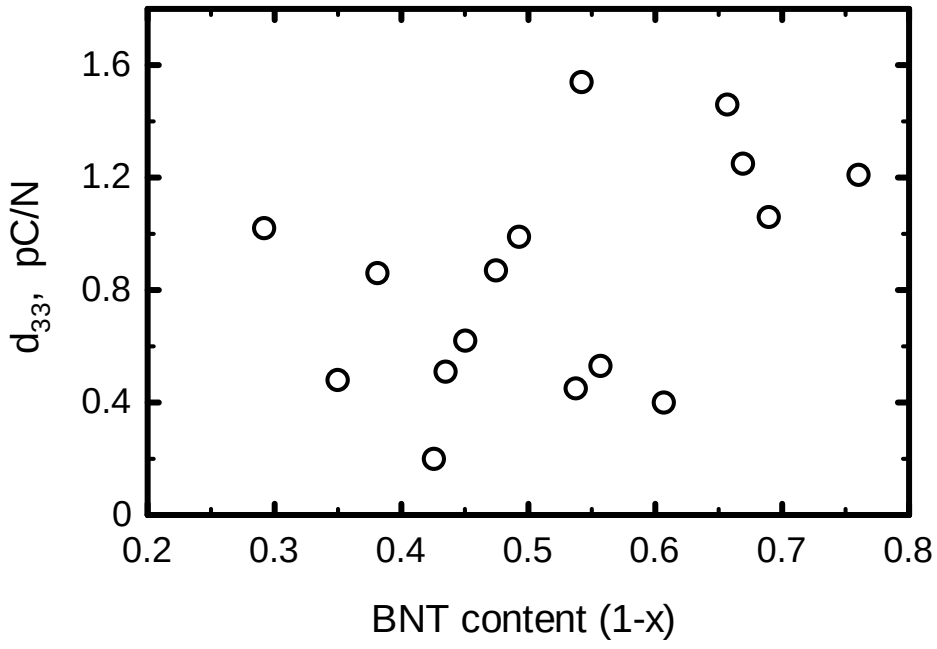

Figure 3.30 Correlation between the piezoelectric constant and the BNT content

3.3.8.2. The Converse Piezoelectric Effect under DC Field

The converse piezoelectric effect of deposited BNT films was examined by the actuation testing. Figure 3.31 shows the unimorph cantilever type actuator used in the testing. Gold was sputtered on the film surface as an electrode, and the titanium substrate was used as the other electrode. The measurement system is shown in Figure 3.32. A thin copper wire was bonded to the gold electrode with conductive epoxy. A DC field was applied on the actuator through the power amplifier, which was used to change the electric field strength. Then we measured the deflection of the tip of its free end by a laser displacement meter (Keyence, LC-2400). A data logger was used to collect the data of the tip deflection and the electric field strength.

As examples, the unimorph cantilever type actuators made from sample G, K and O were discussed here. Figure 3.33 shows the relation of the driving DC field and the tip deflection of unimorph cantilever type actuators for sample G, K and O. It can be seen that the relatively large deflections were obtained for sample G and K in the case of the positive DC field. It was reported by Fujiwara et al. that the deflection was almost linear to the driving electric field for PZT actuator [(14)], which was also synthesized by the hydrothermal method with the same shape and dimension. However, an obvious hysteresis was observed in Figure 3.33 and the deflection was hardly obtained in the negative electric field. On the other hand, it can be also seen that the deflection for sample O was not almost generated in the positive or negative electric field. This was considered the result of the insufficiency of BNT crystallization on the sample O. The above results are considered to be in good accordance with the results of crystallization level and piezoelectric constant for sample G, K and O.

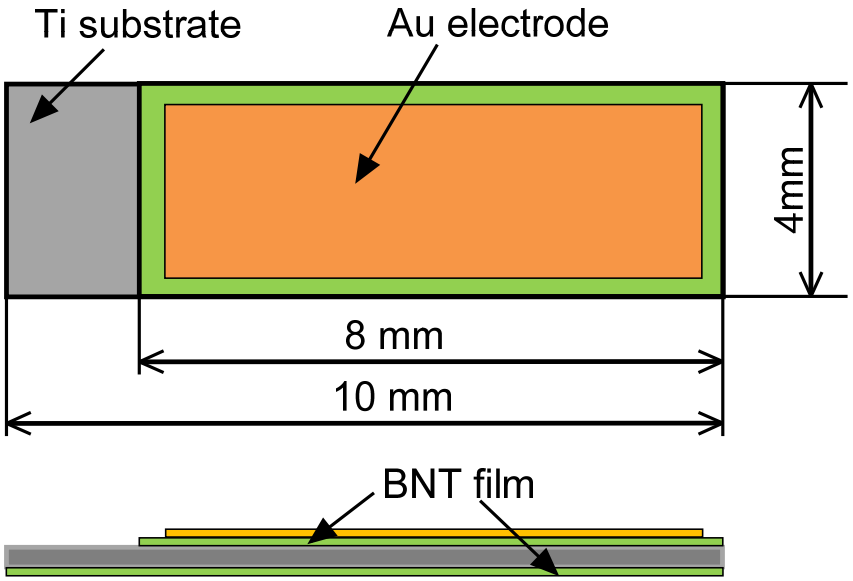

Figure 3.31 Dimensions of unimorph cantilever type actuator

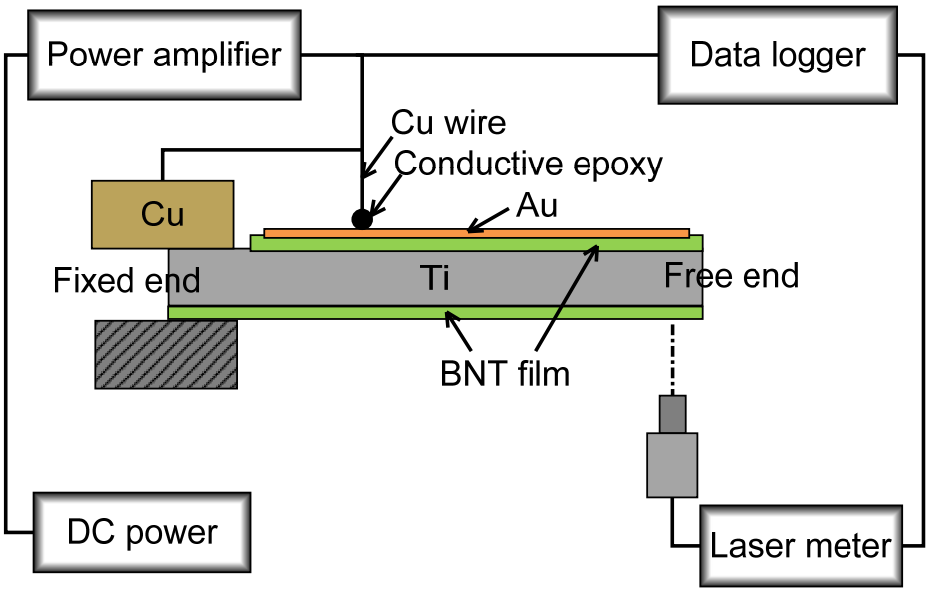

Figure 3.32 Measurement system of the unimorph cantilever type actuator under DC field

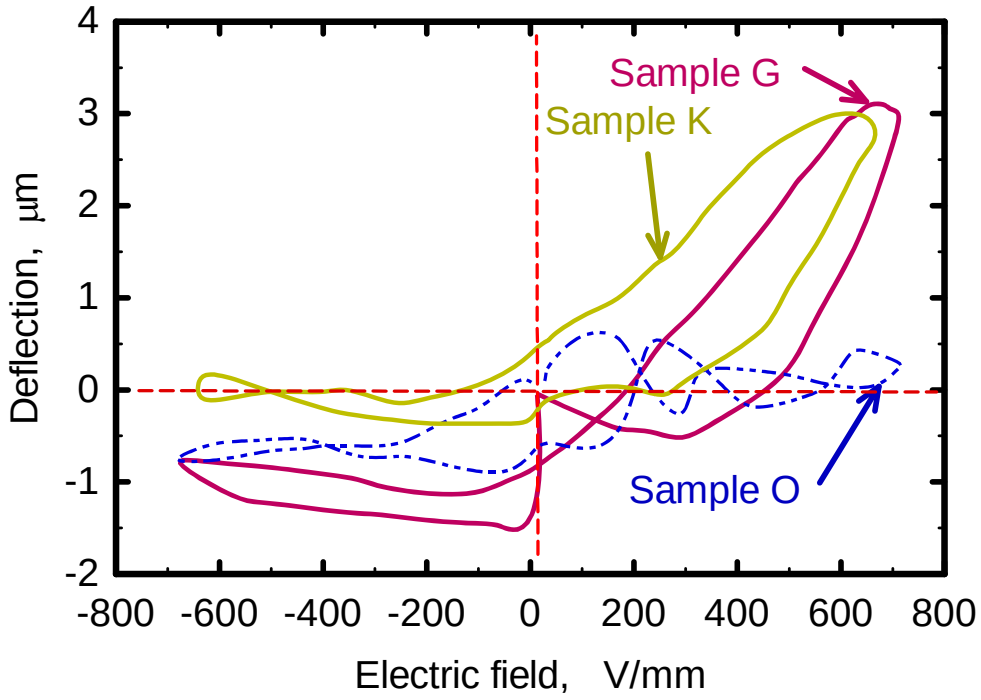

Figure 3.33 Deflection of the unimorph cantilever type actuator under DC field

3.3.8.3. The Converse Piezoelectric Effect under AC Field

The converse piezoelectric effect of deposited BNT films under AC field was measured on the unimorph cantilever type actuator, the same as described in Section 3.3.8.2. Figure 3.34 shows the measurement system. A sinusoidal AC voltage was applied on the unimorph cantilever type actuator through the function generator, and then we monitored the vibration of the tip of its free end on the oscilloscope by using a laser vibrometer (Melectro, V100). The resonance amplitude was obtained by adjusting the input frequency using the function generator. As examples, the unimorph cantilever type actuators made from sample, K and O were discussed here. Figure 3.35 shows the variation of resonance amplitude with applied peak-to-peak voltage $V_{p\text{-}p}$ for sample G, K and O. It can be seen that the resonance amplitude was almost linear to the applied voltage for each sample, and the relatively large resonance amplitudes were obtained for sample G and K. This is considered to be in good accordance with their results of crystallization level and piezoelectric constant.

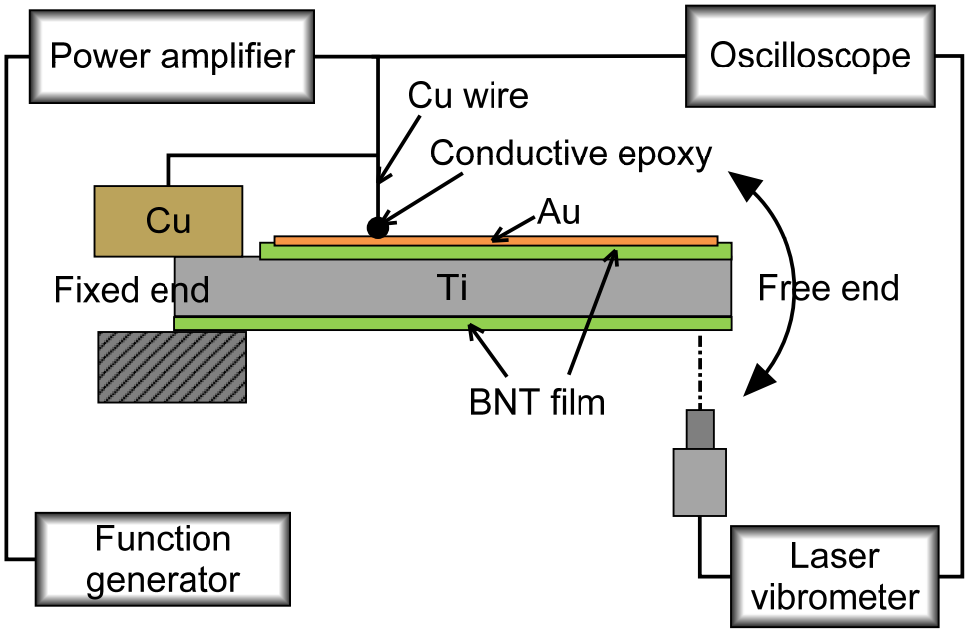

Figure 3.34 Measurement system of the unimorph cantilever type actuator under AC field

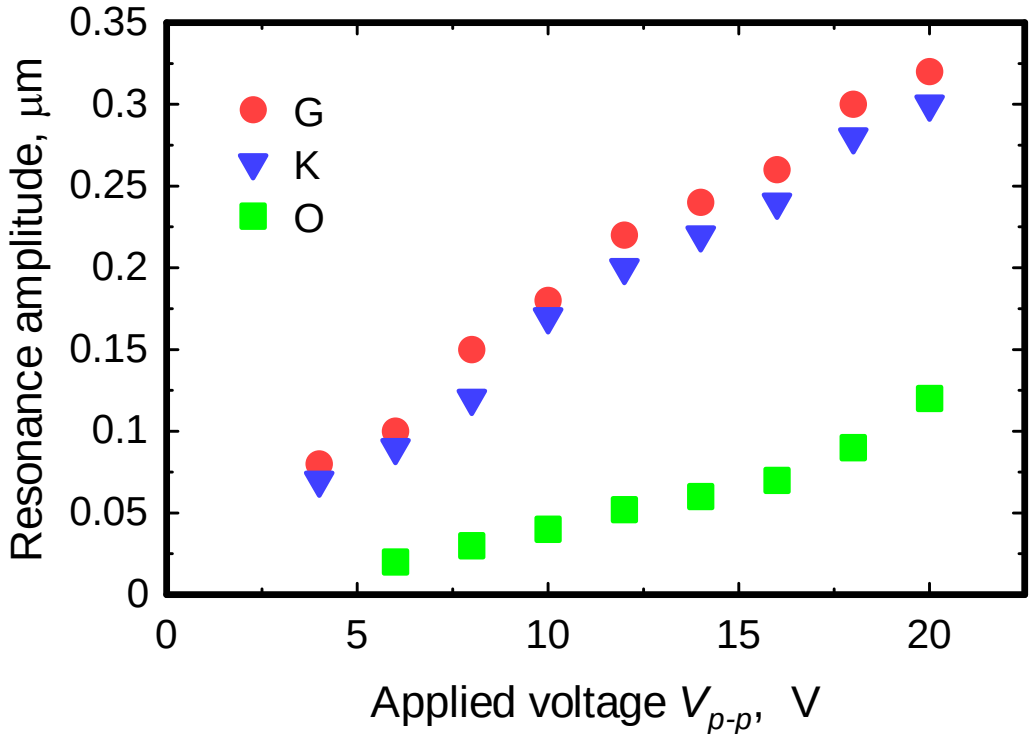

Figure 3.35 Variation of resonance amplitude with applied AC voltage $V_{p\text{-}p}$

3.4. Conclusions

BNT films were successfully synthesized on pure titanium substrates by the hydrothermal method with varying the $Bi(NO_3)_3$ and TiO_2 concentrations of the starting materials. The main conclusions obtained from this chapter are summarized as follows.

(1) The generation of BNT crystal with the rhombohedral crystal structure was confirmed in the deposited films by XRD analysis. Bi_2O_3 impurity was also found, and its amount increased with increasing the $Bi(NO_3)_3$ concentration.

(2) The order of mixing the precursors and the mineralizer for preparing the starting solution influenced greatly the quality of the prepared starting solution, thus affected the crystallization of deposited BNT films. In this study, the order of ($Bi(NO_3)_3$ + TiO_2) + NaOH was used for preparing the starting solution close to a colloid. This is one of necessary conditions for hydrothermal synthesis of well crystallized BNT films.

(3) At the beginning of the hydrothermal synthesis, the titanium substrate reacted with the ions dissolved in the solution to form some nuclei on the substrate surface. Some crystal nuclei were found on the substrate surface after 15 minutes of deposition, and BNT crystals were generated all over the substrate surface after one hour of deposition.

(4) With the evaluation target of the calculated BNT content of deposited films, the optimized synthesis condition was determined as the condition of G, which is as follows: $Bi(NO_3)_3$ of 1.2 mol/l and TiO_2 of 0.5 mol/l. For sample G, the piezoelectric constant was 1.54 pC/N, and the relative permittivity and dielectric loss were 370 and 0.88, respectively.

(5) Deposition speed was relatively high in the 2nd and 3rd deposition. This was primarily attributed to the great amount of the Bi_2O_3 impurity generated in these two depositions. The Bi_2O_3 impurity can be removed by the etching treatment of concentrated nitric acid.

(6) The relative permittivity tended to increase greatly in the case of the $Bi(NO_3)_3$ concentration of 1.6 mol/l. The dielectric loss was positive correlated with the relative permittivity.

(7) The piezoelectric constant was positive correlated with the BNT content when the BNT content is more than 0.6.

(8) The actuation test confirmed the converse piezoelectric effect of deposited BNT films, which greatly depended on the crystallization level of BNT, and so the piezoelectric response of the tested unimorph cantilever type actuator to a DC or AC field was stronger in the case of higher BNT diffraction peaks.

References

(1) M. Demartin Maeder, D. Damjanovic, and N. Setter, Lead Free Piezoelectric Materials, *Journal of Electroceramics*, Vol.13, No.1-3(2004), pp.385-392.

(2) D. Q. Xiao , D. M. Lin and J. G. Zhu, Investigation on the Design and Synthesis of New Systems of BNT-based Lead-free Piezoelectric Ceramics, *Journal of Electroceramics*, Vol.16, No.4(2006), pp.271–275.

(3) K. Prasad, Lily, K. Kumari and K. P. Chandra, Electrical Properties of a Lead-free Perovskite Ceramic: $(Na_{0.5}Sb_{0.5})TiO_3$, *Applied Physics A: Materials Science & Processing*,Vol.88, No.2(2007), pp.377-383.

(4) Y. Wu, H. Zhang, Y. Zhang, J. Y. Ma and D. H. Xie, Lead-free Piezoelectric Ceramics with Composition of $(0.97-x)Na_{1/2}Bi_{1/2}TiO_3$-$0.03NaNbO_3$-$xBaTiO_3$, J*ournal of Materials Science*, Vol.38, No.5(2003), pp.987-994.

(5) S. H. Choy, X. X. Wang and H. L. W Chan, Electromechanical and Ferroelectric Properties of $(Bi_{1/2}Na_{1/2})TiO_3$-$(Bi_{1/2}K_{1/2})TiO_3$-$(Bi_{1/2}Li_{1/2})TiO_3$-$BaTiO_3$ Lead-free Piezoelectric Ceramics for Accelerometer Application, *Applied Physics A: Materials Science & Processing*,Vol.89, No.3(2007), pp.775-781.

(6) X. X. Wang, H. L. W. Chan and C. L. Choy, $(Bi_{0.5}Na_{0.5})_{0.94}Ba_{0.06}TiO_3$ Lead-free Ceramics with Simultaneous Addition of CeO_2 and La_2O_3, *Applied Physics A: Materials Science & Processing*, Vol.80, No.2(2005), pp.333-336.

(7) Y. Q. Huang, L. F. Gao and Y. Hu, Compositional Effects on the Properties of $(1-x)BaTiO_3$-$xBi_{0.5}Na_{0.5}TiO_3$ Ceramics, *Journal of Materials Science: Materials in Electronics*, Vol.18, No.6(2007), pp.605-609.

(8) D. S. Lee, S. J. Jeong and E. C. Park, Characteristic of Grain Oriented $(Bi_{0.5}Na_{0.5})TiO_3$- $BaTiO_3$ Ceramics, *Journal of Electroceramics*, Vol.17, No.2-4(2006), pp.505-508.

(9) J. F. Tressler, S. Alkoy and R. E. Newnham, Piezoelectric Sensors and Sensor Materials, *Journal of Electroceramics*, Vol.2, No.4(1998), pp.257-272.

(10) T. Kanda, T. Morita, M. K. Kurosawa and T. Higuchi, Sensitivity of a Miniaturized Touch Probe Sensor Using PZT Thin Film, *Ultrasonics,* Vol.40, No.1-8(2002), pp.61-65.

(11) S. Euphrasie, S. Daviero-Minaud and P. Pernod, PZT Films Deposited by a Hydrothermal Method and Characterizations, *Material Science and Engineering B*, Vol.104, No.3(2003), pp.180-184.

(12) X. Z. Jing, Y. X. Li and Q. R. Yin, Hydrothermal Synthesis of $Bi_{0.5}Na_{0.5}TiO_3$ Fine Powders, *Material Science and Engineering B*, Vol.99, No.1-3(2003), pp.506-510.

(13) P. Pookmanee, P. Uriwilost and S. Phanickpat, Hydrothermal Synthesis of Fine Bismuth Powders, *Ceramics International*, Vol.30, No.7(2004), pp.1913-1915.

(14) N. Fujiwara, K. Kusukawa, K. Abdul Razak and W. Gao, Piezoelectric Properties of PZT Films Prepared by Hydrothermal Method, *International Journal of Modern Physics B*, Vol.20, No. 25,26 & 27(2006), pp.3805-3810.

Chapter 4

Evaluation of Adhesion Strength between BNT Films and Ti Substrates by a Tensile Test

A deposited film relies on the mechanical properties of a substrate to provide strength. The substrate is always competent for most of applications. However, a failure usually occurs at the interface between the film and the substrate. Therefore the performance and reliability of film/substrate structures are determined to a large extent by the interfacial strength. A quantitative evaluation of the adhesion strength is demanded in the design and fabrication of the film base component. As yet, there is no accepted convention for defining the adhesion strength between the film and substrate. In an effort to quantitatively assess the adhesion strength between the deposited BNT film and titanium substrate, a tensile test, indentation test and scratch test were carried out in this dissertation. In this chapter, the tensile test is presented in detail, and the indentation test and scratch test will be presented in the next two chapters respectively.

4.1. Introduction

The applications of the film/substrate system require that the film adhere sufficiently to its substrate. Therefore, the interfacial adhesion strength between a film and a substrate is often the predominant factor and chief target in determining the performance and reliability of the film/substrate system [(1)]. Quantitative assessment of the adhesion is quite important to understand the film characteristics and develop high quality films. Common methods to evaluate the adhesion of film include pull-off test, scratch test, and indentation test [(2)-(10)]. The pull-off test is accurate and quantitative if the pulling force can be calibrated well normal to the sample surface. The main restriction with this method is that the tested critical force is limited by the strength of the adhesive, normally weaker than 90 MPa [(11)]. Thus, the adhesive usually fails prior to the films.

The tensile test is the most widely used test in determining the mechanical properties of materials. In this chapter, we evaluate the adhesion of deposited BNT films to Ti substrates by the tensile test with the aid of FEM analysis. Titanium substrates were pretreated by chemical polish and mechanical polish respectively prior to BNT film deposition with a view of investigating the effects of substrate surface pretreatments on the adhesion strength of BNT films.

4.2. Experimental

4.2.1. Sample Preparation

BNT films were hydrothermally synthesized on pure titanium substrates which were 1 mm in thickness with a gauge section of 18 mm in length and 6 mm in width. Figure 4.1 shows the dimensions of smooth specimen for the tensile test. In addition, holed specimens, shown in Figure 4.2, were also prepared to investigate the effect of stress and strain concentration on the adhesion strength. The synthesis process for BNT film was performed at the temperature of 150℃ for 24 hours under the optimum condition G, as described in the previous chapter, and shown in Table 4.1. BNT film of about 5 μm thick was obtained on each side of titanium substrate.

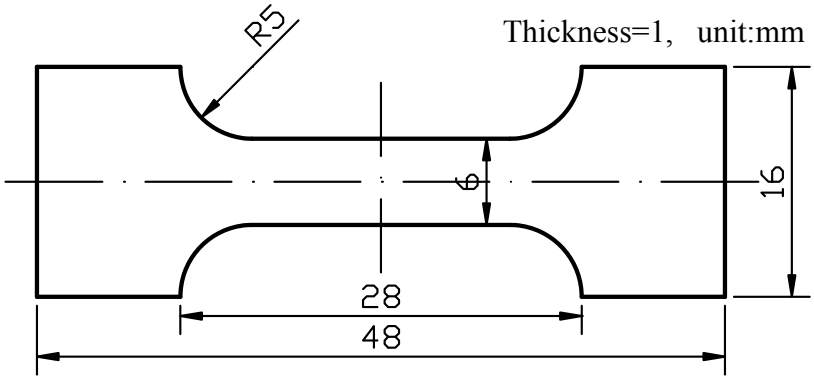

Figure 4.1 Schematic of the smooth specimen for the tensile test

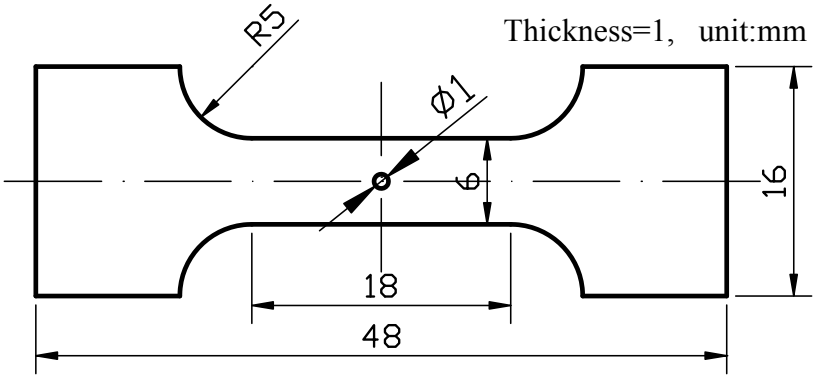

Figure 4.2 Schematic of the holed specimen for the tensile test

Table 4.1 The synthesis condition for depositing BNT film on titanium substrate

$Bi(NO_3)_3 \cdot 5H_2O$	TiO_2	NaOH	Temperature	Time	Rotation
1.2 mol/l	0.5 mol/l	10 mol/l	150℃	24 hr	12 rpm

Heat treatment of titanium substrates prior to BNT film deposition was performed in a furnace (KDF-P90G), in an argon inert atmosphere with a heating rate of 10℃/min from room temperature to 700℃. Table 4.2 shows the annealing condition for titanium substrate. The titanium substrates were placed into the furnace from the beginning of the heating procedure, and then stayed at the annealing temperature 700℃ for 1 hour. After the end of this period the argon flow was used for cooling down the specimens. When the temperature in the furnace reached 300℃, the specimens were removed from the furnace and left to cool down freely in the air. Larger crystal grains were obtained in titanium substrates after the heat treatment.

After the heat treatment, some of smooth and holed titanium substrates were mechanically polished by a 500 grit emery paper. The other substrates were chemically polished by immersing them in a chemical solution with the temperature of 90℃. The chemical solution was prepared by nitric acid (HNO_3), hydrofluoric acid (HF) and distilled water, as shown in Table 4.3. After the pretreatment of mechanical and chemical polish, the substrates were ultrasonically cleaned in a methanol bath followed by a rinse in distilled water.

Table 4.2 The annealing condition for titanium substrate

Heating rate	Temperature	Holding time	Gas
10℃/min	700℃	1 hr	Ar

Table 4.3 The solution prepared for the chemical polish treatment of Ti substrates

Component	Volume	Volume fraction
Distilled water	19 ml	54.3%
HNO_3	12 ml	34.3%
HF	4 ml	11.4%

4.2.2. Tensile Test

A tensile test was carried out using a universal testing machine (SHIMADZU, AG-100kNG). The stress-stain curve was measured on the heat-treated titanium substrate with the tension speed of 0.02 mm/s up to fracture, with a view of examining the ultimate strength and yield strength (for plastic strain of 0.2%) of the heat-treated titanium substrate. During the tensile testing of the BNT deposited specimens, the crosshead of the universal testing machine was manually operated to stop at various appointed displacements, and then the behavior of film exfoliation was investigated by the replica method. Figure 4.3 shows the picture of the specimen being tested in a tensile test using a replica film. The process of the replica method is shown in Figure 4.4. The film exfoliation would adhere to the replica film, so the behavior of film exfoliation can be investigated by observing the applied replica film. In this study, for the smooth specimen, the number of the film exfoliation in the fixed field of vision was measured by the polarized microscopic observation (OLYMPUS, BX60). For the holed specimen, the exfoliation area near the edge of the hole was measured using a laser microscope system (KEYENCE, VK-8510), and then the exfoliation rate was determined by the ratio of the exfoliation area to the gauge section area.

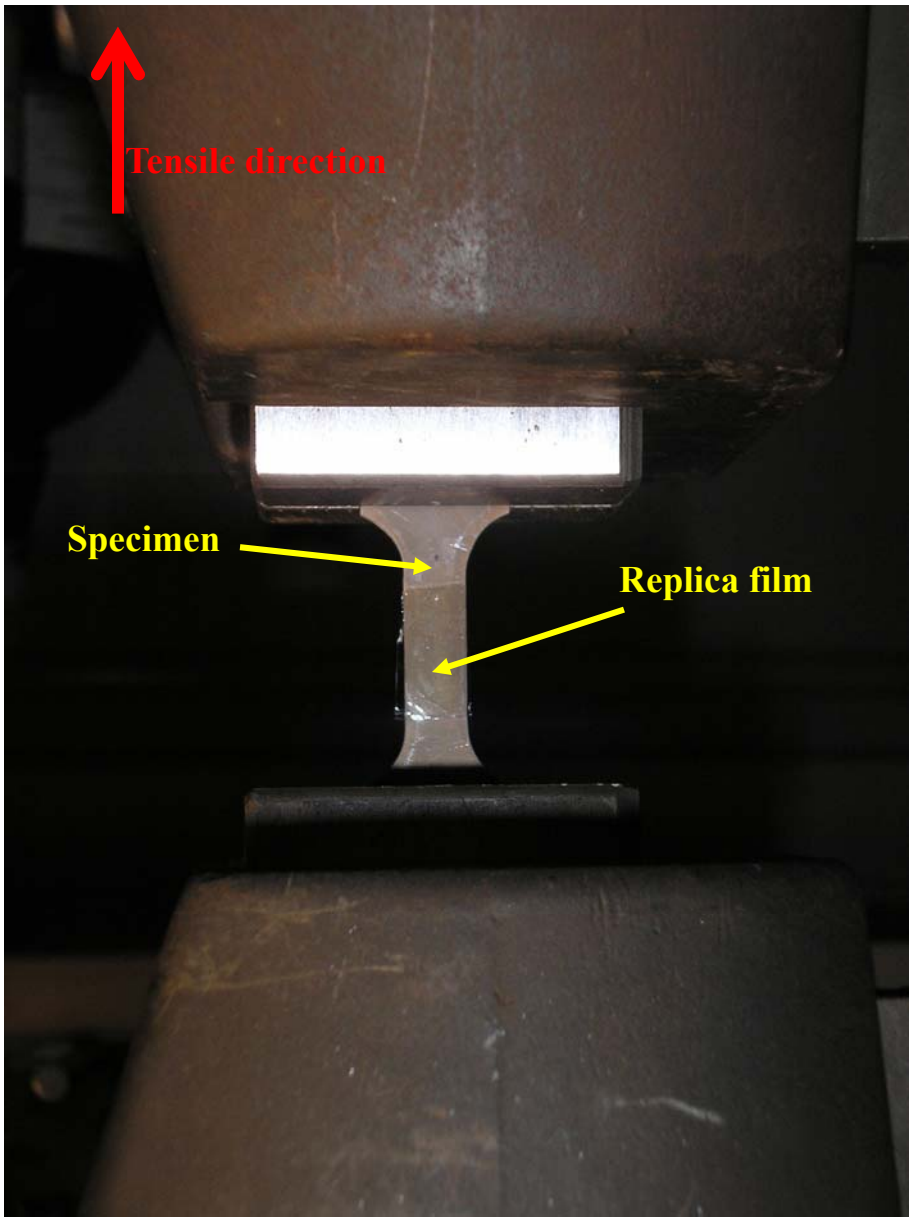

Figure 4.3 Tensile testing of the specimen using a replica film

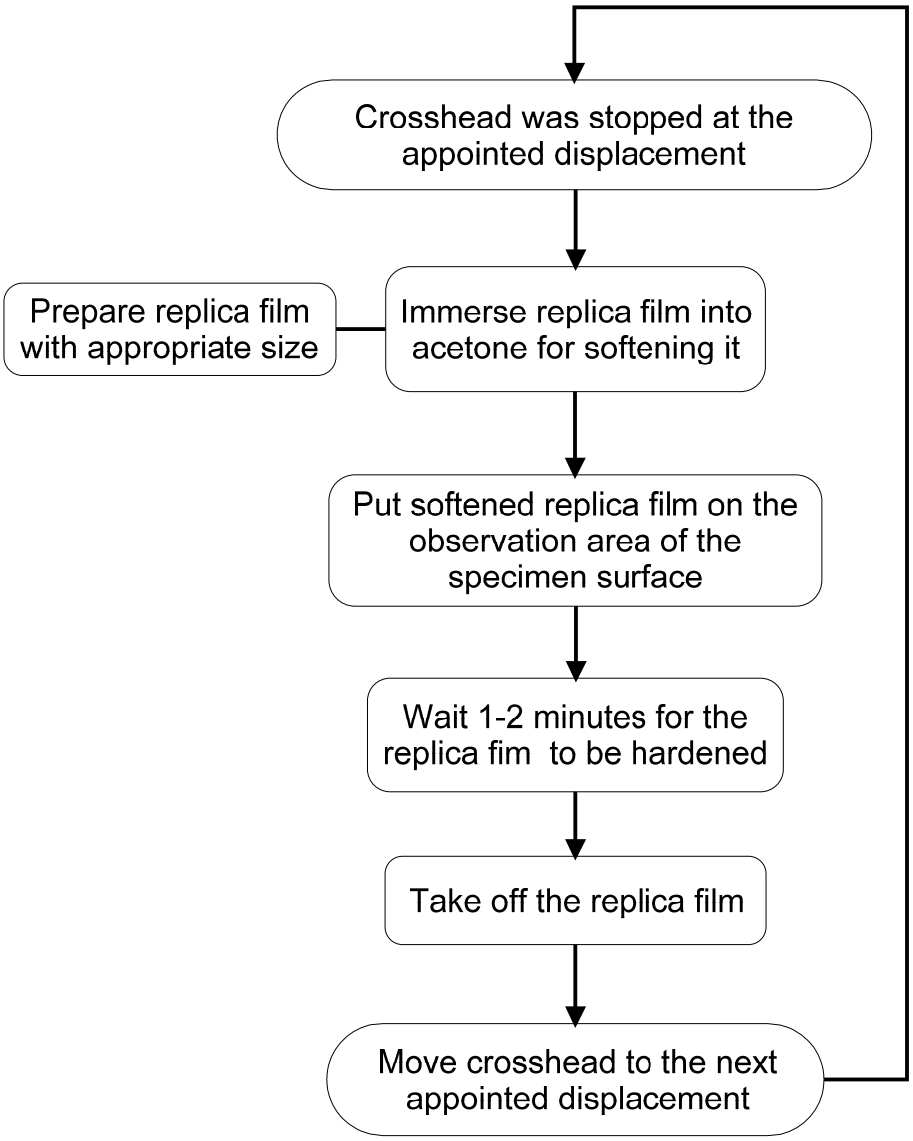

Figure 4.4 The process of the replica method

4.3. Results and Discussion

4.3.1. Heat-treated Titanium Substrate

Figure 4.5 shows the variation of stress with the stroke of crosshead for the tensile test of heat-treated titanium substrate. It can be seen that the ultimate strength is about 350 MPa. Figure 4.6 shows the stress-strain curve of the heat-treated titanium substrate in the first part of tensile test. The yield strength ($\sigma_{0.2}$) and Young's modulus (E) were determined to be 195 MPa and 106 GPa, respectively. These strength data provided reference for the tensile test of BNT deposited specimens.

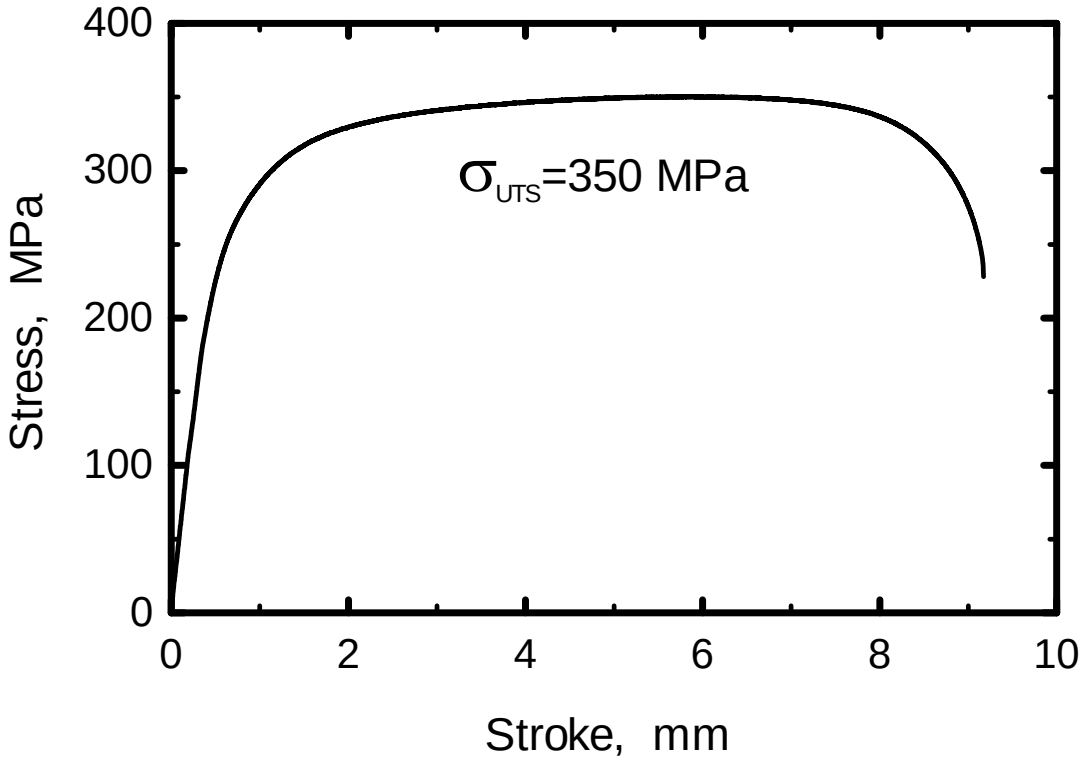

Figure 4.5 Variation of stress with the stroke of crosshead for the tensile test of heat-treated titanium substrate

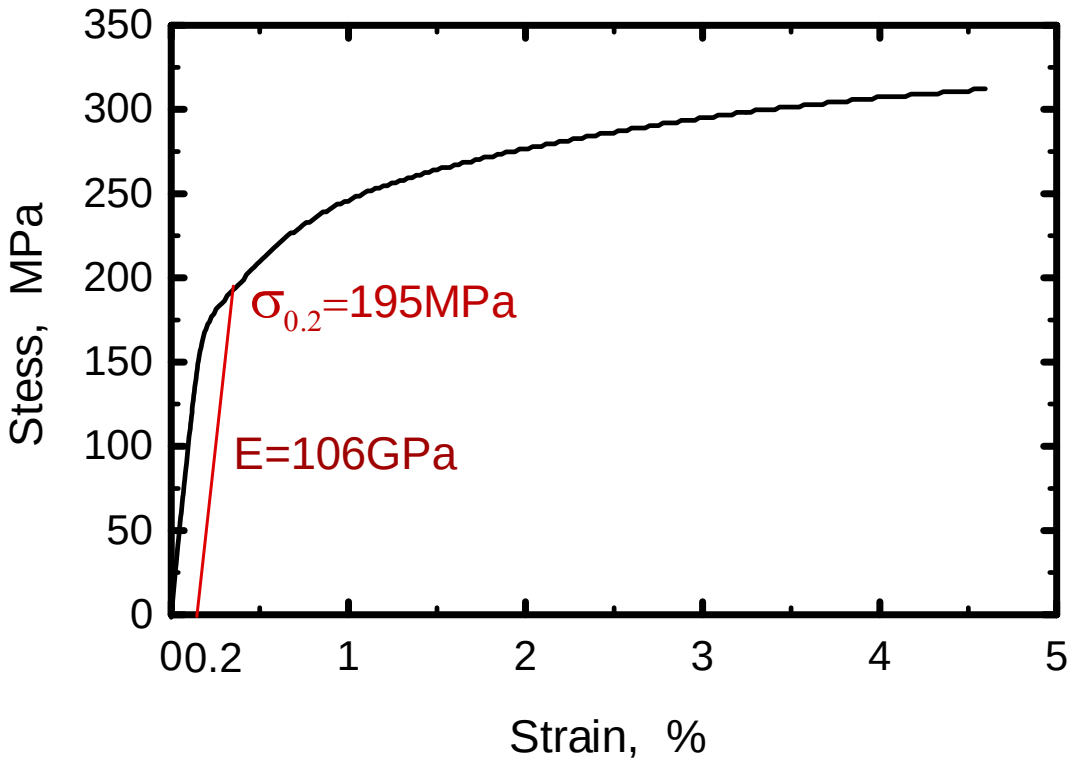

Figure 4.6 Stress-strain curve of the heat-treated titanium substrate in the tensile test

4.3.2. Smooth Specimen

The applied replica films in the tensile test were observed by the polarized microscopic observation, and some of observed results are shown in Figures 4.7 and 4.8. Figure 4.7 shows successive observations with the increase of strain for the mechanically polished (MP) smooth specimen. The critical strain inducing the first film exfoliation was determined to be 1.2% for the MP smooth specimen. Figure 4.8 shows successive observations with the increase of strain for the chemically polished (CP) smooth specimen. The critical strain was determined to be 1.0% for the CP smooth specimen. For both of the MP and CP smooth specimens, the film exfoliation occurred after the yield strength of the substrate, and the number of film exfoliation increased with the increase of train. Figure 4.9 shows the variation of the number of film exfoliation with the strain of Ti substrate for these two smooth specimens. The number of film exfoliation increased

monotonously with the strain up to 3% after the occurrence of the film exfoliation.

In addition, it is noted that the strain in this section indicates the total mechanical strain of titanium substrate in the tensile direction, which was obtained from the finite element (FEM) analysis of the titanium substrate. The FEM analysis was performed using ANSYS Res. 11.0 software package. In the FEM analysis, the titanium substrate was treated as a homogeneous, isotropic, rate-independent and non-linear plastic body. As shown in Figure 4.10, the constraint conditions were set as follows:

(1) The degree of freedom (DOF) of the bottom surface was set zero in the y direction.

(2) The DOF of AB line was set zero in the Z direction.

(3) The DOF of A point was set zero in all of the directions.

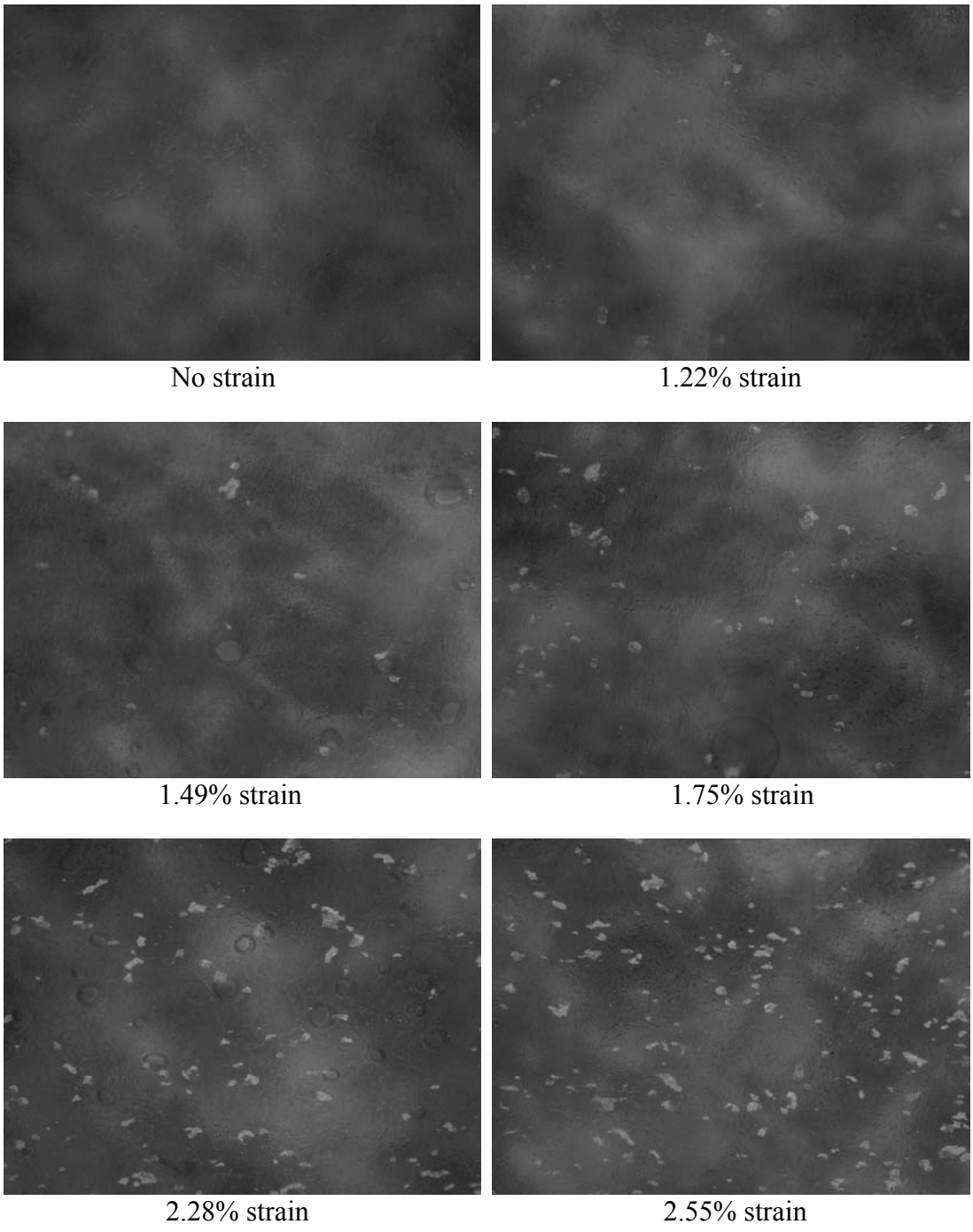

Figure 4.7 Successive observations for the MP smooth specimen

No strain

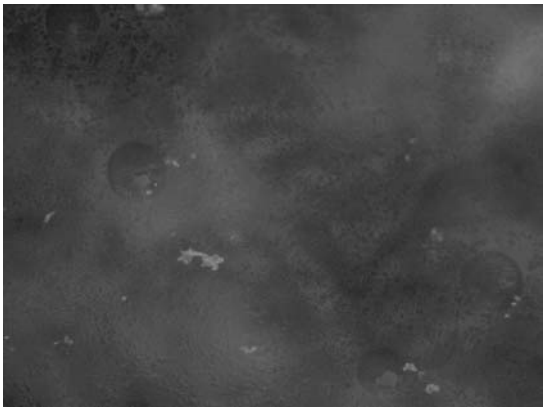

0.99% strain

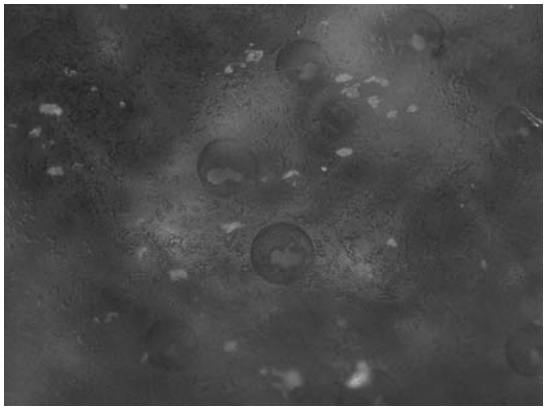

1.28% strain

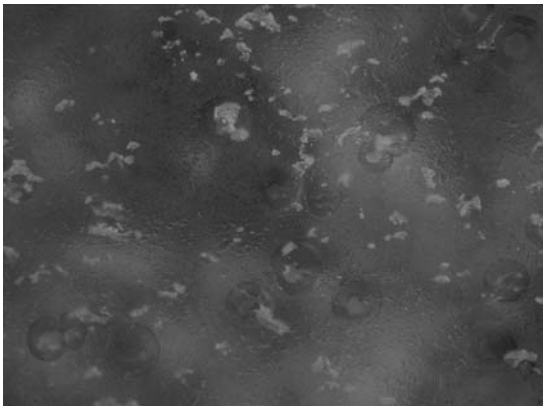

1.58% strain

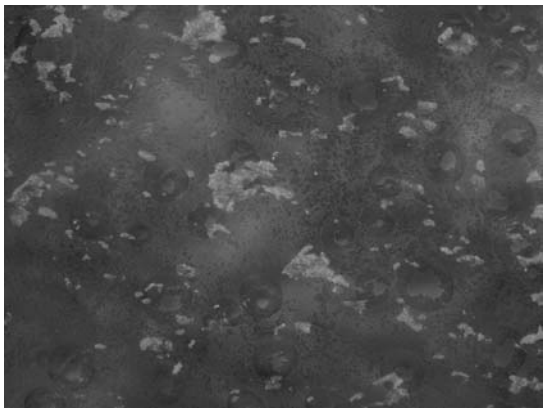

1.87% strain

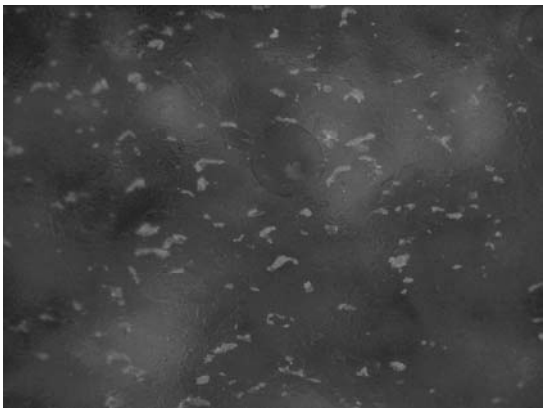

2.46% strain

Figure 4.8 Successive observations for the CP smooth specimen

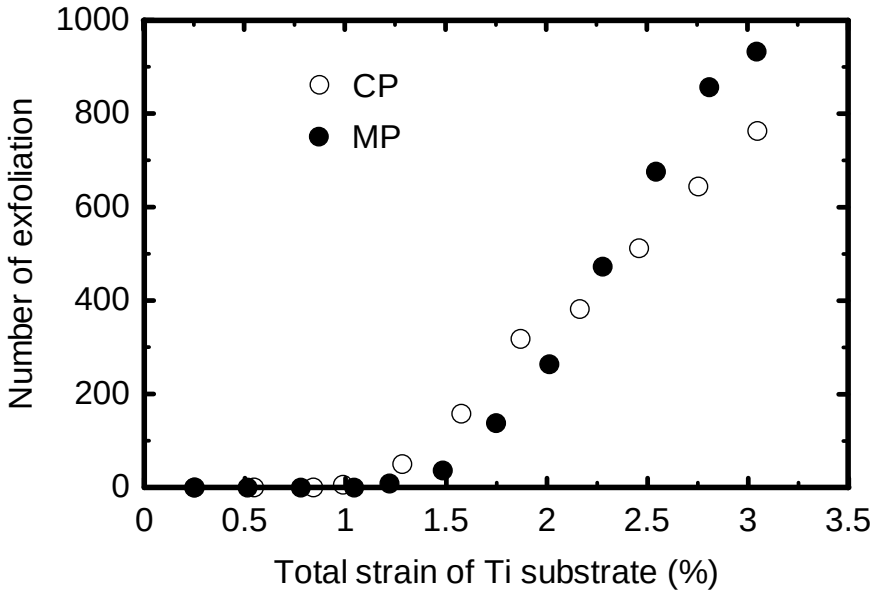

Figure 4.9 Variations of the number of exfoliation with the total strain of Ti substrate for smooth specimens

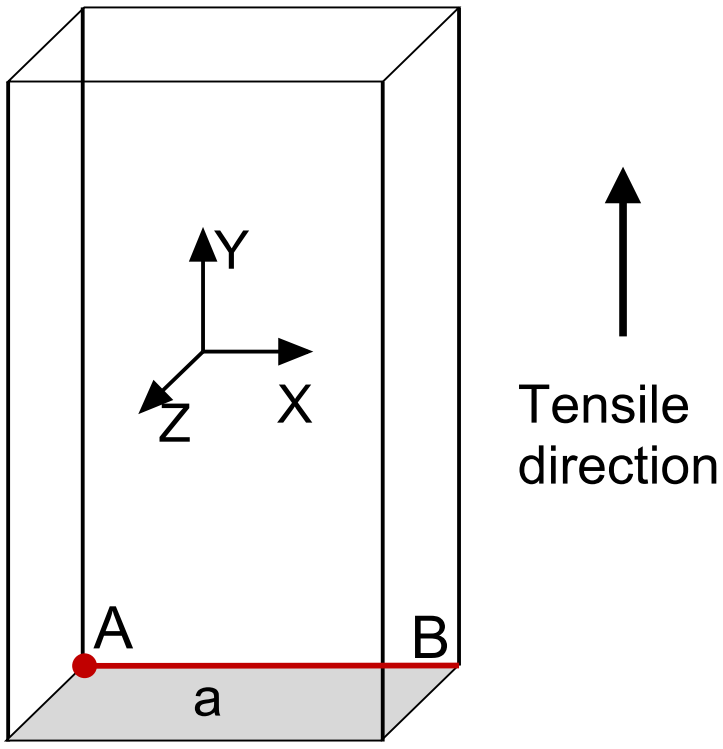

Figure 4.10 Schematic of the constraint condition for the FEM analysis of the titanium substrate in the tensile test

4.3.3. Holed Specimen

The applied replica films in the tensile test were observed by a stereo microscope(OLYMPUS，SZ1145TR-SPT), and some of observed results are shown in Figures 4.11 and 4.12. Figure 4.11 shows successive observations with the increase of strain for the MP holed specimen. The film exfoliation firstly occurred when the maximum strain near the edge of hole reached 1.0%. Figure 4.12 shows successive observations with the increase of strain for the CP holed specimen. The film exfoliation firstly occurred when the maximum strain near the edge of hole reached 0.77%. Therefore, the critical strains for the MP and CP specimens were determined to be 1.0% and 0.77%, respectively. Figure 4.13 shows the variations of exfoliation rate with the total strain of Ti substrate for holed specimens. The exfoliation rate of CP specimen increased more largely than that of MP specimen with further increase of substrate strain after the occurrence of exfoliation. Figure 4.14 shows the comparison of the critical strain between the smooth and holed specimen. The critical strain for the holed specimen is slightly different from that of the smooth specimen. It can be also found that the critical strain for the MP specimen is larger than that of the CP specimen for both of the smooth and holed specimens. This indicates that the pretreatment of the mechanical polish improved the adhesion of deposited BNT film. In addition, for both of the MP and CP holed specimens, the film exfoliation expanded in the direction of 45° angle with the tensile direction.

The above strain in this section was obtained from the FEM analysis of the holed titanium substrate. In the FEM analysis, the constraint conditions were set the same with that of the smooth specimen, as described in Section 4.3.2. Figures 4.15, 4.16 and 4.17 show the contrast between microscopic observation and strain contour plot by FEM analysis for the MP holed specimen under the displacement load of 0.23, 0.26 and 0.32 mm, respectively. It can be found that the exfoliation area was in good agreement with the shape of strain contour. By the contrasts of all the results, it was found that the film exfoliation always occurred in the area where the strain was about more than 1.3%.

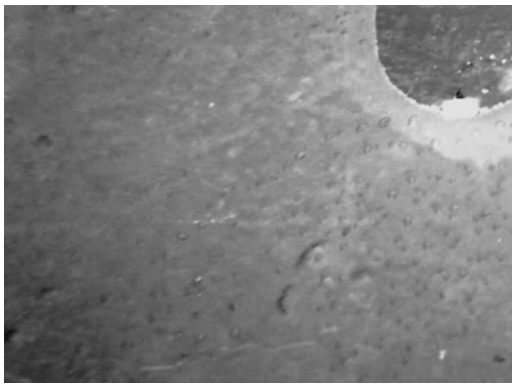

No strain

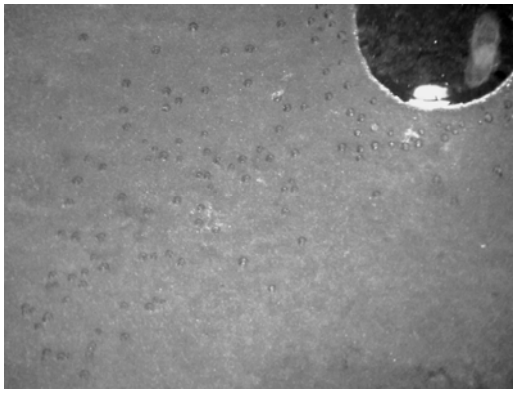

1.07% strain

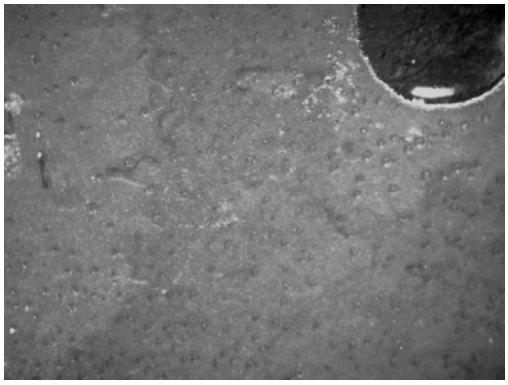

2.41% strain

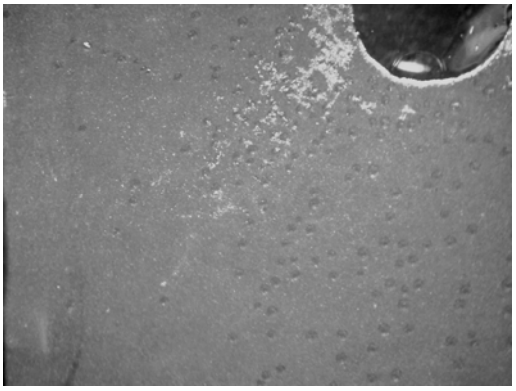

3.62% strain

4.38% strain

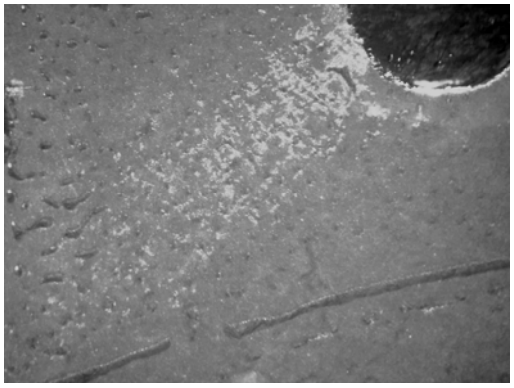

5.15% strain

Figure 4.11 Successive observations for the MP holed specimen

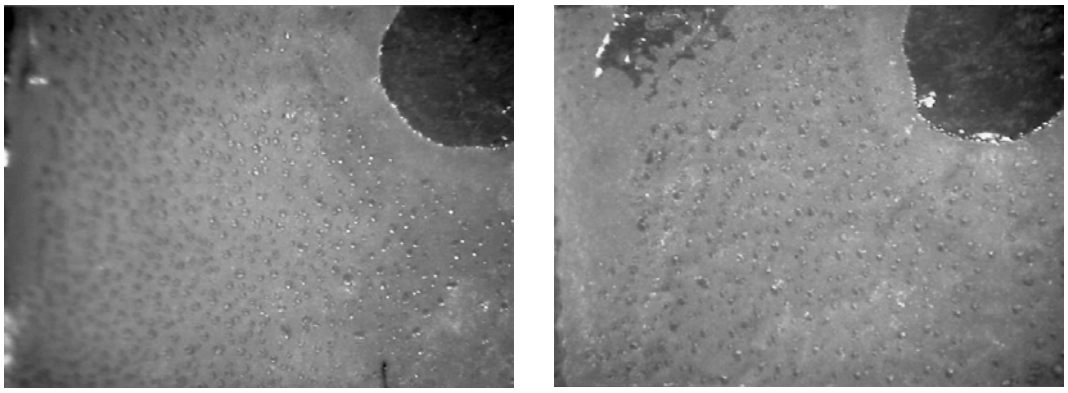

No strain 0.77% strain

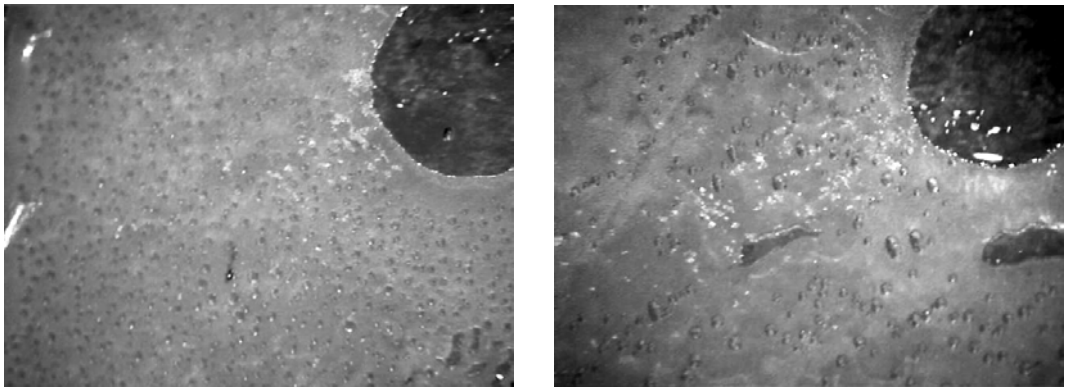

1.10% strain 1.68% strain

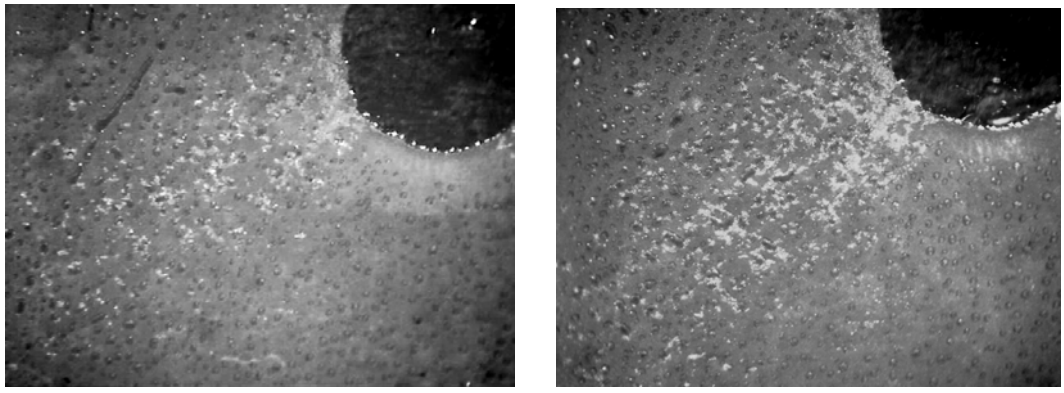

2.13% strain 3.18% strain

Figure 4.12 Successive observations for the CP holed specimen

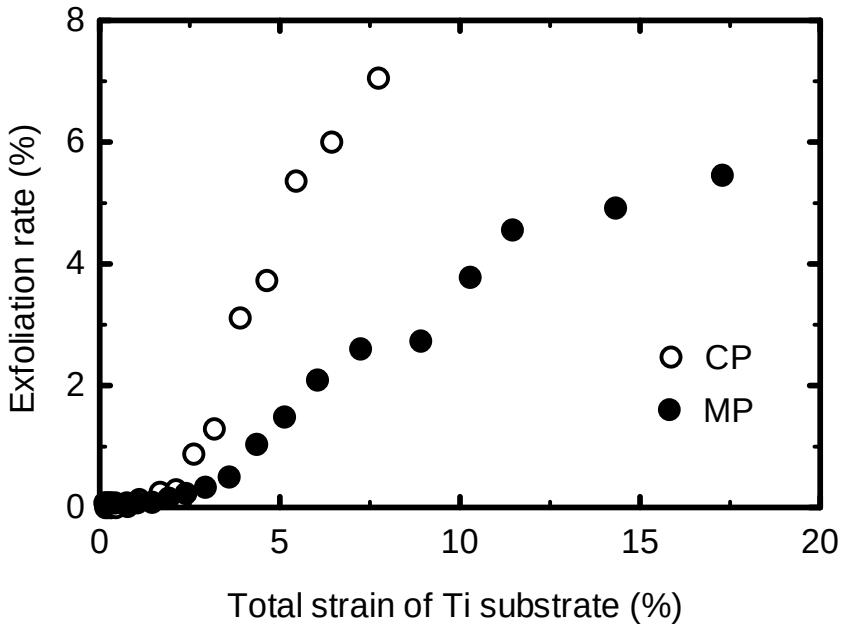

Figure 4.13 Variations of exfoliation rate with the total strain of Ti substrate for holed specimens

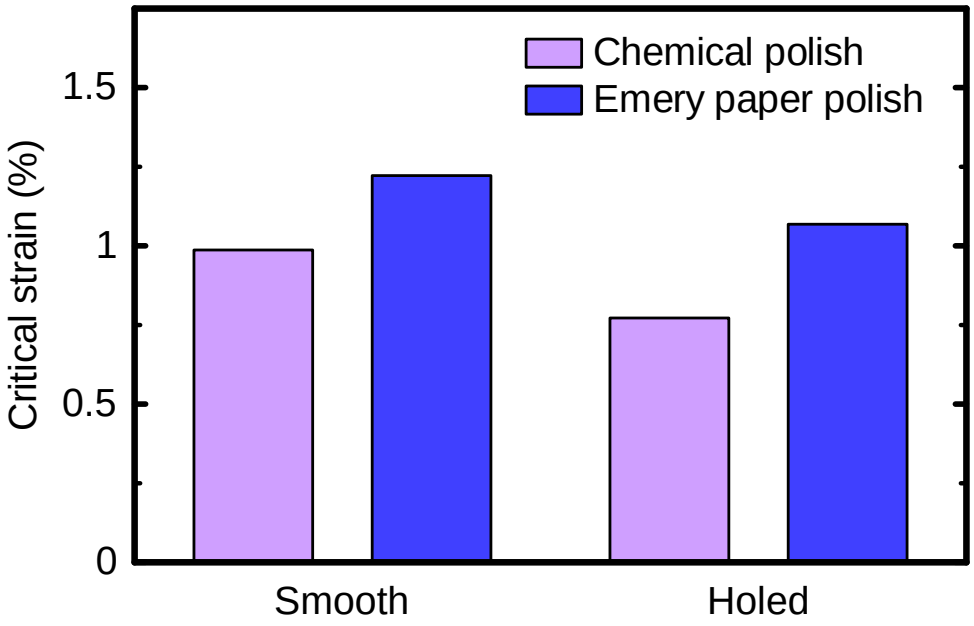

Figure 4.14 Comparison of critical strains for the tensile test of smooth and holed specimens

(a)

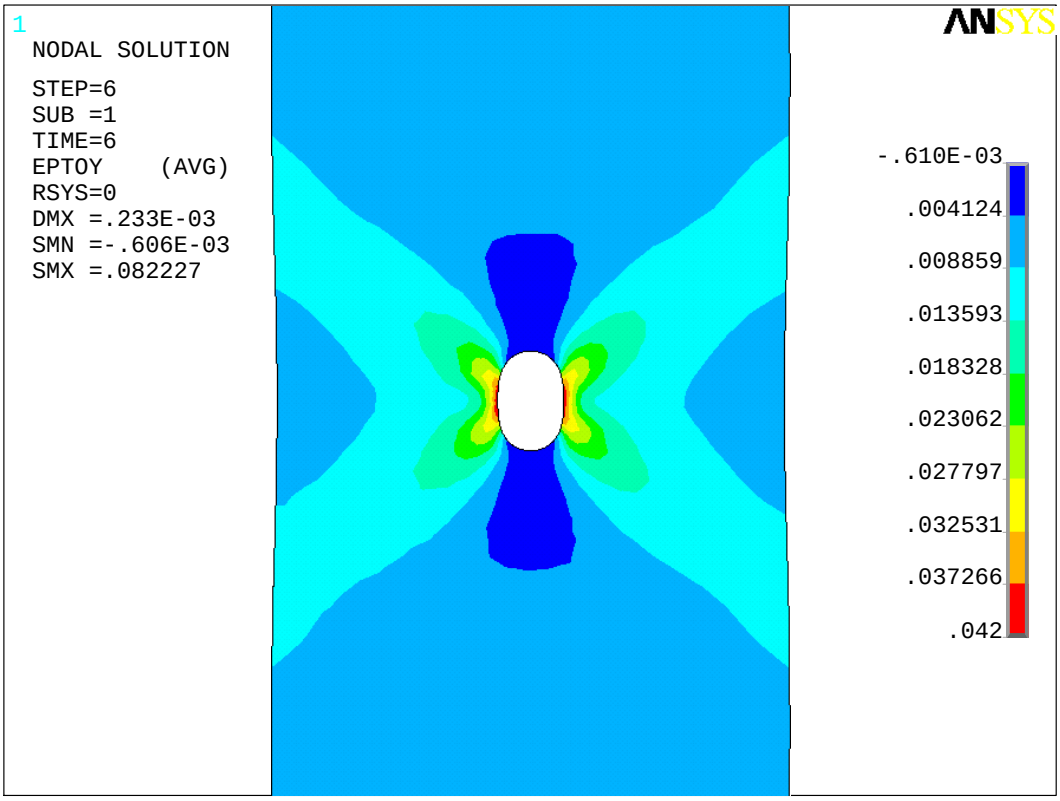

(b)

Figure 4.15 Contrast between (a)microscopic observation and (b) strain contour plot by FEM analysis for the MP holed specimen under the displacement load of 0.23 mm

(a)

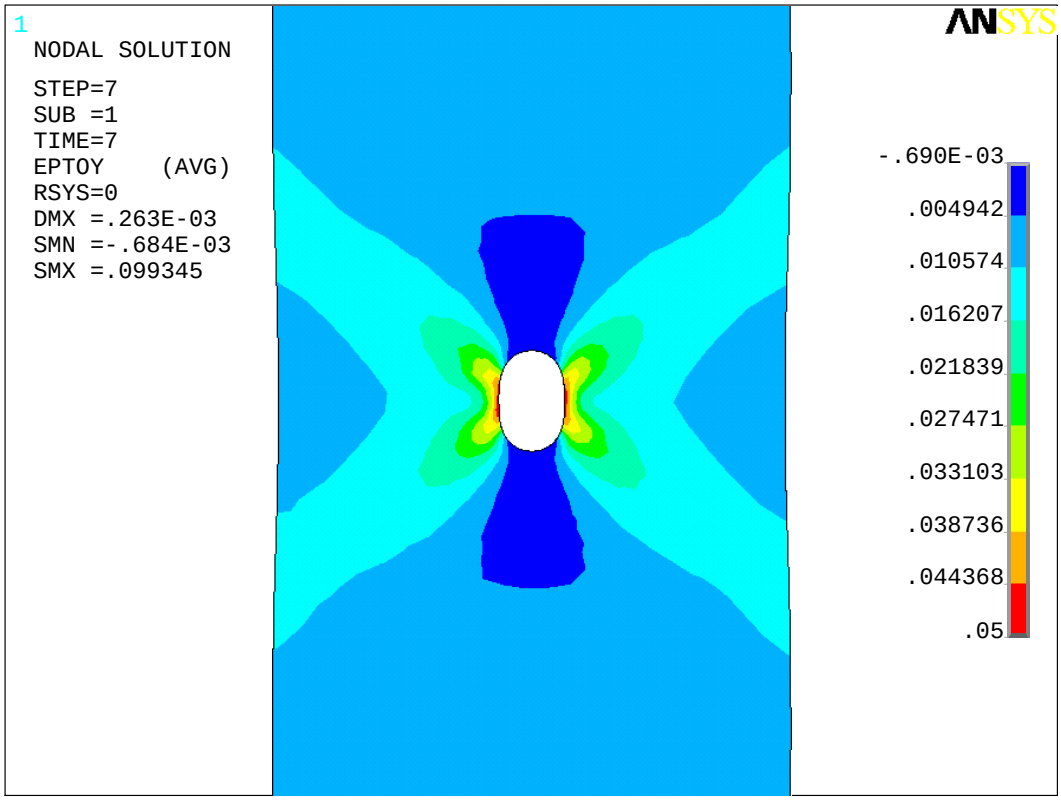

(b)

Figure 4.16 Contrast between (a)microscopic observation and (b) strain contour plot by FEM analysis for the MP holed specimen under the displacement load of 0.26 mm

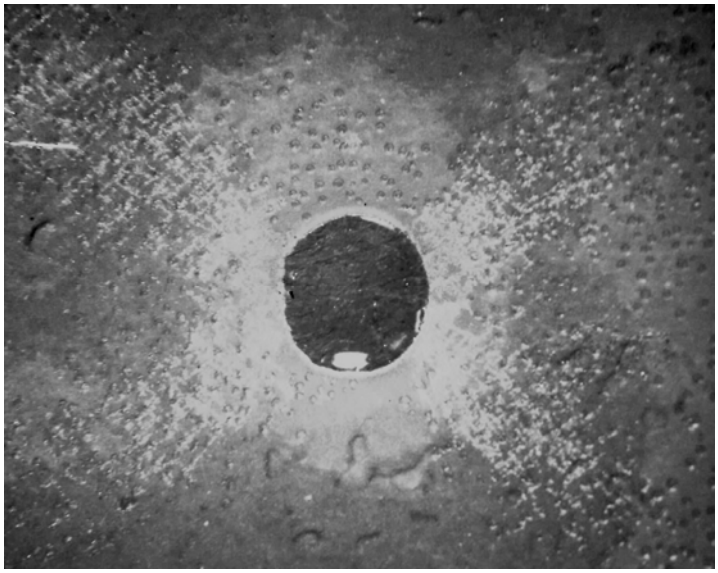

(a)

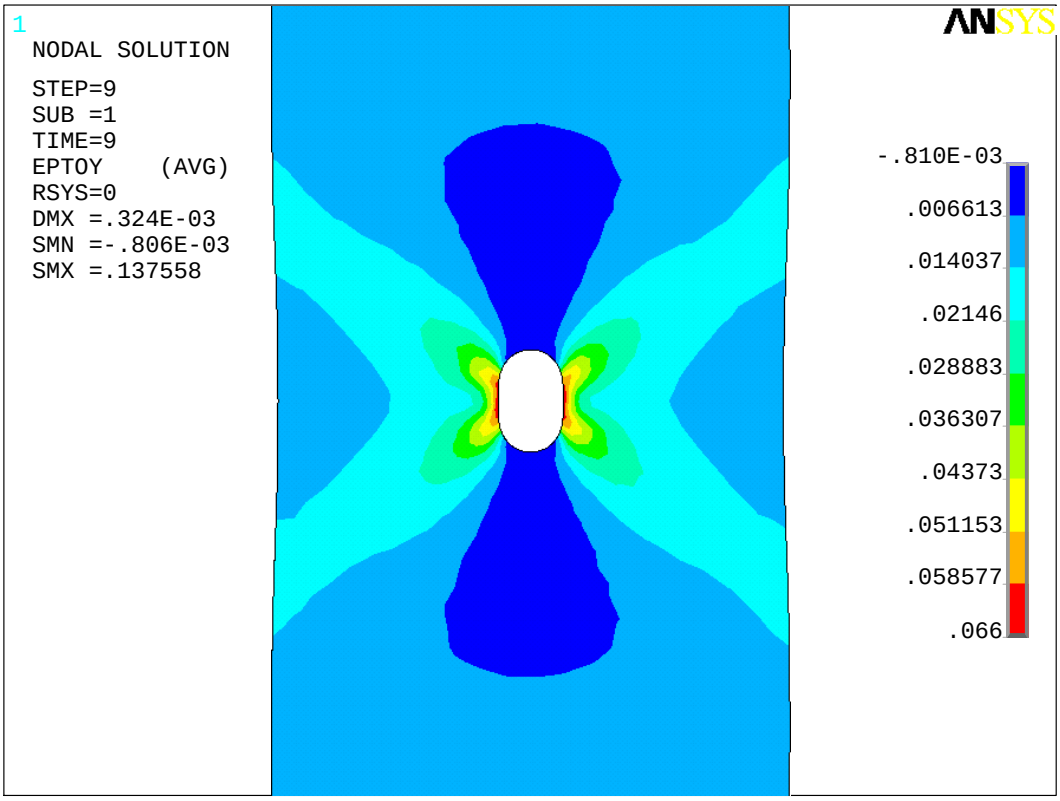

(b)

Figure 4.17 Contrast between (a)microscopic observation and (b) strain contour plot by FEM analysis for the MP holed specimen under the displacement load of 0.32 mm

4.4. Conclusions

In this chapter, tensile tests were performed on the smooth and holed specimens to quantitatively evaluate the adhesion strength of deposited BNT films on titanium substrates. The effects of the substrate pretreatments of the mechanical and chemical polish on the adhesion strength were also investigated. The critical strain was obtained with the aid of FEM analysis. The main conclusions are summarized as follows:

(1) For both of the smooth and holed specimen, the film exfoliation firstly occurred after the yield strength of titanium substrate. The behavior of film exfoliation was attributed to the plastic deformation of the substrate.

(2) For the smooth specimen, the number of exfoliation increased monotonously with the increase of the substrate strain after the occurrence of the film exfoliation. For the holed specimen, the exfoliation area increased monotonously with the increase of the substrate strain after the occurrence of the film exfoliation.

(3) The critical strain was determined to be about 1% for both of the CP and MP specimens.

(4) For the holed specimen, the film exfoliation expanded with increasing the substrate strain in the direction of 45° angle with the tensile direction. The film exfoliation always occurred in the area where the strain was about more than 1.3%. This verified the validity of the obtained critical strain.

References

(1) Teowee, G., Ferroelectric Films, *Journal of Sol-Gel Science and Technology*, Vol.19, (2000), pp. 53-64.

(2) S. Trolier-Mckinstry and P. Muralt, Thin Film Piezoelectrics for MEMS, *Journal of Electroceramics*, Vol.12, (2004), pp. 7-17.

(3) C. J. Xie and W. Tong, Cracking and Decohesion of a Thin Al_2O_3 Film on a Ductile Al–5%Mg Substrate, *Acta Materialia*, Vol.53, No.2 (2005), pp.477-485.

(4) N. Bai and G. H. Yun, Analysis of Film Strain and Stress in a Film-Substrate Cantilever System, *Science in China Series G: Physics, Mechanics & Astronomy*, Vol.51, No.9(2008), pp.1357-1366.

(5) T. Onoki, K. Hosoi, T. Hashida, Y. Tanabe, T. Watanabe, E. Yasuda and M. Yoshimura, Effects of Titanium Surface Modifications on Bonding Behavior of Hydroxyapatite Ceramics and Titanium by Hydrothermal Hot-pressing, *Materials Science and Engineering: C*, Vol.28, No.2(2008), pp.207-212.

(6) I. A. Ashcroft and B. Derby, Adhesion Testing of Glass-ceramic Thick Films on Metal Substrates, *Journal of Materials Science*, Vol.28, No.11 (1993), pp.2989-2998.

(7) C. N. Panagopoulos, V. D. Papachristos and C. Sigalas, Tensile Behaviour of as Deposited and Heat-treated Electroless Ni-P Deposits, *Journal of Materials Science*, Vol.34, No.11 (1999), pp.2587-2600.

(8) M. A. Haque and M. T. A. Saif, A Review of MEMS-based Microscale and NanoscaleTensile and Bending Testing, *Experimental Mechanics*, Vol.43, No.3 (2003), pp.248-255.

(9) Bruno A. Latella, Michel Ignat, Christophe J. Barbé, David J. Cassidy and John R. Bartlett, Adhesion Behaviour of Organically-modified Silicate Coatings on Stainless Steel, *Journal of Sol-Gel Science and Technology*, Vol.26, No.1-3 (2003), pp.765-770.

(10) Örjan Vallin, Kerstin Jonsson and Ulf Lindberg, Adhesion Quantification Methods for Wafer Bonding, *Materials Science and Engineering: R: Reports*, Vol.50, No.4-5 (2005), pp.109-165.

(11) K. L. Mittal, Adhesion Measurement of Thin Films, *Electrocomponent Science and Technology*, Vol.3, (1976), pp.21-42.

Chapter 5

Evaluation of Adhesion Strength between BNT Films and Ti Substrates by an Indentation Test

An indentation method has long been used to characterize the mechanical properties of materials as quantitatively as conventional testing techniques such as uniaxial compression and tension. In this chapter, the indentation method will be used to quantitatively evaluate the adhesion strength of deposited BNT films on titanium substrates. The relation of the film delamination and the substrate strain will be discussed with the aid of FEM analysis.

5.1. Introduction

Historically, an indentation method is used as a testing method of hardness. Recently, some researchers have developed depth-sensing indentation technique to accurately measure mechanical properties of materials [(1)-(5)], such as elastic modulus and elasto-plastic properties. Attempts have also been made to determine the fracture toughness of coatings and the coating-substrate interface strength via indentation [(6)-(10)]. An indentation test was used to evaluate the adhesion of diamond-like carbon (DLC) film to its substrate in some literatures [(11)-(12)].

In this chapter, the adhesion strength of BNT deposited films on titanium substrates was evaluated under Vickers indentation through investigating the delamination response of the BNT films to the applied load. Three dimensional finite element analysis was employed to simulate the indentation test and thus to determine the strain distributions in the substrate under the indentation loads. The delamination mechanisms of the BNT films under Vickers indentation were discussed in terms of the strain results.

5.2. Experimental

5.2.1. Sample Preparation

BNT films were hydrothermally synthesized on pure titanium substrates which were 0.05 mm in thickness. Some of titanium substrates (MP) were mechanically polished using a 1000 grit emery paper. The other substrates (CP) were chemically polished in the chemical solution, as shown in Table 4.3. The synthesis process was performed at the temperature of 150℃ for 24 hours under the optimum condition G, as described in Table 4.1. BNT film of about 5 μm thick was obtained on each side of titanium substrate. In order to remove the loose structure in the top layer of the BNT deposited specimens, the deposited film surfaces were slightly polished using an emery paper before the Vickers indentation test.

5.2.2. Vickers Indentation Test

Vickers indentation tests were carried out on the BNT deposited specimens using a microhardness tester, as shown in Figure 5.1. The indenter tip was a Vickers tip with a pyramidal square base and a 136-degree angle between opposing faces. The indentations were performed under a set of discrete loads (0.98, 2.94, 4.9 and 9.8 N), with a 15 s hold under the maximum load. After indentation, the morphologies of indentations were observed by the laser microscope, and the indentation edge length and the delamination area of BNT film around the indentation were measured using the laser microscope system. Figure 5.2 shows the schematic illustration of indentation test.

Figure 5.1 The Vickers indentation tester

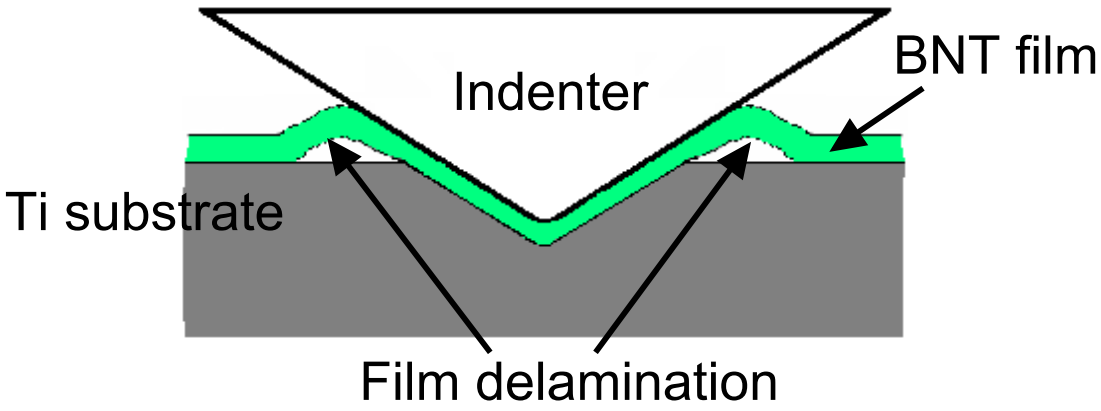

Figure 5.2 Schematic illustration of indentation test

5.3. Results and Discussion

5.3.1. Vickers Indentation Test

An indentation in the film deposited substrate may cause the following failure modes: (1) the substrate cracking; (2) the film cracking and localized exfoliation; and (3) the adhesion failure at the film/substrate interface and the film delamination [13]. In this study, we can firstly rule out the possibility of the first mode because Ti substrate is ductile. In addition, no film cracking was observed at lower indentation load before the generation of film delamination. Therefore, we can rule out the possibility of the second mode. The above results suggest that Vickers indentation induced the adhesion failure at the BNT film/Ti substrate interface, and then caused the film delaminations. This failure type was confirmed as localized convexity on microscopic observations.

Figure 5.3 shows the microscopic observation of Vickers indentation under 4.9 N indentation load. On titanium substrate, no convexity around the indentation was found, while film delamination was found around the indentation on the CP specimen due to the convexity, which was formed due to the difference of deformation between film and substrate under indentation load. Figure 5.4 shows film delamination around the indentation for the CP specimen under 0.98, 2.94, 4.9 and 9.8 N indentation loads, respectively. Figure 5.5 shows the variation of film delamination area with applied indentation load for CP and MP specimens. Compared with CP specimen, the MP specimen exhibited relatively good adhesion when the indentation load was lower than 5 N. For both of the MP and CP specimens, the delamination area increased monotonously with increasing the indentation load after the beginning of film delamination. As shown in Figure 5.6, the indentation depth also increased monotonously with increasing the applied indentation load for the CP specimen.

(a) (b)

Figure 5.3 Microscopic observation of indentation under 4.9 N indentation load: (a) titanium substrate; (b) the CP specimen

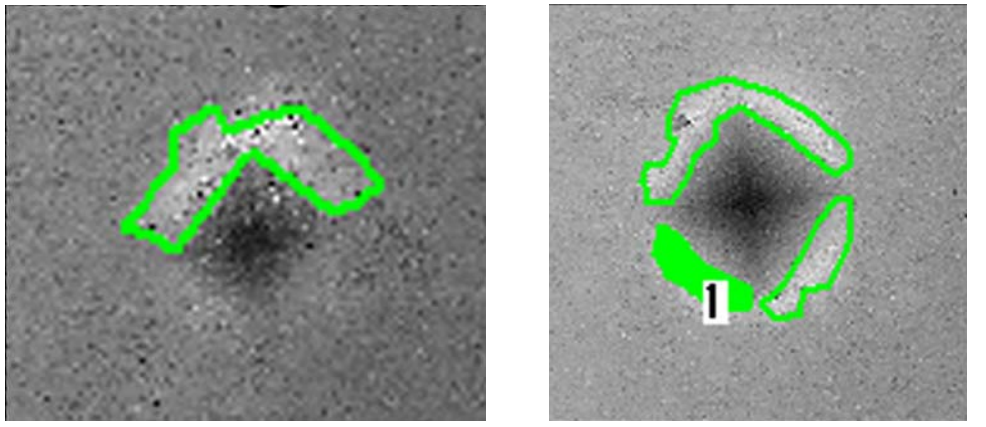

(a) (b)

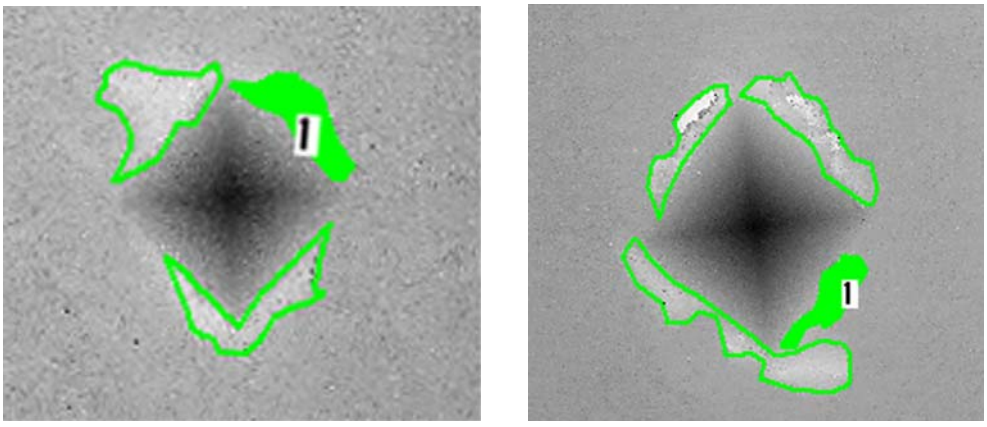

(c) (d)

Figure 5.4 Film delamination around the indentation for the CP specimen under various indentation loads: (a) 0.98N; (b) 2.94N; (c) 4.9N; (d) 9.8N

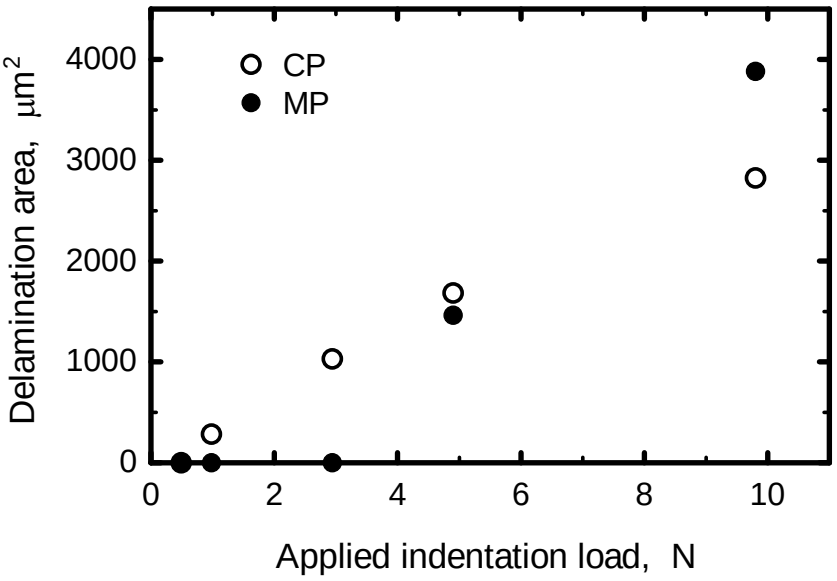

Figure 5.5 Variation of film delamination area with applied indentation load for CP and MP specimens

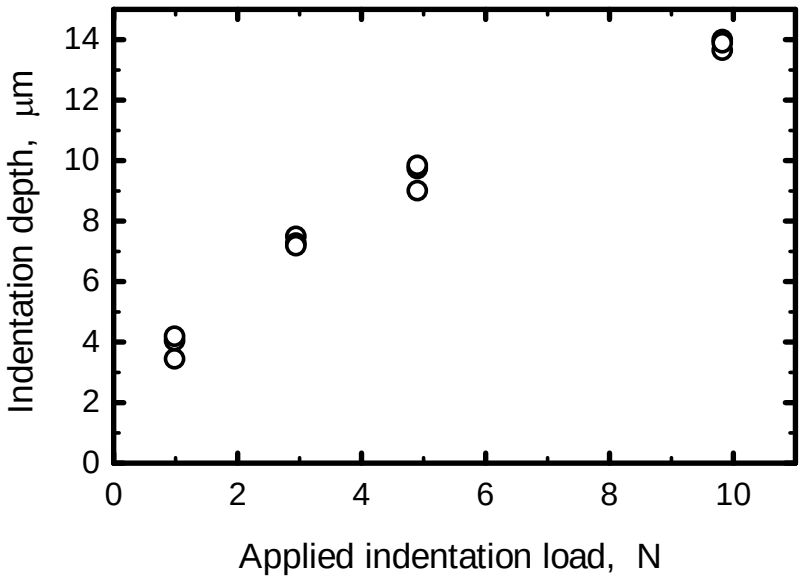

Figure 5.6 Variation of indentation depth with applied indentation load for CP specimen

5.3.2. FEM Analysis

In order to investigate the strain field where film delaminations occurred, three-dimensional FEM analysis of Vickers indentation was performed using ANSYS Res. 11.0 software package. A three dimensional finite element model was developed to computationally simulate the Vickers indentation experiment. The Vickers indenter was modeled as a rigid body. The model material was treated as a homogeneous, isotropic, rate independent and nonlinear plastic body. Due to the symmetry, one fourth model of the indentation was studied, as shown in Figure 5.7. The meshing was denser near the indentation where the substrate is expected to deform while a coarse mesh was used in the other regions. This was done to decrease the computation time and increase efficiency. The indenter was constrained in all directions. The displacement load which was obtained from the experimental results of indentation depth was applied on the bottom surface of the model. Surface-to-surface (CONTA174 and TARGE170) and node-to-surface (CONTA175 and TARGE170) contact elements were used.

Figure 5.8 shows the comparison of the experimental and FEM simulated results on the indentation edge length. The results from the FEM analysis are in close agreement with the experimental results. This indicates that the above FEM model is valid for this analysis.

Figures 5.9, 5.10, 5.11 and 5.12 show the plastic shear strain (γ_{xy}) field on the indentation surface after the 0.98, 2.94, 4.9 and 9.8 N load indentation, respectively. The extent of solid lines in each drawing shows the area where film delaminations occurred. Based on a comprehensive consideration of the same mapping under all the indentation load levels, we can conclude that the critical plastic in-plane strain on the substrate which induces film delaminations is about 0.2.

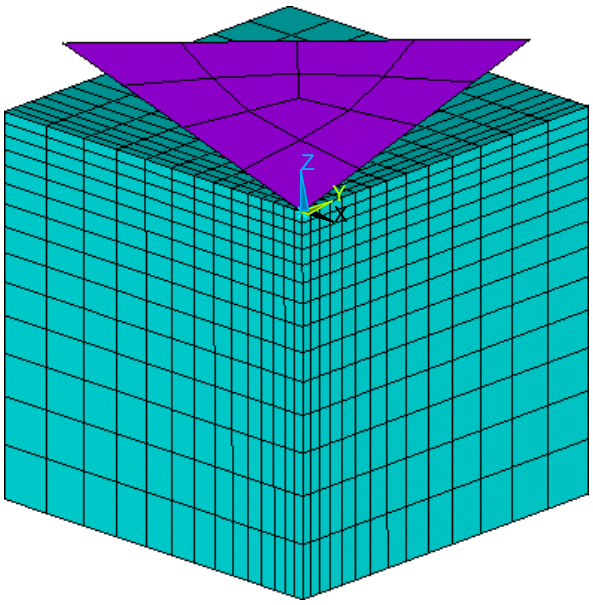

Figure 5.7 Three-dimensional mesh model used for the FEM analysis of one fourth of indentation

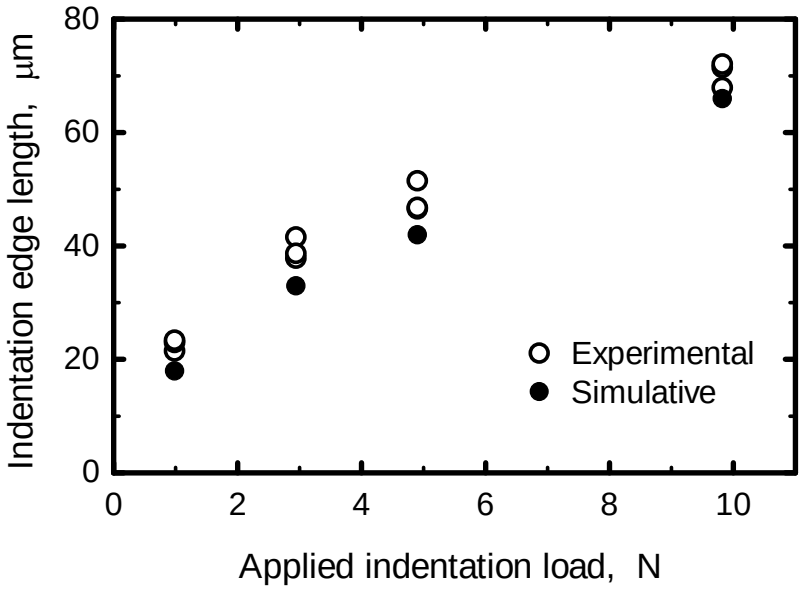

Figure 5.8 Comparison of experimental and FEM simulated results of the indentation edge length

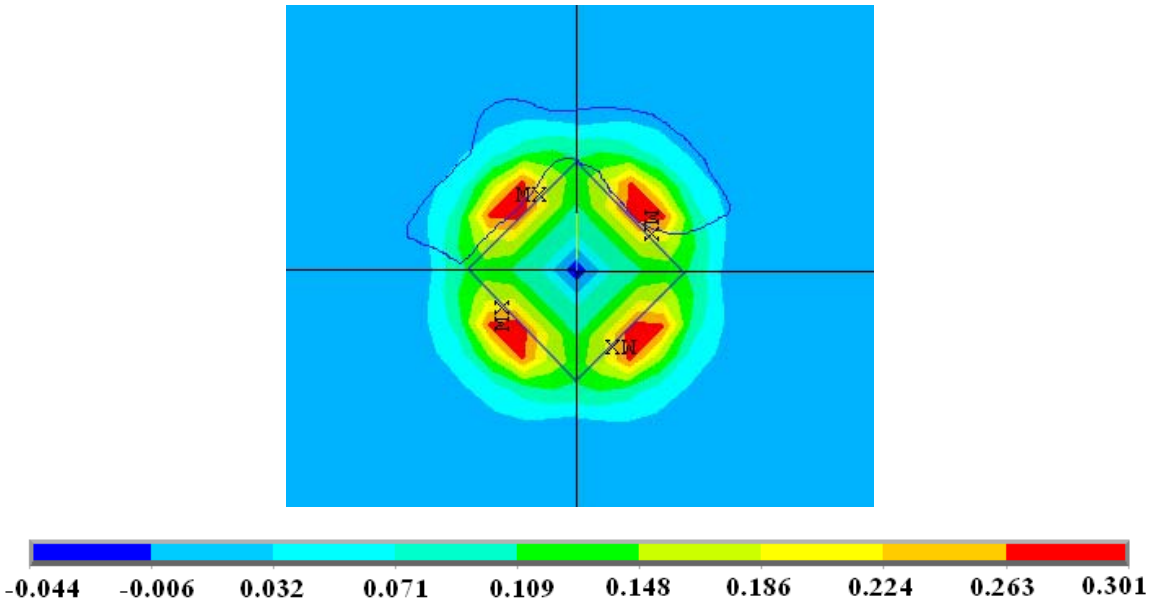

Figure 5.9 In-plane plastic shear strain γ_{xy} field determined in FEM and delaminated area under 0.98 N indentation load

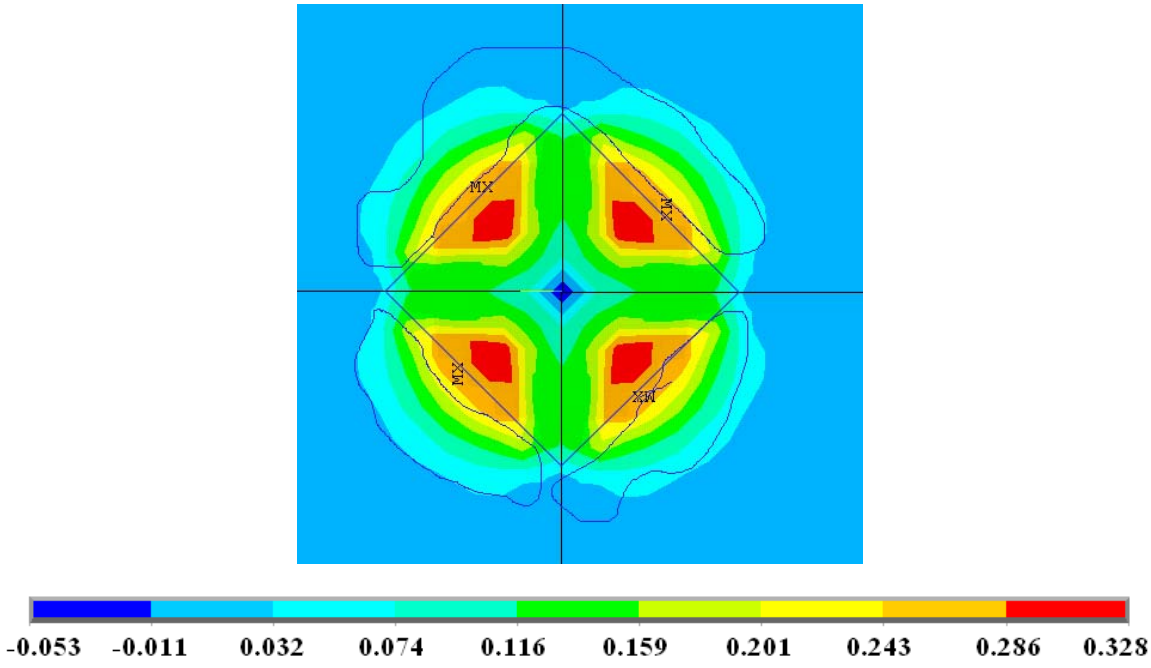

Figure 5.10 In-plane plastic shear strain γ_{xy} field determined in FEM and delaminated area under 2.94 N indentation load

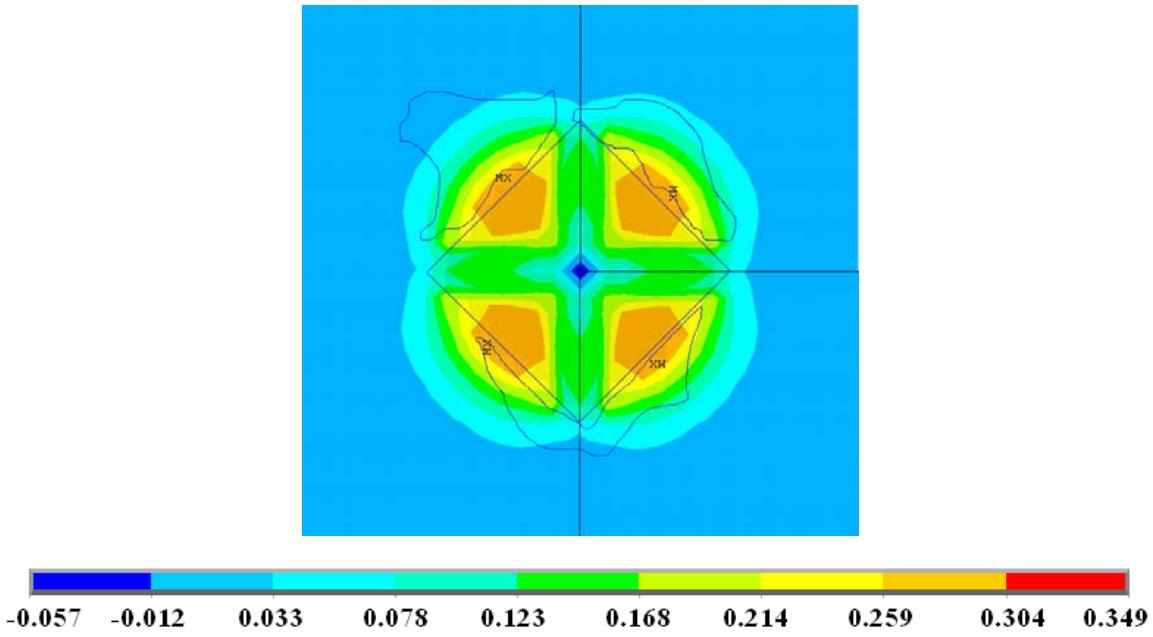

Figure 5.11 In-plane plastic shear strain γ_{xy} field determined in FEM and delaminated area under 4.9 N indentation load

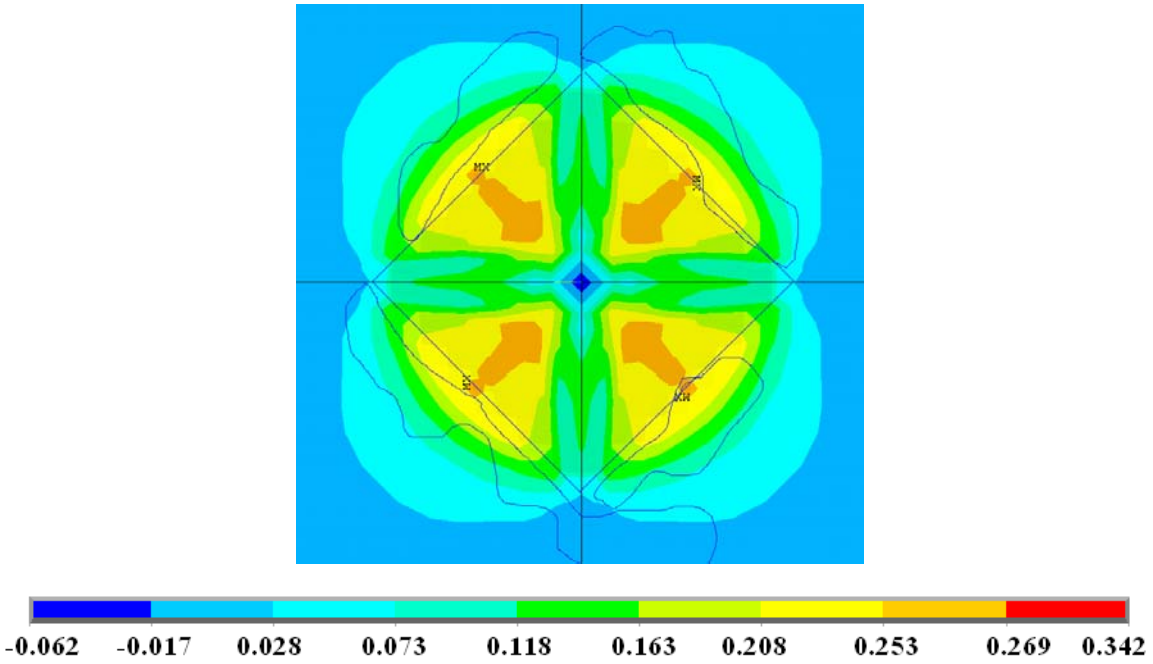

Figure 5.12 In-plane plastic shear strain γ_{xy} field determined in FEM and delaminated area under 9.8 N indentation load

5.4. Conclusions

In this chapter, Vickers indentation tests were carried out on the MP and CP specimens to quantitatively evaluate the adhesion strength of deposited BNT films on titanium substrates. The relation between the film delamination and the shear strain of titanium substrate was studied with the aid of FEM analysis. The main conclusions are summarized as follows:

(1) The MP specimen exhibited better adhesion than the CP specimen under the indentation load lower than 5 N. However, the delamination area for the MP specimen increased more greatly than that of the CP specimen with further increase of the indentation load.
(2) The delamination area increased monotonously with increasing the indentation load after the beginning of film delamination.
(3) The BNT film delamination induced by the indentation was primarily attributed to the plastic deformation of Ti substrate, and the critical shear strain γ_{xy} was evaluated to be about 0.2 with the aid of FEM analysis.

References

(1) Jaroslav Menčík, Determination of Mechanical Properties by Instrumented Indentation, *Meccanica*, Vol.42, No.1 (2007), pp.19-29.

(2) W. W. Gerberich, D. E. Kramer, N. I. Tymiak, A. A. Volinsky, D. F. Bahr and M. D. Kriese, Nanoindentation-induced Defect–interface Interactions: Phenomena, *Methods and Limitations*,Vol.47, No.15-16 (1998), pp.4115-4123.

(3) X. J. Zheng, Y. C. Zhou, J. M. Liu and A. D. Li, Interfacial Adhesion Analysis of $Pb(Zr_{0.52}Ti_{0.48})O_3$ (PZT) Thin Films by Nano-indentation Test, *Physics Letters A*,Vol.304, No.3-4 (2002), pp.110-113.

(4) L. L. Mishnaevsky and D. Gross, Micromechanisms and Mechanics of Damage and Fracture in Thin Film/Substrate Systems, *International Applied Mechanics*,Vol.40, No.2 (2004), pp.140-155.

(5) P. Davies, B. R. K. Blackman and A. J. Brunner, Standard Test Methods for Delamination Resistance of Composite Materials: Current Status, *Applied Composite Materials*,Vol.5, No.6(1998), pp.345-364.

(6) A. P. Buang, R. Liu, X. J. Wu and M. X. Yao, Cracking Analysis of HVOF Coatings under Vickers Indentation, *Journal of Coatings Technology and Research*,Vol.5, No.4 (2008), pp.513-534.

(7) I. M. Low and C. Shi, Vickers Indentation Responses of Epoxy Polymers, *Journal of Materials Science Letters*,Vol.17, No.14 (1998), pp.1181-1183.

(8) D. F. Bahr, C. L. Woodcock, M. Pang, K. D. Weaver and N. R. Moody, Indentation Induced Film Fracture in Hard Film – Soft Substrate Systems, *International Journal of Fracture*,Vol.119, No. 4 (2003), pp.339-349.

(9) A. Jain, V. Gupta and S. N. Basu, A Quantitative Study of Moisture Adsorption in Polyimide and Its Effect on the Strength of the Polyimide/Silicon Nitride Interface, *Acta Materialia*, Vol.53, No.11 (2005), pp.3147-3153.

(10) K. K. Bamzai, P. N. Kotru and B. M. Wanklyn, Investigations on Indentation Induced Hardness and Fracture Mechanism in Flux Grown DyAlO Crystals, *Applied Surface Science*,Vol.133, No.3 (1998), pp.195-204.

(11) V. P. Poliakov, C. J. de M. Siqueira, W. Veiga, I. A. Hümmelgen, C. M. Lepienski, G. G. Kirpilenko and S. T. Dechandt, Physical and Tribological Properties of Hard Amorphous DLC Films Deposited on Different Substrates, *Diamond and Related Materials*,Vol.13, No.4-8 (2004), pp.1511-1515.

(12) B. D. Beake, S. R. Goodes, J. F. Smith, R. Madani, C. A. Rego, R. I. Cherry and T. Wagner,

Investigating the Fracture Resistance and Adhesion of DLC Films with Micro-impact Testing, *Diamond and Related Materials*,Vol.11, No.8 (2002), pp.1606-1609.

(13) Alex A. Volinsky, Neville R. Moody and William W. Gerberich, Fiducial Mark and CTOA Estimates of Thin Film Adhesion, *International Journal of Fracture*,Vol.120, No.1-2 (2003), pp.431-439.

Chapter 6

Evaluation of Adhesion Strength between BNT Films and Ti Substrates by a Scratch Test

A scratch test is one of common methods to quantitatively evaluate the adhesion strength between a film and its substrate. In the scratch testing, the adhesion strength of film can be further investigated by the microscopic observation of film damage, the measurement of friction force and the detection of acoustic emission (AE). This chapter presents the scratch test performed on the self-made scratch tester to quantitatively evaluate the adhesion strength of deposited BNT films on titanium substrates.

6.1. Introduction

A scratch method has been used to determine the practical adhesion strength and mechanical failure mode of thin film, ceramic coatings on metal, ceramic, and polymer substrates [(1)-(7)]. Conventional scratch testing employs a diamond stylus of defined geometry and tip size to draw across the surface of the test sample a scratch track at a constant speed. As the normal force is increased, the stylus produces progressive mechanical damage in the coating through a combination of elastic/plastic indentation stresses and frictional forces in the coating-substrate system. At a specific applied normal force a recognizable failure mode is observed in the coating, this normal force is known as the critical load (L_c). The scratch adhesion test is operated in two modes: constant load scratch testing and progressive load testing. In constant load testing, the applied normal force remains at a set level throughout the test. While for progressive load testing, the applied normal force is linearly increased as the test advances. Damage assessment of the coating is performed by a microscopic observation of the scratch channel. Other measurements taken to characterize the failure mechanism of the coating include the tangential force and acoustic emission.

Recently, a scratch method has been developed to evaluate the adhesion strength of TiN and DLC film on their substrates [(8)-(14)]. In this chapter, we employ the self-made scratch tester to investigate the adhesion strength of deposited BNT films on titanium substrates. The critical force was determined from the variations of the tangential force and AE signals with the normal force, and then used to quantitatively evaluate the adhesion strength of BNT films.

6.2. Experimental

6.2.1. Sample Preparation

BNT films were hydrothermally synthesized on pure titanium substrates which were 0.2 mm in thickness. Some of titanium substrates (MP) were mechanically polished using an emery paper. Some of substrates (CP) were chemically polished in the chemical solution, as shown in Table 4.3. Table 6.1 shows the surface treatments of Ti substrates. After the pretreatment, the substrates were ultrasonically cleaned in a methanol bath followed by a rinse in distilled water. The surface roughness Ra was measured for all the substrates to be deposited using a laser microscope.

The synthesis process of BNT film was performed at the temperature of 150℃ for 24 hours under the optimum condition G, as described in Table 4.1. BNT film of about 5 μm thick was obtained on each side of titanium substrate.

.

Table 6.1 Surface treatments of Ti substrates prior to the deposition of BNT films

Sample	Pretreatment method
AR	As received with calendering
E240	Mechanical polish by a 240 grit emery paper
E1000	Mechanical polish by a 1000 grit emery paper
CP	Chemical polish by pickling in the prepared solution

6.2.2. Scratch Tester

In this study, scratch tests were performed on the BNT deposited samples using the self-made scratch tester with a diamond indenter. As shown in Figure 6.1, this tester system consists of an indenter head, an adjustable stage, a step motor and AE system, and it employed a sliding conical diamond indenter with apex angle 120º and spherical tip radius of 50 μm. As shown in Figure 6.2, the indenter head is the core part of the self-made scratch tester. AE sensor was used to detect the signal of acoustic emission. Strain gauges on the cantilever beam and flat spring were used to detect the signals of normal force and tangential force. We performed experiments in the condition of only normal load and only tangential load respectively, and then made the regression analysis of the obtained experimental data, which were shown in Figures 6.3 and 6.4, respectively. As a result, the following two equations were obtained to calculate the normal force and the tangential force by the output voltages of gauges during the scratch testing.

$$F_t = -\frac{V_{s2}}{6.12} \tag{6.1}$$

$$F_n = -\frac{V_{s1} - V_{s2}/6.12}{1.25} \tag{6.2}$$

Where F_t is the tangential force;

F_n is the normal force;

V_{s1} is the output voltage of sensor1, which indicates the gauge on the flat spring;

V_{s2} is the output voltage of sensor2, which indicates the gauge on the cantilever beam.

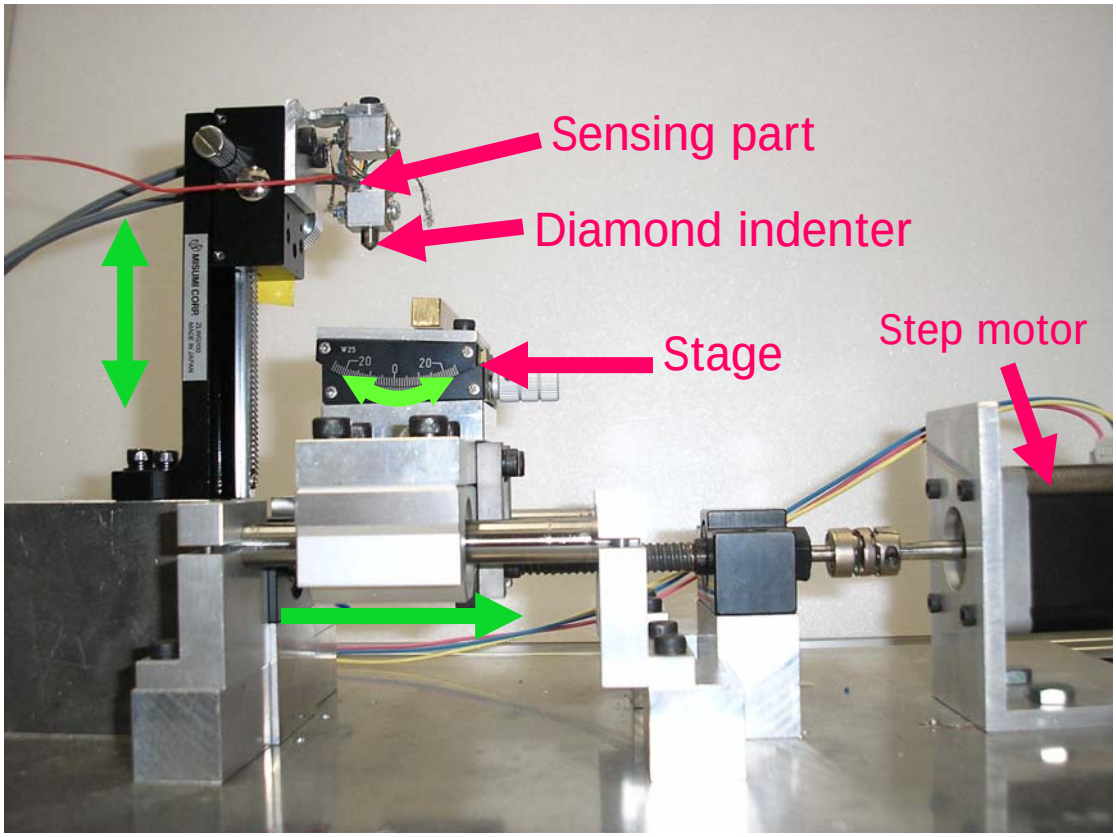

Figure 6.1 The self-made scratch tester

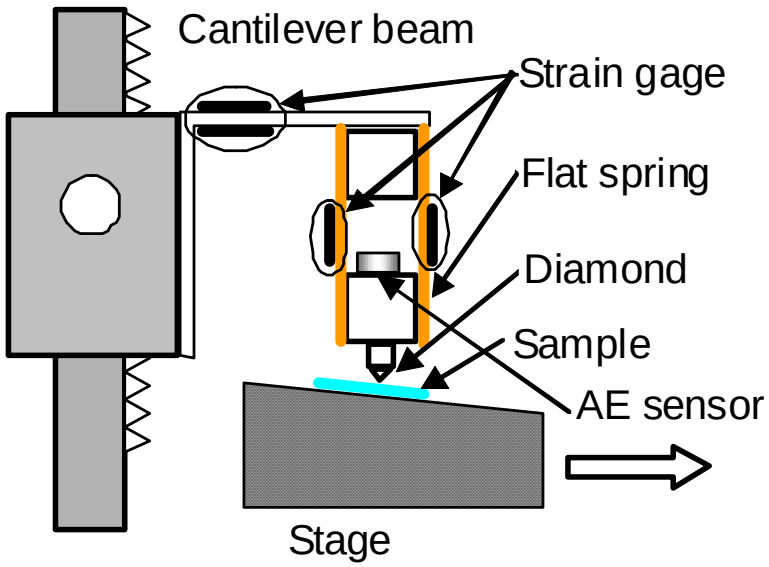

Figure 6.2 Schematic of the indenter head of the self-made scratch tester

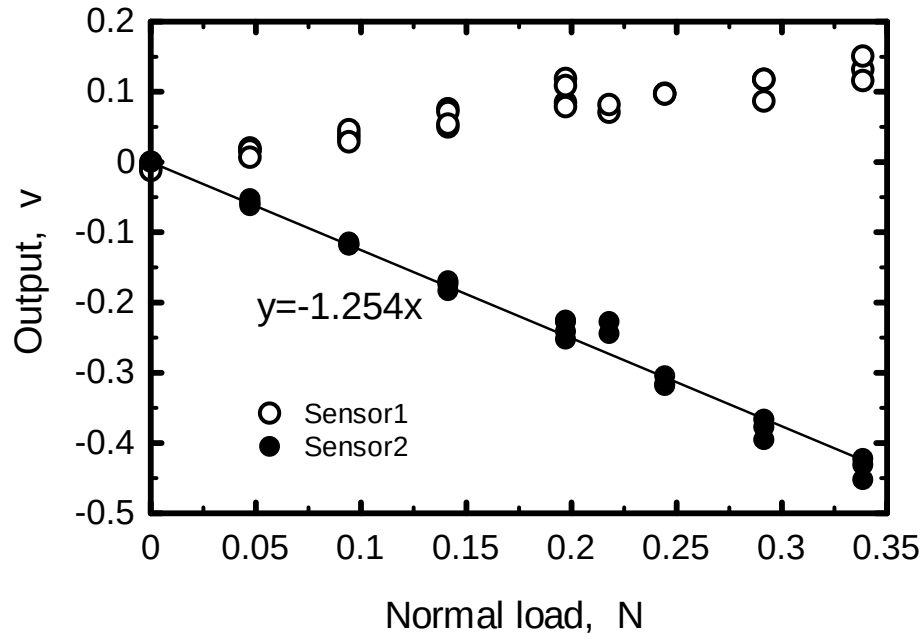

Figure 6.3 The output voltage as a function of applied normal load

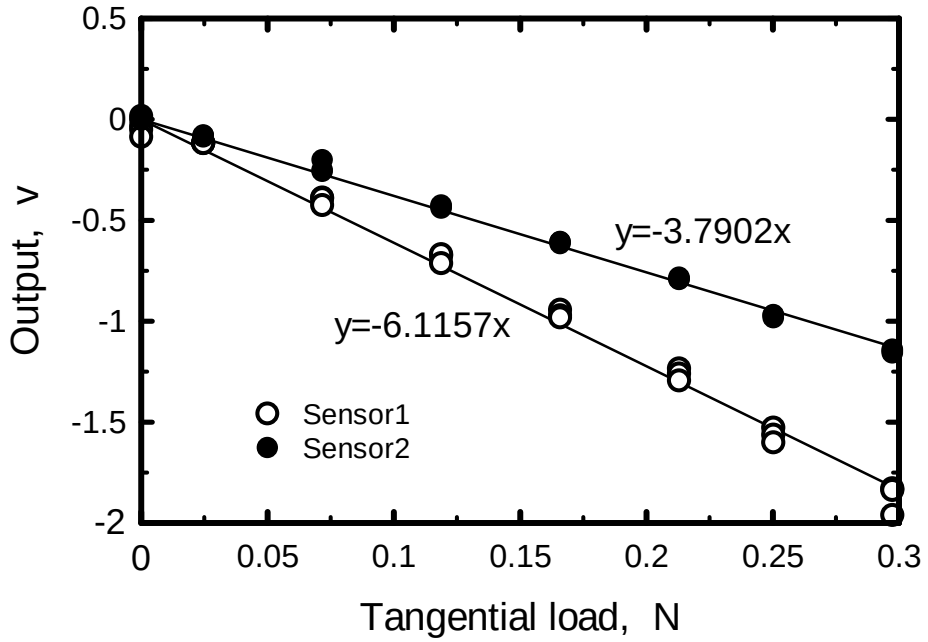

Figure 6.4 The output voltage as a function of applied tangential load

6.2.3. Scratch Test

Figure 6.5 shows the schematic illustration of the scratch testing. During the scratch testing, the signals of normal force, tangential force and acoustic emission were simultaneously recorded. In this study, the stage was adjusted to a slope with an angle of 3º. As a consequence, the normal load imposed on the sample increased continuously during the scratching test. Scratch tests were carried out at a scratching speed of 3 mm/min over about 2 mm scratch distance. After scratching, the scratch channels were observed by SEM.

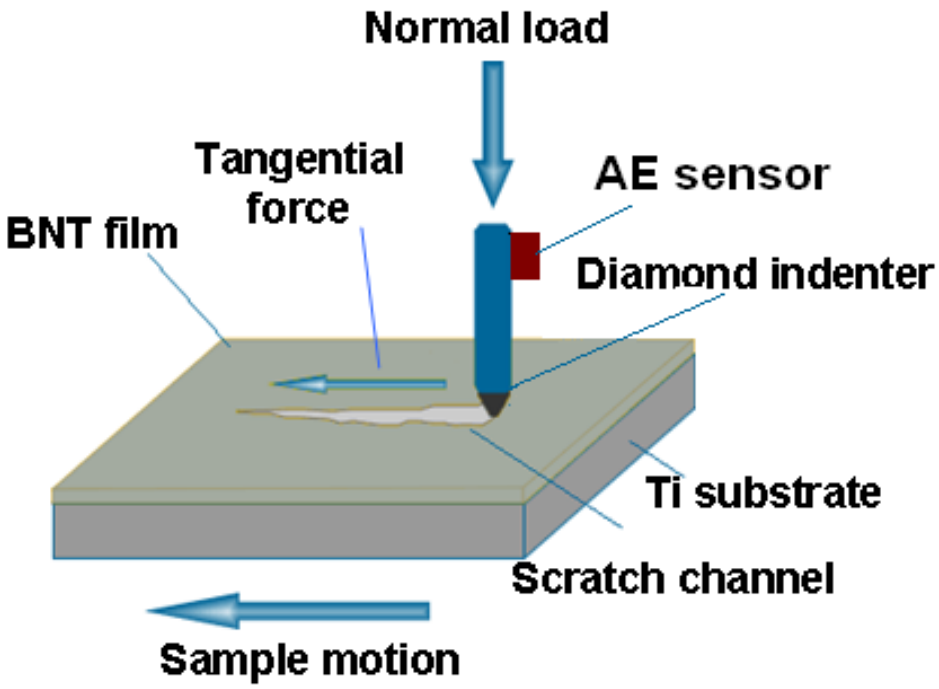

Figure 6.5 Schematic of the scratch testing

6.3. Results and Discussion

6.3.1. Microscopic Observation of Scratch

Figures 6.6, 6.7, 6.8 and 6.9 show SEM images of the different parts of the scratch channel for sample AR, E240, E1000 and CP respectively. These SEM observations of the scratched samples showed that the scratch channels were composed of two stages before and after the diamond indenter reached the film/substrate interface. The first stage, at low normal force, involved the film deformation which didn't cause adhesion failures of BNT films. In the second stage, the film exfoliations were observed around the scratch channel owing to the deformations of film and substrate. The spot of the scratch channel where the indenter tip just reached the titanium substrate was determined by the EDX element analysis of the bottom of scratch channel.

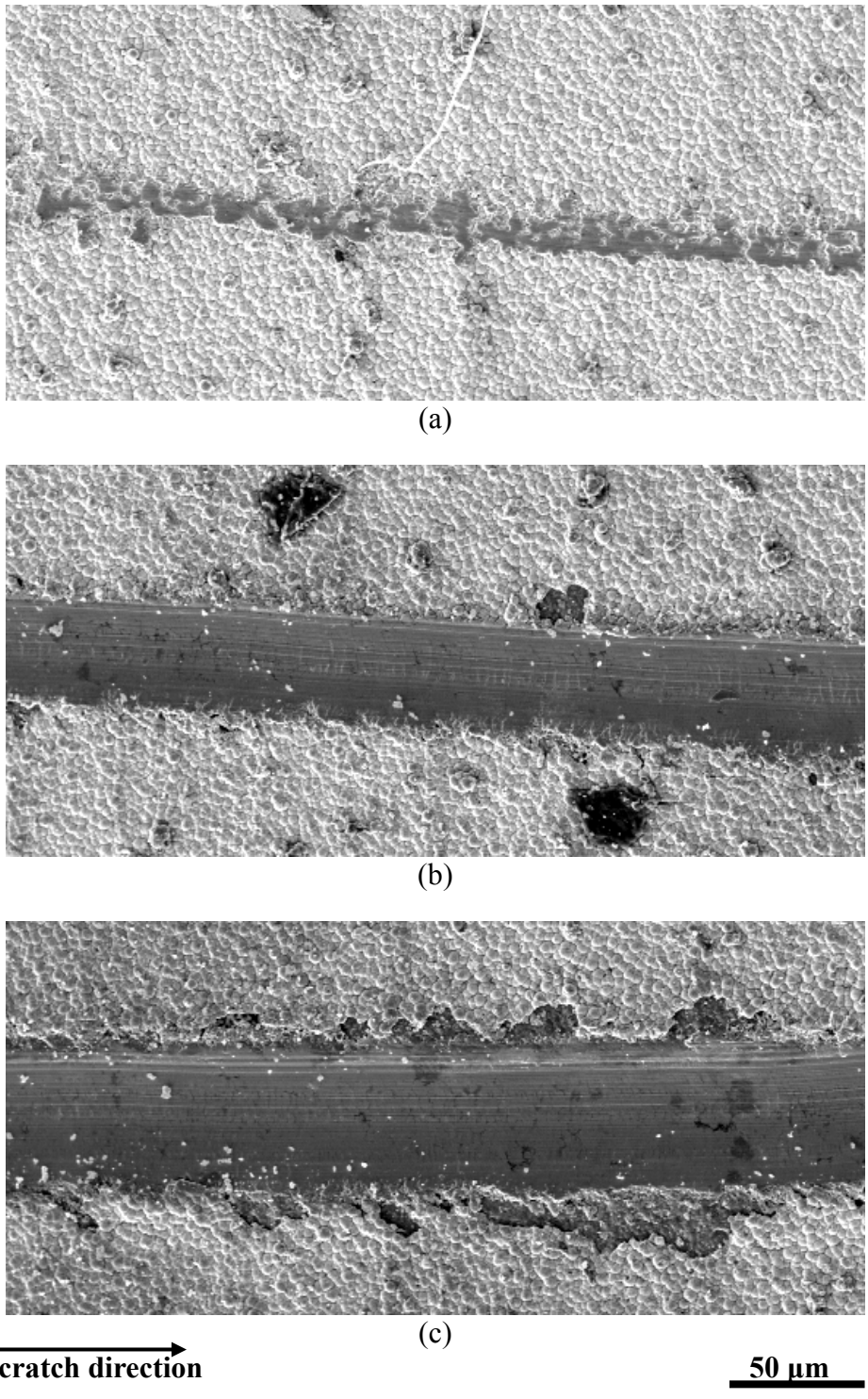

Figure 6.6 SEM images of the different parts of the scratch channel (AR): (a) the fore part; (b) the middle part; (c) the rear part

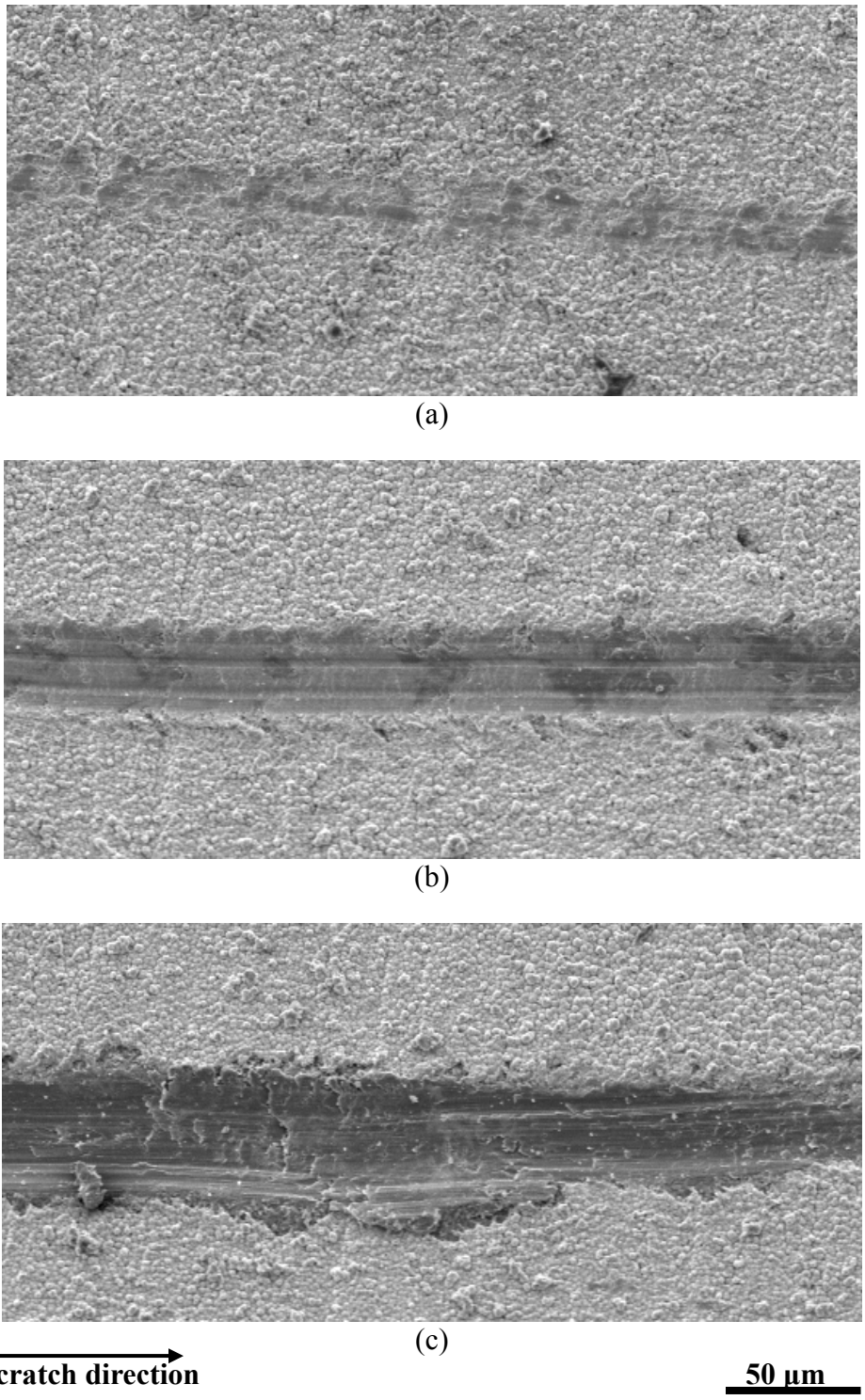

Figure 6.7 SEM images of the different parts of the scratch channel (E240): (a) the fore part; (b) the middle part; (c) the rear part

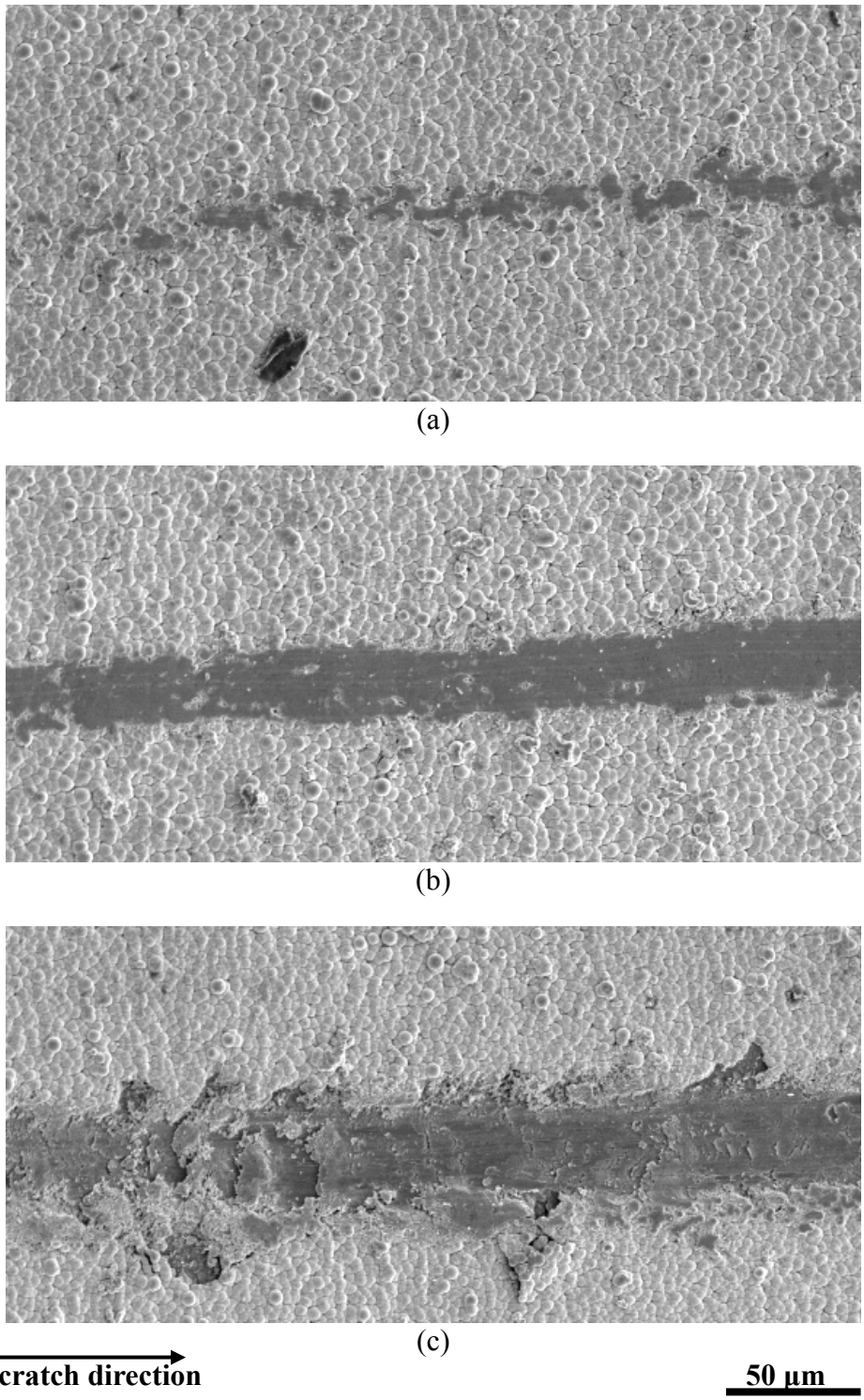

Figure 6.8 SEM images of the different parts of the scratch channel (E1000): (a) the fore part; (b) the middle part; (c) the rear part

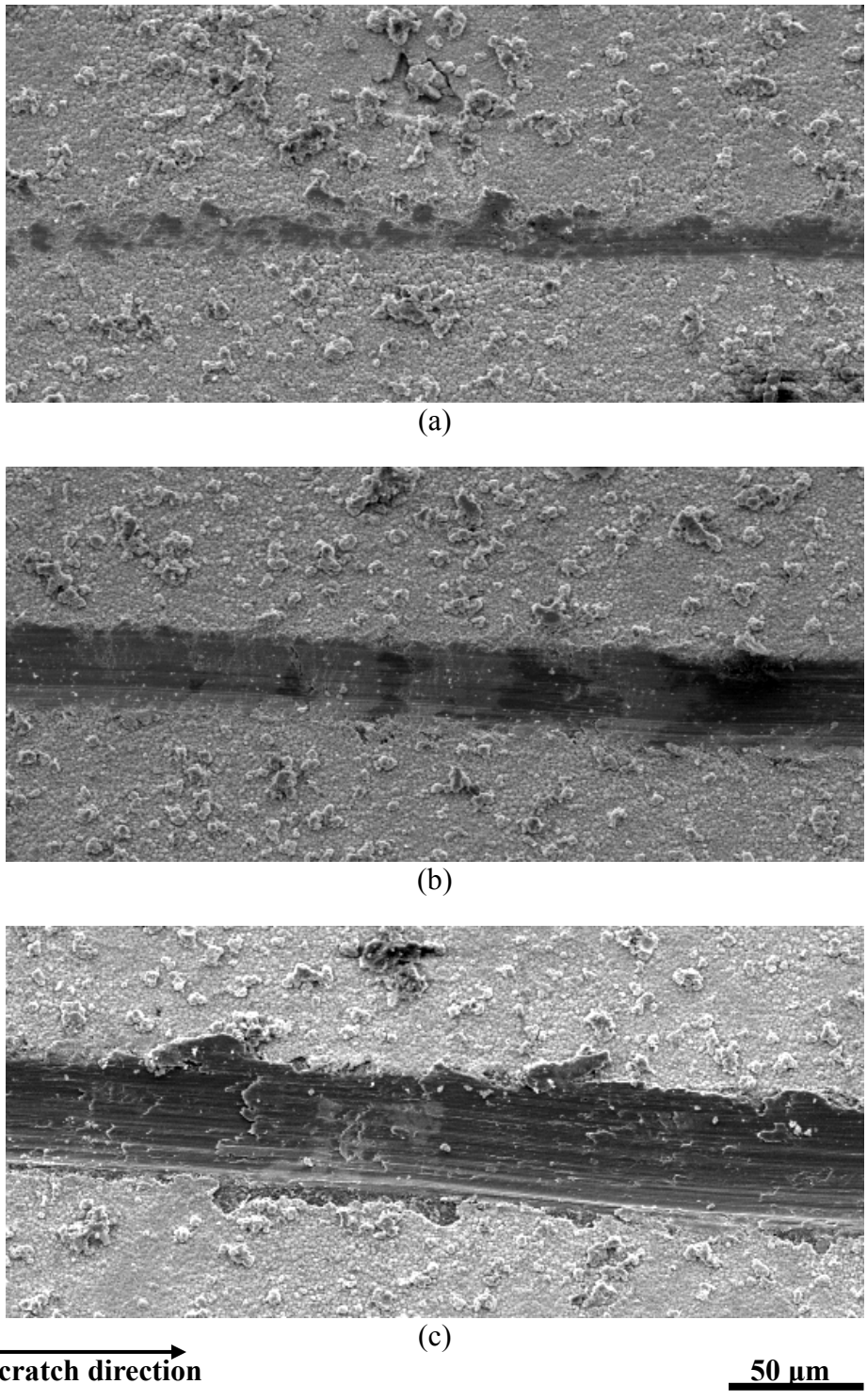

Figure 6.9 SEM images of the different parts of the scratch channel (CP): (a) the fore part; (b) the middle part; (c) the rear part

6.3.2. Adhesion Strength

In the scratch test of adhesion, the adhesion strength of film was evaluated by investigating the critical force (load). Generally, the critical force is deduced from the following three ways:

(1) The microscopic investigation of film exfoliation;

(2) The friction coefficient (F_t/F_n);

(3) AE signal.

In Section 6.3.1, it was found that the film exfoliation occurred after the indenter tip reached the titanium substrate by SEM observation of the scratch channel. In this section, we will investigate the critical force by the last two methods. Figures 6.10, 6.11, 6.12 and 6.13 show the variations of the tangential force (F_t) and AE signal with the normal force (F_n) during the scratch test for sample AR, E240, E1000 and CP respectively. As the mechanical properties of the film and substrate are different, there is a turning point in the slope of F_t-F_n and AE-F_n curve respectively, when the indenter reaches the film/substrate interface. At this turning point, the normal force is regarded as the critical normal force which, if sufficiently large, induces adhesion failure. Two critical forces (L_T and L_{AE}) were determined from the F_t-F_n and AE-F_n curves. The small difference between L_T and L_{AE} was found in Figures 6.10, 6.11, 6.12 and 6.13, and thus can be neglected. In this study, L_T was used to assess the adhesion strength of BNT film on its substrate.

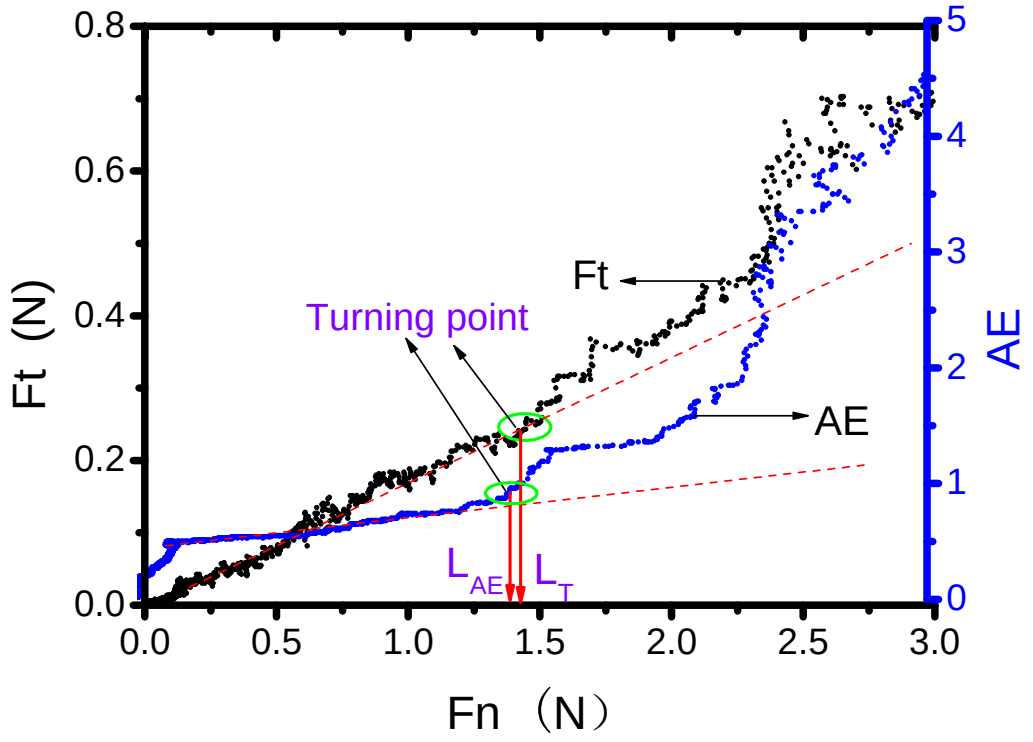

Figure 6.10 Variations of the tangential force and AE signal with the normal force (AR): L_T =1.4 N and L_{AE}=1.42 N

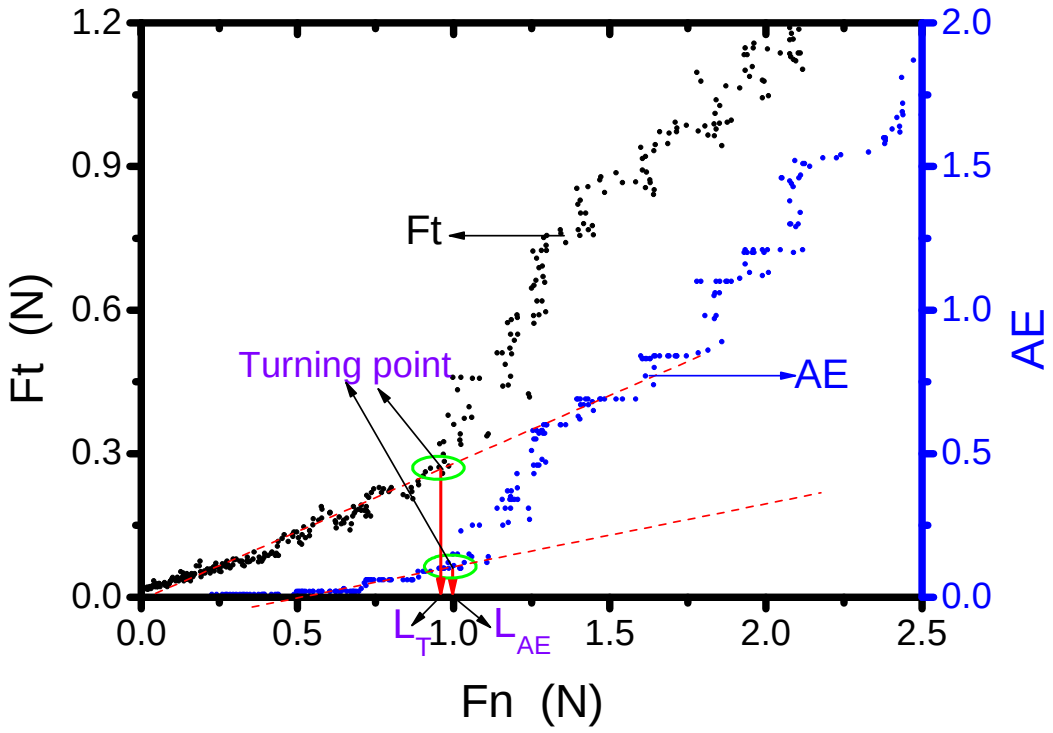

Figure 6.11 Variations of the tangential force and AE signal with the normal force (E240): L_T =0.95 N and L_{AE}=1.0 N

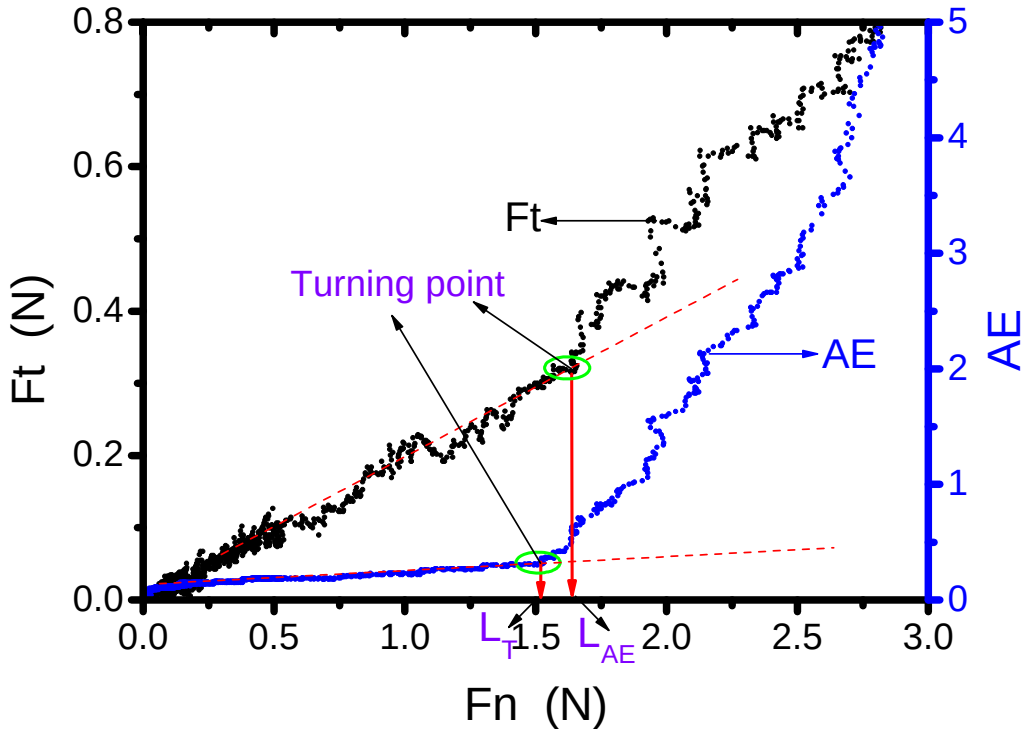

Figure 6.12 Variations of the tangential force and AE signal with the normal force (E1000): L_T =1.5 N and L_{AE}=1.65 N

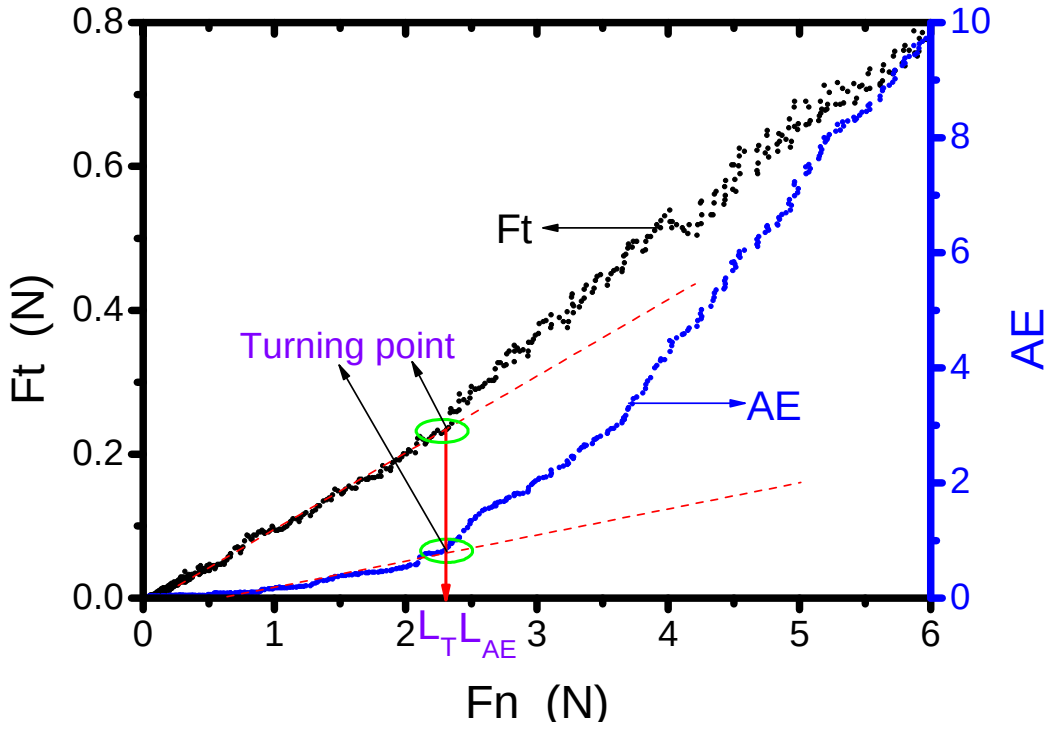

Figure 6.13 Variations of the tangential force and AE signal with the normal force (CP): L_T =2.3 N and L_{AE}=2.3 N

The critical force obtained by the scratch test for each sample and the surface roughness for each substrate were shown in Figure 6.14 and Figure 6.15, respectively. It was reported that the increase in the mechanical interlock between the film and the substrate by surface roughening resulted in the improvement of the adhesion of film [8]. However, it can be found from Figure 6.16 that the CP sample was largest in the critical normal force, and the critical normal force decreased almost monotonously with the increase of substrate roughness. It may be a factor that a plastic deformation layer was produced on substrate surface after mechanical polish.

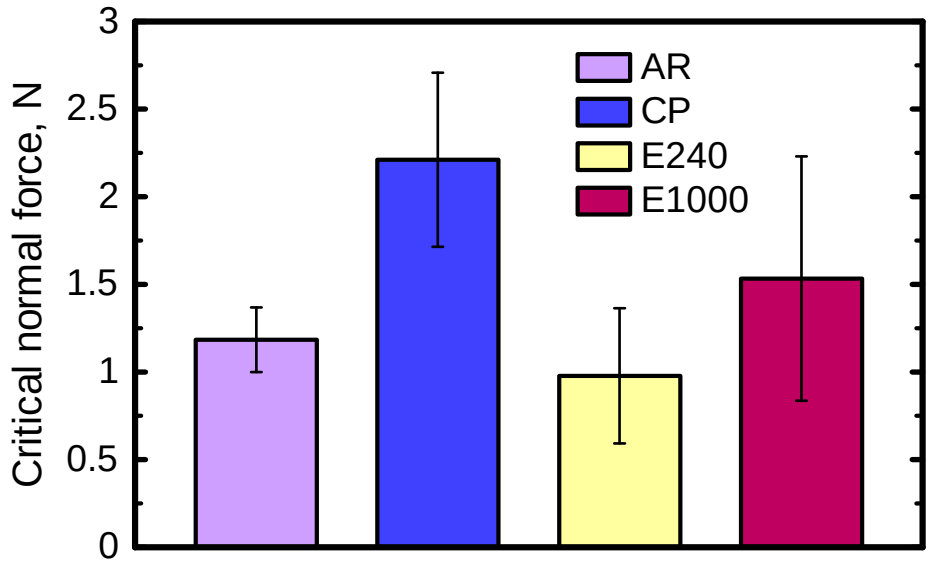

Figure 6.14 The critical normal force for various samples

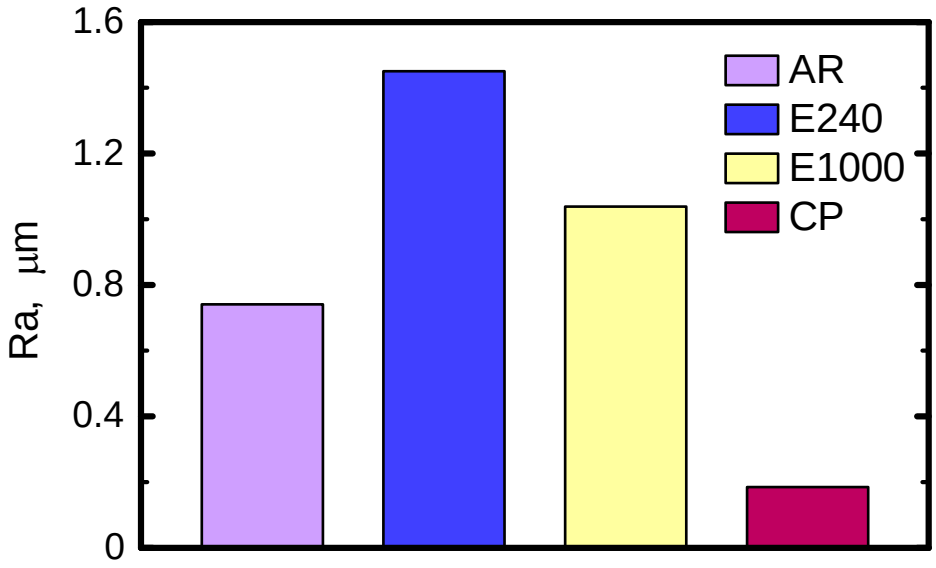

Figure 6.15 Surface roughness of various substrates

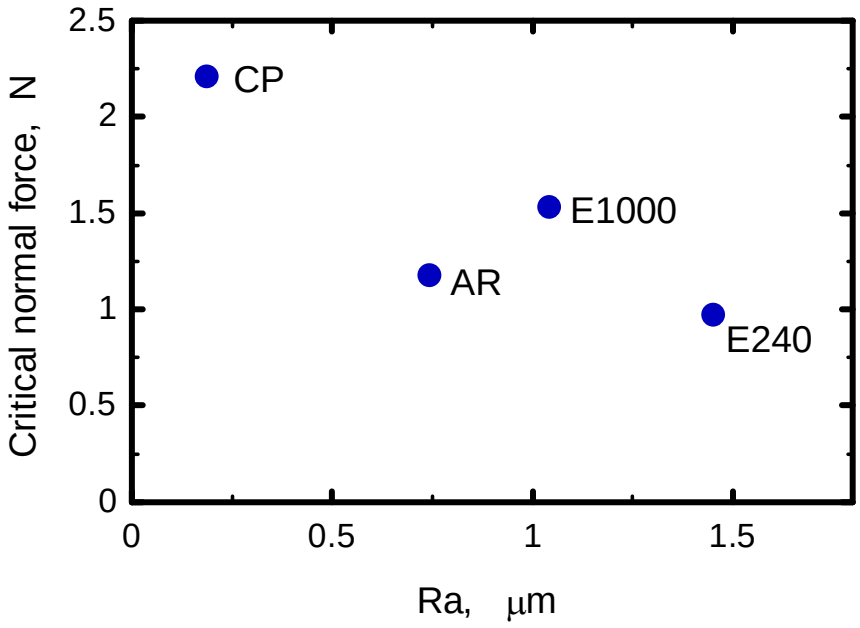

Figure 6.16 Correlation between the critical normal force and substrate roughness

6.4. Conclusions

In this chapter, Scratch tests were performed to quantitatively evaluate the adhesion strength of deposited BNT films on titanium substrates using the self-made scratch tester. Some of titanium substrates were pretreated by chemical polish and mechanical polish respectively prior to BNT film deposition with a view of investigating the effects of substrate surface pretreatments on the adhesion of BNT films. The critical force was determined by investigating SEM images of scratch channels and the relations between the normal force, tangential force and AE signal. The main conclusions are summarized as follows:

(1) Scratch test is an effective method for evaluating the adhesive strength of BNT films on Ti substrates in the scratch condition.
(2) No exfoliation of BNT film was found before the indenter tip reached the titanium substrate. The film exfoliations occurred around the scratch channel owing to the deformations of film and substrate after the indenter tip reached the titanium substrate.
(3) Comparing the critical forces between samples, it was demonstrated that chemical polish and mechanical polish using a 1000 grit emery paper were pretreatments of titanium substrate surface, which improved the adhesion strength of BNT films on the Ti substrates. The chemical polish was better in comparison.

References

(1) I. A. Ashcroft and B. Derby, Adhesion Testing of Glass-Ceramic Thick Films on Metal Substrates, *Journal of Materials Science*, Vol.28, No.11 (1993), pp.2989-2998.

(2) B. D. Beake, A. A. Ogwu and T. Wagner, Influence of Experimental Factors and Film Thickness on the Measured Critical Load in the Nanoscratch Test, *Materials Science and Engineering: A*, Vol.423, No.1-2 (2006), pp.70-73.

(3) C. Charitidis, Y. Panayiotatos and S. Logothetidis, A Quantitative Study of the Nano-scratch Behavior of Boron and Carbon Nitride Films, *Diamond and Related Materials*, Vol.12, No.3-7 (2003), pp.1088-1092.

(4) X. J. Zheng, Y. C. Zhou, J. M. Liu and A. D. Li, Determination of Interfacial Fracture Energy of PZT Ferroelectric Thin Films by Nano-scratch Technique, *Journal of Materials Science Letters*, Vol.22, No.10 (2003), pp.743-745.

(5) H. Ichimura and Y. Ishii, Effects of Indenter Radius on the Critical Load on Scratch Testing, *Surface and Coatings Technology*, Vol.165, No.1 (2003), pp.1-7.

(6) S. J. Bull, R. I. Davidson, K. Harvathova, D. Mitchell and J. R. Preliminary Investigation into the Application of Scratch Testing to Marine Coatings, *Journal of Materials Science*, Vol.37, No.22 (2002), pp.4937-4943.

(7) A. Hodzic, J. K. Kim and Z. H. Stachurski, The Nano-scratch Technique as a Novel Method for Measurement of an Interphase Width, *Journal of Materials Science Letters*, Vol.19, No.18 (2000), pp.1665-1667.

(8) S. Kamiya, H. Nagasawa, K. Yamanobe, H. Hanyu and M. Saka, A Comparative Study of the Mechanical Properties of PVD Coatings Evaluated by New Techniques and Conventional Methods, *Thin Solid Films*, Vol.469-470 (2004), pp.248-253.

(9) M. H. Staia, E. S. Puchi and C. Julia Schmutz, Adhesion of CVD TiN on 316L Surgical Obtained in a Mass Transfer Regime Stainless Steel, *Journal of Electronic Materials*, Vol.26, No.9 (1997), pp.980-986.

(10) Jingze Tian, Qing Zhang, Lifang Xia, S. F. Yoon, J. Ahn, E. S. Byon, Q. Zhou, S. G. Wang, J. Q. Li and D. J. Yang, A Study of Interface and Adhesion of c-BN Film on Si(1 0 0) Modified by Nitrogen Plasma Based Ion Implantation Technique, *Materials Research Bulletin*, Vol.39, No.7-8 (2004), pp.917-922.

(11) D. Sheeja, B. K. Tay, C. Q. Sun and Y. Q. Fu, Characterization of Ti-containing Amorphous Carbon Films Prepared on Titanium Substrates, *Journal of Materials Science*, Vol.38, No.3(2003), pp.421-425.

(12) B. Y. Tang, Y. H. Wang, L. P. Wang, X. F. Wang, H. X. Liu, Y. H. Yu and T. Sun, Adhesion Strength of Tin Films Synthesized on GCr15-bearing Steel Using Plasma Immersion Ion Implantation and Deposition, *Surface and Coatings Technology*, Vol.186, No.1-2 (2003), pp.153-156.

(13) L. Y. Huang, K. W. Xu, J. Lu, Bruno Guelorget and H. Chen, Nano-scratch and Fretting Wear Study of DLC Coatings for Biomedical Application, *Diamond and Related Materials*, Vol.10, No.8 (2001), pp.1448-1456.

(14) K. H. Lai, C. Y. Chan, M. K. Fung, I. Bello, C. S. Lee and S. T. Lee, Mechanical Properties of DLC Films Prepared in Acetylene and Methane Plasmas Using Electron Cyclotron Resonance Microwave Plasma Chemical Vapor Deposition, *Diamond and Related Materials*, Vol.10, No.9-10 (2001), pp.1862-1867.

Chapter 7
Summary

As indicated in Chapter 1, this dissertation has focused on two issues: one is the development of the hydrothermal method to deposit BNT film on titanium substrate, and the other is the quantitative assessment of the adhesion strength of deposited BNT films by a tensile test, indentation test and scratch test.

In the hydrothermal synthesis of BNT films on titanium substrates, $Bi(NO_3)_3 \cdot 5H_2O$, TiO_2 and NaOH were used as starting materials. We employed a 2-step process: nucleation and crystal growth. The properties of deposited BNT films were characterized using SEM, EDX, XRD, LCR and other instruments, and then investigated with respect to the concentrations of $Bi(NO_3)_3$ and TiO_2 starting materials. The main conclusions are summarized as follows.

(1) The generation of BNT crystal with the rhombohedral crystal structure was confirmed in the deposited films by XRD analysis. Bi_2O_3 impurity was also found, and its amount increased with increasing the $Bi(NO_3)_3$ concentration.
(2) The order of mixing the precursors and the mineralizer for preparing the starting solution influenced greatly the quality of the prepared starting solution, thus affected the crystallization of deposited BNT films. In this study, the order of ($Bi(NO_3)_3$ + TiO_2) + NaOH was used for preparing the starting solution close to a colloid. This is one of necessary conditions for hydrothermal synthesis of well crystallized BNT films.
(3) At the beginning of the hydrothermal synthesis, the titanium substrate reacted with the ions dissolved in the solution to form some nuclei on the substrate surface. Some crystal nuclei were found on the substrate surface after 15 minutes of deposition, and BNT crystals were generated all over the substrate surface after one hour of deposition.

(4) With the evaluation target of the calculated BNT content of deposited films, the optimized synthesis condition was determined as follows: $Bi(NO_3)_3$ of 1.2 mol/l and TiO_2 of 0.5 mol/l.

(5) Deposition speed was relatively high in the 2nd and 3rd deposition. This was primarily attributed to the great amount of the Bi_2O_3 impurity generated in these two depositions. The Bi_2O_3 impurity can be removed by the etching treatment of concentrated nitric acid.

(6) The relative permittivity tended to increase greatly in the case of the $Bi(NO_3)_3$ concentration of 1.6 mol/l. The dielectric loss was positive correlated with the relative permittivity.

(7) The actuation test confirmed the piezoelectric activity of deposited BNT films, and it was noted that the piezoelectricity strength of the deposited BNT film was greatly dependent on the crystallization level of BNT. The piezoelectric response of the tested unimorph cantilever type actuator was stronger in the case of higher BNT diffraction peaks.

In an effort to quantitatively assess the adhesion strength between the deposited BNT film and titanium substrate, a tensile test, indentation test and scratch test were carried out in this dissertation. The critical force or substrate strain inducing film exfoliation or delamination was determined with the aid of FEM analysis in their respective load condition. The main conclusions are summarized as follows.

(1) In the tensile test, the film exfoliation firstly occurred after the yield strength of titanium substrate for both of the smooth and holed specimens. With the aid of FEM analysis of titanium substrate, the critical strain was determined to be about 1% for both of the CP and MP specimens.

(2) In the Vickers indentation test, the film delamination area increased monotonously with increasing the indentation load after the beginning of film delamination. The critical shear strain γ_{xy} was evaluated to be about 0.2 with the aid of FEM analysis.

(3) In the scratch test, no exfoliation of BNT film was found before the indenter tip reached the titanium substrate. The film exfoliations occurred around the scratch channel owing to the deformations of film and substrate after the indenter tip reached

the titanium substrate. Comparing the critical forces between samples, it was demonstrated that chemical polish and mechanical polish using a 1000 grit emery paper were pretreatments of titanium substrate surface, which improved the adhesion strength of BNT films on the Ti substrates. The chemical polish was better in comparison.

(4) The adhesion strength of deposited BNT film was sensitive to the property of substrate surface. Film adhesion measurements showed that the appropriate pretreatment of titanium substrate such as chemical polish and mechanical polish can improve the adhesion strength of BNT films on titanium substrates.

(5) In practical evaluation of film adhesion, which test method to use depends mainly on the comparability of the results to actual operational environments of the film/substrate system. Much more researches are needed to establish a reliable and versatile method for measuring the adhesion strength of film on its substrate.

ACKNOWLEDGEMENTS

I would first like to express my deepest appreciation to my advisor, Professor Kazuhiro KUSUKAWA, for all his support, encouragement, and guidance throughout this research. This research work would not have been realized without his guidance over the years of my Ph.D. study. His enthusiasm for research and devotion to science always inspire me and direct me during my research work. Thanks for all the encouragement and good advice throughout the thesis work. His enthusiasm and broad knowledge are truly invaluable for my future career.

I would take this opportunity to thank all the members in our lab, Strength of Materials Laboratory.

Finally, I would like to thank my wife and my family for their encouragement and continuous support during my Ph.D. study.